

NASA Contractor Report 159086

Final Report Design Study of Prestressed Rotor Spar Concept

D. Gleich

**ARDE INC.
Mahwah, N.J. 07430**

**CONTRACT NAS 1-13816
JANUARY 1980**



**National Aeronautics and
Space Administration**

**Langley Research Center
Hampton, Virginia 23665
AC 804 827-3966**

FINAL REPORT
DESIGN STUDY OF
PRESTRESSED ROTOR SPAR CONCEPT

by
D. Gleich

Prepared Under Contract No. NAS1-13816
January 1980

Submitted by:
ARDE, INC.
19 Industrial Avenue
Mahwah, New Jersey 07430

for
National Aeronautics & Space Administration

FOREWARD

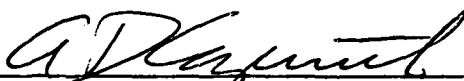
This report is submitted by ARDE, INC. in fulfillment of Contract NAS1-13816 and covers the period from March, 1975 to June, 1976. The program manager and principal investigator was Mr. David Gleich. The principal subcontractor was Kaman Aerospace Corporation. Mr. Justin Barzda was the key Kaman technical investigator. Mr. Carl Swindlehurst was the Army technical project manager.

Prepared by:

Approved by:



David Gleich



A. D. Cozewith

DESIGN STUDY OF THE PRESTRESSED
ROTOR SPAR CONCEPT *

by

D. Gleich

ABSTRACT

A design study of the prestressed composite spar concept as applied to the Bell Helicopter 540 Rotor System of the AH-1G helicopter was performed. The stiffness, mass and geometric configurations of the Bell blade were matched, to give a dynamically similar prestressed composite blade. A multi-tube, prestressed composite spar blade configuration was designed for superior ballistic survivability at low life cycle cost. Principal structural elements include three (3) prestressed composite spar tubes, KEVLAR 49 fiber skins and interconnections, a Nomex honeycomb afterbody and KEVLAR 49 fiber nose and trailing edge members. The tube liners were designed to provide redundant attachment to the rotor hub. An outer skin ply of #120 woven fiberglass cloth increases tear resistance to external damage. The composite spar prestresses, imparted during fabrication, are chosen to maintain compression in the high strength cryogenically stretchformed 304-L stainless steel liner and tension in the overwrapped HTS graphite fibers under operating loads. This prestressing results in greatly improved crack propagation and fatigue resistance as well as enhanced fiber stiffness properties. Advantages projected for the prestressed composite rotor spar concept include increased operational life and improved ballistic survivability at low life cycle cost.

* The contract research effort which lead to the results of this report was financially supported by the U. S. Army Research and Technology Laboratories (AVRADCOM), Structures Laboratory.

CONTENTS

	<u>PAGE</u>
SUMMARY	vii
1.0 INTRODUCTION	1
2.0 SYMBOLS	4
3.0 DESCRIPTION OF THE PRESTRESSED ROTOR SPAR CONCEPT AND BLADE CONFIGURATION	9
4.0 TECHNICAL DISCUSSION	22
4.1 Structural Analysis	22
4.2 Performance Analysis	37
4.3 Fabrication Considerations	38
4.4 Alternative Applications	46
5.0 BLADE COST ESTIMATE	48
6.0 CONCLUSIONS AND RECOMMENDATIONS	52
7.0 APPENDICES	55
8.0 REFERENCES	90
9.0 DISTRIBUTION LIST	92

LIST OF FIGURES

<u>Figure No.</u>	<u>Description</u>	<u>Page</u>
3-1	Blade General Arrangement	10
3-2	Blade Basic Cross Section	11
3-3	Sketch, Prestressed Composite Spar Tube	13
3-4	Root End Structure	17
3-5	Tip Structure	21
4-1	Axial Stiffness VS Blade Station	23
4-2	Out-of-Plane Bending Stiffness VS Blade Station .	24
4-3	In-Plane Bending Stiffness VS Blade Station . . .	25
4-4	Distributed Weight VS Blade Station	26
4-5	Neutral Axis Chordwise Location VS Blade Station	27
4-6	Centroidal Axis Chordwise Location VS Blade Station	28
4-7	Torsional Stiffness VS Blade Station	29
4-8	Sketch of Root End Metal Liner Head Cross-Section	33
4-9	Sketch, Prestressed Composite Spar Tube Notation Description	35
4-10A	Blade Fabrication	39
4-10B	Blade Structure Build Up	40
4-11	Prestressed Composite Spar Tube Fabrication . . .	42
4-12	Spline Filament Winding Machine	45
7-1	CF Force Distribution - 540 Rotor	56
7-2	Limit Chordwise Moment - 540 Rotor	57
7-3	Limit Chordwise Moment - 540 Rotor	58
7-4	Limit Beamwise Moment - 540 Rotor	59
7-5	Fatigue Condition - In Plane Moment	60

LIST OF FIGURES

(Continued)

<u>Figure No.</u>	<u>Description</u>	<u>Page</u>
7-6	Fatigue Condition - Out of Plane Moment	61
7-7	Tube Cross-Sections	66
7-8	Fiber Strain Due to Bending	74
7-9	Fiber Forces and Widths	74
7-10	Fiber Strain Due to Torsion	77
7-11	Fiber Width	78
7-12	Differential Fiber Force	78
7-13	Sketch, Fiber and Metal Initial Stress	80
7-14	Idealized Stress-Strain Curve for Stainless Steel	84
7-15	Constrictive-Wrap Buckling Strengths for Cylindrical Tubes	86

LIST OF TABLES

<u>Table No.</u>	<u>Description</u>	<u>Page</u>
4-1	Margins of Safety for Station 1.156 to 1.27 . . .	30
4-2	Station 2.032 Ultimate Load Conditions	31
4-3	Results of Fatigue Condition Stress Analysis For Station 2.032	32
5-1	Life Cycle Cost Comparison	51
7-1	Material Property Summary	63
7-2	Blade Section Properties, Station 2.032	65
7-3	Blade Section Properties, Station 1.27	68
7-4	Station 1.27 Tubes Ultimate Margins of Safety . .	70
7-5	Section B-B Ultimate Margins of Safety	71
7-6	Section C-C Ultimate Margins of Safety	72

DESIGN STUDY OF THE PRESTRESSED
ROTOR SPAR CONCEPT

by

D. Gleich

SUMMARY

The prestressed composite rotor spar consists of a 304-L cryogenically stretchformed stainless steel liner overwrapped with isotenoid fibers. The spar is prestressed. The high strength metal liner is under initial compression and the fibers are pretensioned. The prestresses are selected to maintain compression in the liner and tension in the fibers under operating loads. This prestressing results in greatly improved crack propagation and fatigue resistance as well as enhanced fiber stiffness. Potential benefits of this prestressed composite construction include significantly increased safe operational spar life, improved ballistic impact resistance and attractive weight/stiffness trade-offs at low life cycle costs.

A prestressed composite spar rotor blade (AK-76) was designed for the Bell Helicopter 540 rotor system of the AH-1G helicopter. The mass and stiffness distribution of the 540 blade were closely matched, as required, to give a dynamically similar prestressed composite spar blade (AK-76). Geometric configuration, interfaces and actual loads of the 540 blade were used in the design of the prestressed composite spar rotor blade. Cost estimates were made. Advantages of the AK-76 and its application to other rotor systems were evaluated.

A multi-spar AK-76 blade configuration was designed for improved survivability and utilization of simple circular cylindrical shapes. The primary structural elements are:

- (1) A three (3) tube prestressed composite spar assembly consisting of high strength (cryogenically stretchformed) 304-L tubular liners (isotenoid) overwrapped with HTS graphite fibers. Tubes were connected by KEVLAR 49 fibers and foam fillers.

- (2) Fiber skins with outer ply of woven fiberglass cloth.
- (3) A nomex honeycomb afterbody.
- (4) Kevlar 49 Nose and trailing edge members.
- (5) Aluminum alloy root end connection.
- (6) Polyurethane elastomer boot over the leading edge for erosion protection.

The primary program objective has been met by the AK-76 prestressed composite spar rotor blade design. An advanced helicopter rotor blade structure has been defined which incorporates the ARDE, INC. prestressed composite spar and which is functionally equivalent to the current AH-1G helicopter Model 540 rotor blade. Advantages projected for the AK-76 prestressed composite spar rotor blade include:

- . Low life cycle cost; more than 40% savings compared to Model 540 blade projected.
- . Increased operational life and improved ballistic survivability due to spar prestressing restraining crack propagation, low stresses in blade structural members, redundant survivable load paths, ability of spar to survive ballistic over pressures and use of materials insensitive to defects and stress raisers.
- . Reliability, safety and economic benefits provided by prestressed composite spar are indicated for articulated, hingeless and rigid rotor systems.
- . Improved corrosion resistance of composite construction.
- . Most damage-vulnerable afterbody structure is readily field repaired.
- . Prestressed isotensoid spar tube fiber wrap develops full uniaxial fiber stiffness potential due to minimization of need for shear transfer to and from fibers through the resin. Permits advantageous weight/stiffness trade-offs to be made.

- . Simple, reliable and structurally efficient blade rotor attachment is facilitated by use of composite metal liner for root-end connection. Effective redundant root attachments are made possible by prestressed metal/fiber construction.
- . Non-destructive inspection for spar cracks by gas leakage detection techniques are enhanced by prestressed construction. Gas introduced inside the hollow composite spar tubes can be highly pressurized, thereby significantly increasing the effective sensitivity of the gas detection instrumentation.

Use of commercial products or names of manufacturers in this report does not constitute official endorsement of such products or manufacturers, either expressed or implied, by the National Aeronautics and Space Administration.

1.0 INTRODUCTION

1.1 Background

There is a need for improved operational life, "fail-safe" and structurally efficient helicopter blades. Considerable work^{(1), (2)} has been done on composite structures, which can be applied to meet this need. Stiffness can be tailored at good weight trade-offs compared to homogeneous material designs and redundant load carrying capability is inherent in this type of configuration. These composite structures generally consist of fiber-metal constructions in which the fibers, imbedded in a resin matrix, are attached to the metal primarily by adhesively bonded joints (shear-type connections). The operational life of this construction (measured by fatigue and crack propagation rate considerations) is a strong function of the effectiveness of these joints.

Another approach to composite metal-fiber construction, aimed at a further significant improvement of operational life and fail-safe helicopter blade structures, consists of a compressively prestressed metal liner overwrapped with pretensioned fibers. Prestressing is achieved by stretch-forming a metal liner overwrapped with fiber. Strength and toughness are achieved by accomplishing the stretchforming with 304L at cryogenic temperature. Prestressing provides bearing between the fiber and metal which in turn minimizes the need for adhesive bonds between the fibers and metal liner or between the fibers themselves. The fiber resin matrix primarily provides protection against fiber abrasion and moisture. By regulating the magnitude of the metal liner compressive prestress, so that the liner is always in compression under operational blade loads, liner crack propagation is retarded and significant improvements in liner fatigue life are obtained. Fiber pretensioning also provides substantial increases in fiber fatigue cycle life compared to zero pretensioned fibers at the same maximum service stress levels. Theoretical considerations as well as test data from prior programs indicate that these crack propagation and fatigue life advantages are attained at good stiffness weight trade-offs compared to homogeneous material and other types of composite material blades.^{(5), (6)} Finally, in addition to inherent redundant load carrying capability and relatively high structural damping capacity, the option exists to provide even more enhanced torsional, bending and extensional stiffness properties at little weight penalty by winding additional fibers at selected angles subsequent or prior to the metal prestressing operation.

Following ARDE's demonstration of design principles and fabrication techniques for prestressed metal-fiber pressure vessels under various NASA contracts^{(3); (4)}, contractual effort was started and successfully completed under NAS1-10028 to demonstrate the crack propagation characteristics of a prestressed composite. Subscale oval-shaped cross-section prestressed composite spar structural models about .91 meters long were designed and successfully fabricated. Special tooling required for prestressed composite spar fabrication was designed, built and proven. The prestressed state of these composite spars, determined and verified by means of structural theory coupled with spar inspection data, was in the desired design range. Suitable spar fiber wrap patterns, together with compatible spar metal liner head closure shapes needed to properly anchor the fibers, were determined and verified. Following under contract NAS1-11594, additional prestressed composite spar specimens were fabricated using the same .91 meters long design configuration. These spar specimens were then evaluated by means of crack propagation tests under axial and alternating bending stresses. Ballistic tests were also conducted. The test data demonstrated the superior crack propagation and fatigue life properties of the prestressed composite spar construction (compared to current metal spar configurations). Test results equivalent to about 1500 continuous hours of flight in the damaged condition at much higher operating stresses than current spars, were obtained. Propagation of artificially introduced fatigue cracks did not occur until alternating bending stress levels of $\pm 207 \times 10^6 \frac{\text{N}}{\text{m}^2}$ were applied (compared to $\pm 69 \times 10^6 \frac{\text{N}}{\text{m}^2}$ for current metal spars). Structural design theory was confirmed by agreement between measured and predicted strains. The design technology for the composite prestressed spar construction was thus confirmed by these experimental results. Damage from three (3) 7.62mm projectile hits on an unloaded but prestressed composite spar specimen consisted solely of three (3) small holes due to the projectile penetrations. No fragmentation or crack propagation occurred, implying high ballistic resistance. Rotor design approaches were identified by spar specimen constructions that evolved and were proven during testing. Further improved

structural performance prestressed composite spar configurations utilizing higher stiffness and lower density fibers (KEVLAR 49 and graphite) were defined.

Based on the successful results described above, the next step of demonstrating the prestressed composite advantages for application to a rotor system was undertaken under NAS1-13816 as reported herein. Comparison was made to the model 540 rotor system of the Bell AH-1G Helicopter.

1.2 Program Objective and Description

The primary program objective was to evaluate the potential benefits of the prestressed rotor spar concept in a realistic application and to project applicability to other rotor systems. The prestressed composite spar rotor blade design study, using the Bell 540 system as the prescribed model, consisted of a six (6) task effort:

- . Blade structural design
- . Blade performance evaluation
- . Manufacturing process study
- . Cost estimation
- . Alternative applications (other rotor systems and advanced design blade)
- . Program management and documentation

ARDE, INC. was responsible for overall program management, technical direction and documentation as well as detailed technical effort related to the prestressed composite spar. Kaman's work concerned the design, analysis, fabrication definition and cost estimation of the overall AK-76 blade configuration which utilized the prestressed composite spar.

The design specification (constraints) desired that the new AK-76 prestressed composite rotor blade be dynamically similar to the existing Model 540 rotor system. Because of the limited scope of the study, it was agreed to approach this similarity by matching the stiffness, mass distribution, geometric configuration and support interfaces. These various factors and results are described in detail in Sections 4 and 5 herein.

2.0 SYMBOLS

Symbols used in the text are listed and defined in this section.

A	=	Cross Sectional Area, m^2
A_t	=	Tube Area, m^2
b	=	Fiber Width, m
c	=	Critical Buckling Coefficient, dimensionless
C_x	=	Extreme Fiber Distance From x Centroidal Axis, m
C_y	=	Extreme Fiber Distance From y Centroidal Axis, m
CF	=	Centrifugal Force, N
D	=	Diameter, m
D_f	=	Fiber Diameter, m
D_{fj}	=	Diameter of j^{th} Fiber, m
D_m	=	Metal Diameter, m
dA_f	=	Differential Fiber Area, m^2
dA_m	=	Differential Metal Area, m^2
dF_f	=	Differential Fiber Force, N
dT_f	=	Differential Fiber Torque, $m-N$
dM	=	Differential Moment, $m-N$
dM_f	=	Differential Fiber Moment, $m-N$
dM_m	=	Differential Metal Moment, $m-N$
E	=	Young's Modulus, N/m^2
E_f	=	Fiber Young's Modulus, N/m^2
E_{fj}	=	Young's Modules of j^{th} Fiber, N/m^2
E_j	=	Young's Modules of j^{th} Component of Element, N/m^2
E_m	=	Metal Young's Modulus, N/m^2

E_p = Plastic Young's Modulus, N/m^2
 F = Allowable Stress of Force, N/m^2 or N
 F_a = Allowable Vibratory (alternating) Stress, N/m^2
 F_{bru} = Allowable Bearing Ultimate Stress, N/m^2
 F_e = Endurance Limit for Completely Reversed Bending
 $(R = -1)$ N/m^2
 F_{su} = Allowable Shear Ultimate Stress, N/m^2
 F_{tu} = Ultimate Tensile Strength, N/m^2
 F_u = Allowable Ultimate Stress, N/m^2
 F_x = Force Component Parallel to x Axis, N
 F_y = Force Component Parallel to y Axis, N
 f = Stress, N/m^2
 f_f = Fatigue Stress, N/m^2
 f_i = Initial Stress, N/m^2
 f_s = Steady Component of Fatigue Stress, N/m^2
 f_u = Ultimate Stress, N/m^2
 f_v = Vibratory Component of Fatigue Stress, N/m^2
 G = Shear Modulus, N/m^2
 G_m = Metal Shear Modulus, N/m^2
 I_f = Fiber Moment of Inertia, m^4
 I_m = Metal Moment of Inertia, m^4
 I_{oyy} = Moment of Inertia of an Element abouts its centroidal
y-y Axis, m^4
 I_{xx} = Moment of Inertia about x-x Axis, m^4
 I_{yy} = Moment of Inertia about y-y Axis, m^4
 J_m = Metal Polar Moment of Inertia, m^4
 K_{bc} = Composite Bending Stiffness, Nm^2
 K_{bf} = Fiber Bending Stiffness, Nm^2

K_{bm} = Metal Bending Stiffness, Nm^2
 K_{tc} = Composite Torsional Stiffness, Nm^2
 K_{tm} = Metal Torsional Stiffness, Nm^2
 L = Length, m
 M = Moment, m-N
 M_c = Composite Moment, m-N
 MS = Margin of Safety, dimensionless
 MS_f = Fatigue Margin of Safety, dimensionless
 MS_u = Ultimate Margin of Safety, dimensionless
 M_x = Moment about x Axis (out-of-plane moment), m-N
 M_y = Moment about y Axis (in-plane moment), m-N
 M_{xs} = Steady Component of Moment about x-Axis, m-N
 M_{xv} = Vibratory Component of Moment about x-Axis, m-N
 M_{ys} = Steady Component of Moment about y-Axis, m-N
 P_f = Equivalent Tube Fatigue Load, N
 P_u = Equivalent Tube Ultimate Load, N
 R = Minimum to Maximum Stress Ratio, dimensionless
 R_f = Fiber Radius, m
 R_b = Applied to Allowable Bending Stress Ratio, dimensionless
 R_c = Applied to Allowable Compressive Stress Ratio, dimensionless
 r = Radius, m
 S_o = Fiber Length Before Straining, m
 T = Torque, m-N
 T_f = Fiber Torque, m-N
 T_m = Metal Torque, m-N
 t = Thickness, m

t_f	=	Fiber Thickness, m
t_{fj}	=	Thickness of j^{th} Fiber ($j = 1, 2, \dots$), m
t_m	=	Metal Thickness, m
w	=	Weight per Unit Length, N/m
X	=	Chordwise Coordinate or Tube Longitudinal Direction, m
\bar{X}_{na}	=	Chordwise Centroidal Coordinate, m
X_o	=	Fiber Axial Length Before Straining, m
Y_o	=	Fiber Hoop Length Before Straining, m
Z	=	Distance of Tube Element From Neutral Axis, m
α	=	Fiber Helix Wrap Angle, rad
$d\alpha$	=	Differential Fiber Helix Angle, rad
α_j	=	Helix Wrap Angle of j^{th} Fiber, rad
ΔS	=	Increment of Fiber Length, m
ΔX	=	Increment of Axial Fiber Length, m
ΔY	=	Increment of Hoop Fiber Length, m
ϵ_f	=	Fiber Strain, m/m
ϵ_x	=	Metal Longitudinal Strain, m/m
ϵ_θ	=	Metal Hoop Strain, m/m
K	=	Bending Curvature, m^{-1}
θ	=	Angle of Twist Per Unit Length, rad/m
ρ	=	Density, kg/m^3
σ	=	Stress, N/m^2
σ_{cr}	=	Critical Buckling Stress, N/m^2
σ_f	=	Fiber Stress, N/m^2
σ_{fb}	=	Fiber Stress Due to Bending, N/m^2

- σ_{fji} = Initial Stress (Prestress) in j^{th} Fiber, N/m^2
 σ_{fx} = Axial Component of Fiber Stress, N/m^2
 $\sigma_{f\theta}$ = Hoop Component of Fiber Stress, N/m^2
 σ_m = Metal Stress, N/m^2
 σ_{mb} = Metal Bending Stress, N/m^2
 σ_{mx} = Metal Axial Stress, N/m^2
 $\sigma_{m\theta}$ = Metal Hoop Stress, N/m^2
 σ_{mxi} = Metal Initial Axial Stress, N/m^2
 $\sigma_{m\theta i}$ = Metal Initial Hoop Stress, N/m^2
 Σ = Summation, takes dimension of items summed

3.0 BLADE CONFIGURATION DESCRIPTION

3.1 General

Preliminary design studies were performed to evaluate the ARDE, INC. "prestressed spar" as a helicopter rotor blade spar. The design goal for this phase was to design a blade structure which matched the physical characteristics of the AH-1G Model 540 Blade.

The general structural arrangement of the candidate design, AK-76, defined by the studies is shown in Figure 3-1. The AK-76 blade has the same external dimensions - airfoil section, chord, planform, and hub attachment interfaces - as the Model 540 blade. Mass and stiffness distributions of both blades match closely.

The blade basic cross section is shown in Figure 3-2. The principal structural elements are: three prestressed spar tubes, aramid (KEVLAR 49) fiber skins, a noncorrosive polyamide (Nomex) honeycomb afterbody, and rugged (Kevlar 49) nose and trailing edge members. A polyurethane elastomer boot over the leading edge protects the nose from erosion. Redundant load transfer doublers and fittings interfacing with the AH-1G standard hub and drag brace attachments are integrated into the root end structure.

The following sections describe the blade structure and design features in more detail.

3.2 Structural Description

3.2.1 Spar Structure

Primary elements are the three prestressed spar tubes, shear transfer layups, a filament wrap over the tubes, a preformed nose block, and a spar filament overwrap. Cavities between the tubes are foam-filled.

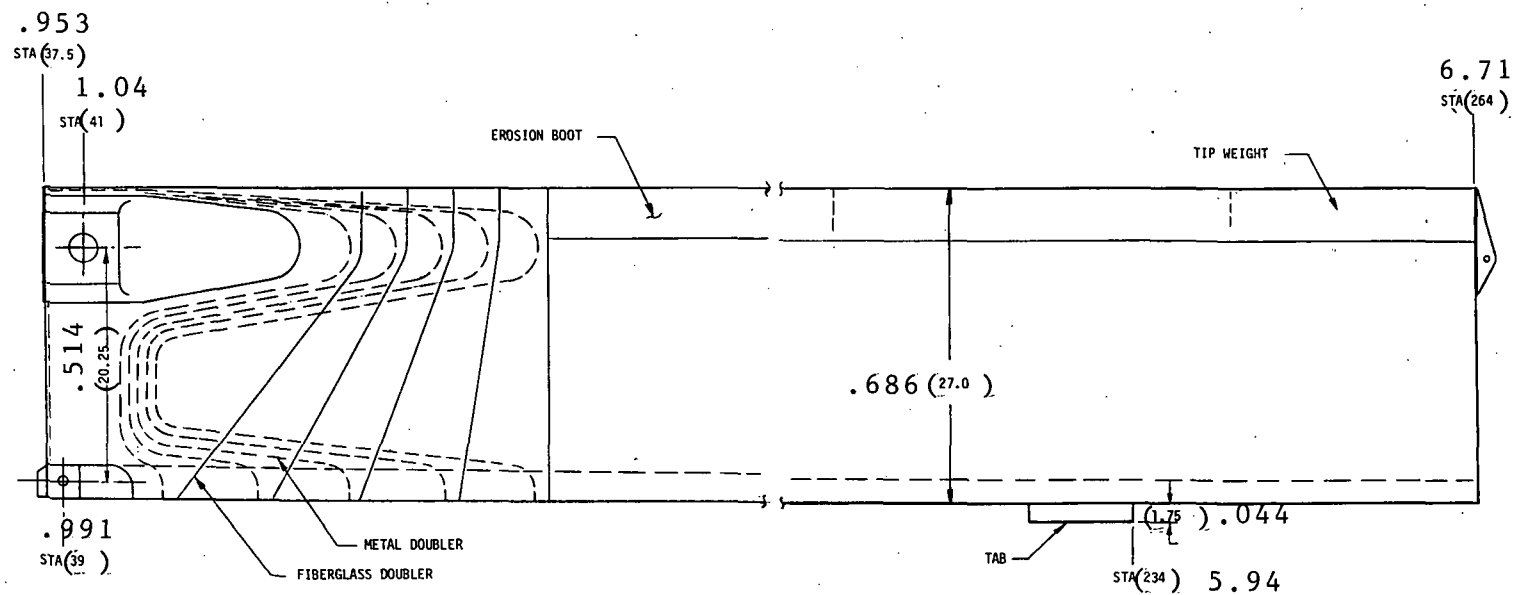


Figure 3-1 Blade General Arrangement

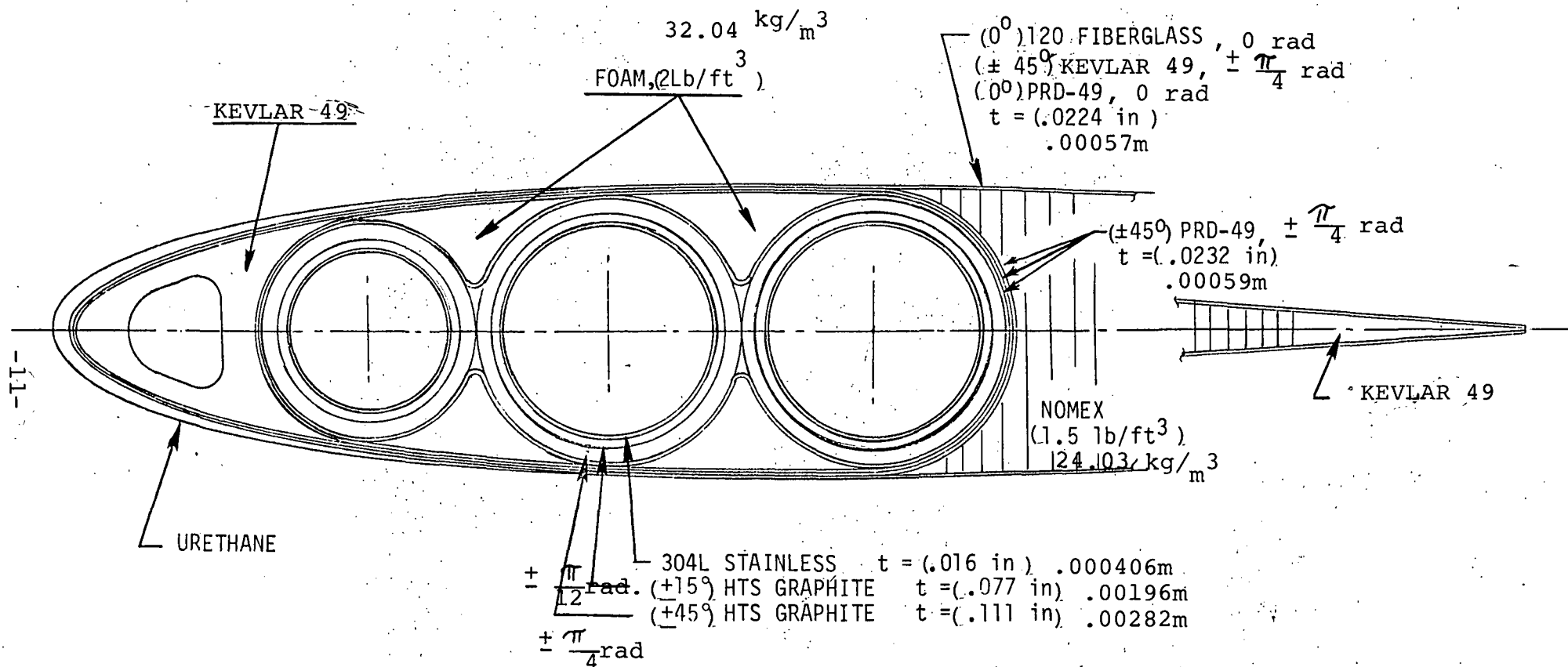


Figure 3-2 Blade Basic Cross Section

3.2.1.1 Prestressed Spar Tube

These composite structures consist of an inner 304-L stainless steel liner, .000406m thickness, overwrapped with HTS graphite fibers in a geodesic* fiber wrap pattern as sketched on Figure 3-3. The 304-L liner has a tubular (circular cylindrical) body section with heads welded to the tube ends for load transfer and fiber support. The inboard head is a "rod end" type to facilitate spar tube attachment to the aluminum root attachment fitting. The outboard head, simpler in shape, is provided with a threaded hole for spar tube processing and pressurization during fabrication, tip weight attachment and non-destructive crack inspection by tracer gas leak monitoring techniques. The heads are shaped and the fibers wrapped in such a manner to permit the fibers to be anchored on the heads without "slipping", compatible with the geodesic fiber wrap. No fibers appear on the two (2) flat surfaces of the inboard rod end head region in the vicinity of the pin holes (see Figure 3-3). Feasibility of this type of fiber wrap has been verified experimentally by a projected fiber wrap vendor (Hercules, ABL). Two (2) HTS graphite fiber orientations are used. The inner windings, .00196m fiber plus resin thickness at $\pm \frac{\pi}{12}$ rad. orientation, provide primarily bending stiffness. The outer windings, .00282m fiber plus resin thickness at $\pm \frac{\pi}{4}$ rad. orientation, provide torsional and bending stiffness. The graphite fibers, sandwiched between metal and overwrapped KEVLAR 49 and glass fibers, are well protected against impact and abrasive type damage. The middle and aft tubes are identical in size and design. The forward tube is similar in design but smaller in diameter (see Figure 3-2).

The fiber overwrapped spar tube is prestressed during its fabrication process as detailed in Section 4.3. The whole 304-L liner (including the heads and welds) is precompressed and the fibers are pretensioned. The prestress magnitudes are selected to keep the metal liner in compression and the fibers in tension under the operating conditions of centrifugal, bending, and

* A geodesic is a curve of minimum length between two points on the surface. The geodesic curve contains the principal normals to the surface. Thus normal forces alone can hold the constant tension fiber in equilibrium by bearing on the surface, like a cable on a frictionless pulley.

$\pm \frac{\pi}{4}$ rad

($\pm 45^\circ$) HTS Graphite Torsion
& Bending Fibers

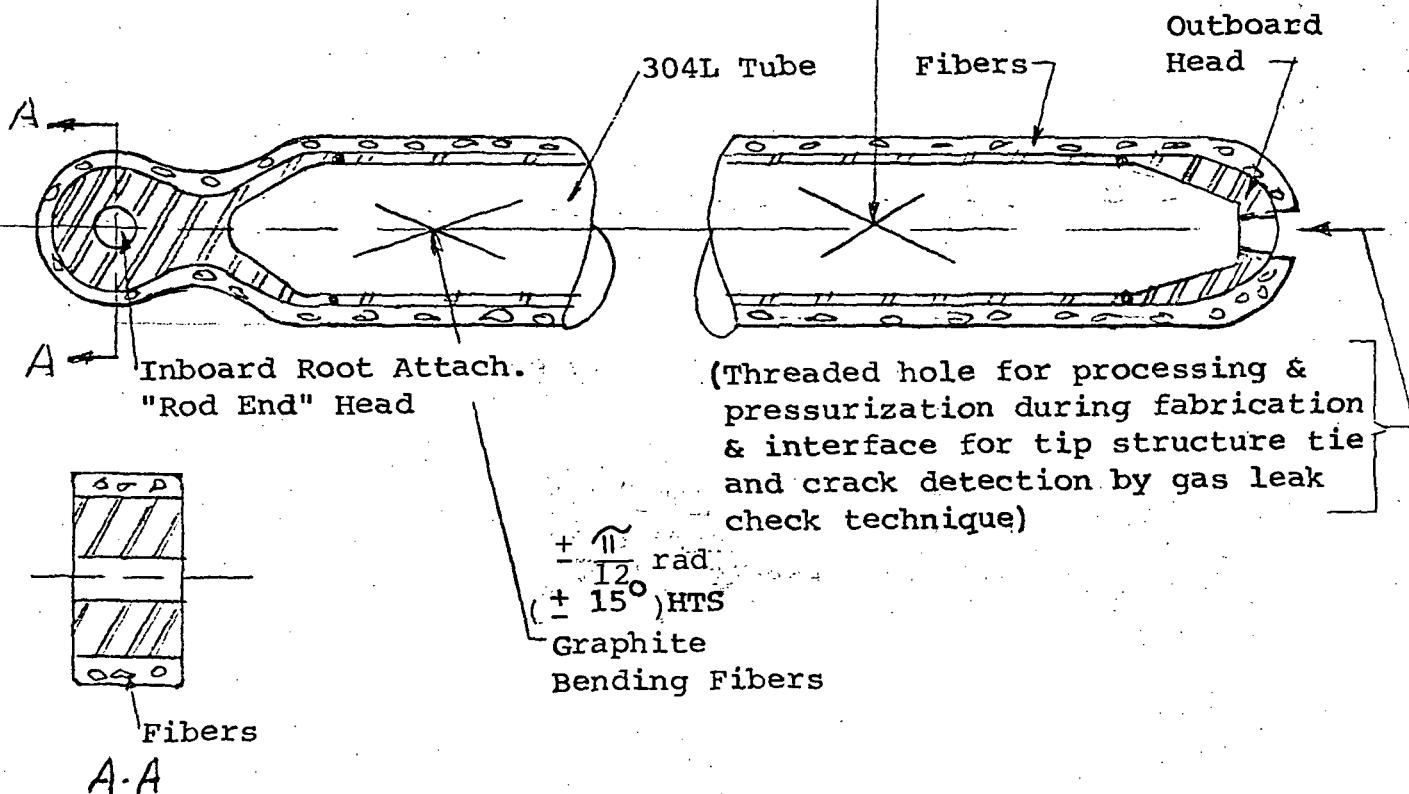


Figure 3-3 Sketch, Prestressed Composite Spar Tube

torsional loads as discussed in Section 4.1. The prestressed state provides crack growth resistance, enhanced fatigue properties and allows higher strain levels in the metal liner. The net fiber tension prevents the fibers from losing effectiveness under compression and the geodesic fiber wrap minimizes the need for shear transfer to and from the resin. Both of these factors result in achievement of the full fiber and full cross-section stiffness potential.

3.2.1.2 Shear Transfer Layup

Transfer of torsional and normal load shears from tube to tube is assisted by a layup of KEVLAR 49 fibers at $\pm \frac{\pi}{4}$ rad. orientation joining the peripheries of the tubes.

3.2.1.3 Tubes Filament Wrap

Premolded foam fillers are placed into the cavities between the shear transfer layup and filament wrap before the winding operation (See Figure 3-2). The selected foam will have sufficient shear and crush strength to transfer the estimated shear stresses and back up the filament wrap. The tubes are unitized into a structural system by a $\pm \frac{\pi}{4}$ rad. KEVLAR 49 filament wrap over the entire span of the tubes and foam. The windings extend over the root end and tip fittings.

3.2.1.4 Nose Block

The nose block is a preformed unidirectional KEVLAR 49 fiber structure designed to back up the leading edge skin and absorb forces from impact of the leading edge with obstacles such as small branches and small-arms bullets.

3.2.1.5 Spar Filament Overwrap

A $\pm \frac{\pi}{4}$ rad. KEVLAR 49 filament wrap forms the outer surface of the spar structural system, binding the tube structure and nose block together as an integral structure.

3.2.2 Afterbody

The afterbody is a non-corrosive Nomex honeycomb core sandwiched between the afterbody skins and bonded to the spar, skins, and trailing edge spline. The core with .00635m cells is structurally adequate, lightweight and easily field repairable.

3.2.3 Skins

Skins are four-ply layups of fiberglass and KEVLAR 49 fibers. A spanwise unidirectional KEVLAR 49 fiber ply is sandwiched between plies with $\pm \frac{\pi}{4}$ rad. orientation of KEVLAR 49 fibers. An outer ply of #120 woven fiberglass cloth increases tear resistance to external damage.

3.2.4 Trailing Edge Spline

The trailing edge spine is a KEVLAR 49 member with spanwise unidirectional orientation of fibers. The spline can be filament wound using fabrication techniques developed by Kaman for the AH-1Q improved blade.

3.2.5 Erosion Boot

The erosion boot is a vulcanized component made from Goodrich "Estane" thermoplastic polyurethane elastomer. Urethanes exhibit excellent resistance to sand erosion - superior to most metals. Among urethanes, "Estane" was superior in resistance to rain erosion in tests for the AH-1Q improved blade development. Promising techniques are being developed for field repair of erosion damage.

3.2.6 Root End Attachment

The root end attachment structural system is shown in Figure 3-4. The main structural element is a forged 7075-T73 aluminum alloy fitting which joins the rod end attachments of the spar tubes and blade retention bolt. The fitting is contoured to nest inside the skin structure and is thus protected from handling and environmental nicks and scratches. A simple, structurally effective, redundant load path, high cycle life and high ballistic resistance root end connection is provided.

Blade retention loads are transmitted via the primary load path through the spar tube metal "rod end" heads directly to the aluminum fitting and rotor by steel pin shear reactions. This direct load transfer minimizes shear loads in the fiber/resin spar tube wrap. Loads are transmitted to the fiber wrap primarily by bearing.

A redundant (secondary) load path is also provided. Fiberglass and aluminum doublers, starting at station 2.032 and building up to a maximum thickness at the blade retention bolt, are used to transmit blade loads to the rotor by shear transfer. The doublers are also designed to transmit the blade flatwise bending loads to the rotor hub, relieving tube bending near the root end.

Steel bushings are used to protect the softer aluminum root connection fitting pin hole surfaces from bearing stress and wear effects. All steel/aluminum interfaces are coated with Loctite to prevent moisture-induced dissimilar metal "battery action" type of corrosion. The aluminum fitting will be coated with a zinc chromate primer.

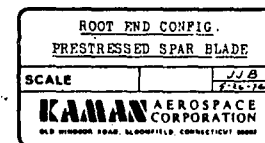
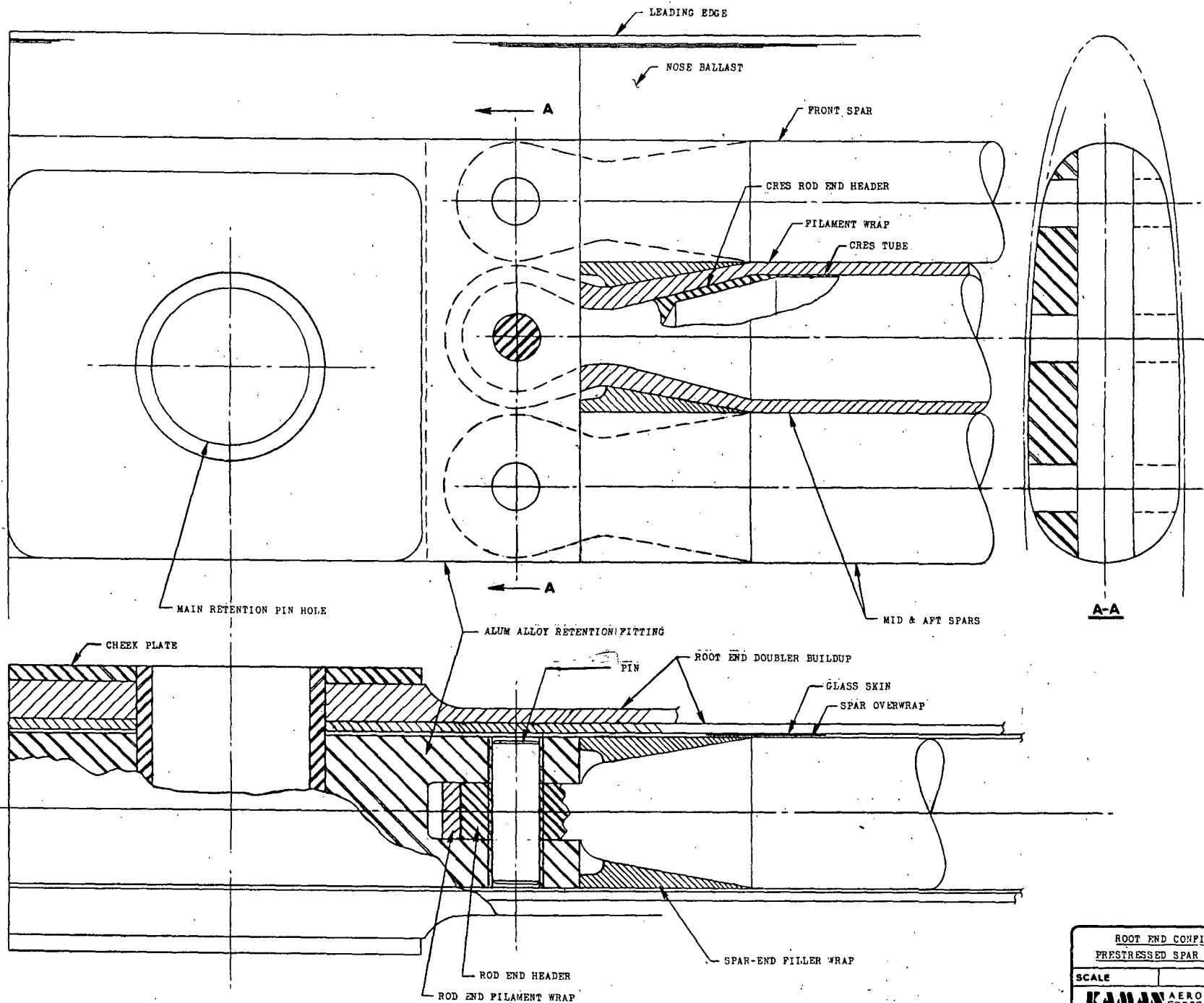


Figure 3-4 - Root End Configuration Prestressed Spar Blade

- Note: (1) Metal to metal hub attachment.
 (2) Spar can act like a pressure vessel for:
 (a) Retarding overpressure due to ballistic effect.
 (b) Ready inspection by high pressure helium leak test.

3.3 Repairability and Maintainability

Compared to the baseline Model 540 blade, the advanced concept AK-76 blade is considered to be superior in inherent reliability, damage tolerance, and repairability. The aft structure, in particular, lends itself to easy field repair by personnel of a skill level found at the direct support maintenance level. The repair techniques and field tools have been developed, demonstrated and qualified. The following discussion describes the repairability and maintainability features of the blade.

3.3.1 Spar

- Corrosion resistant materials virtually eliminate corrosion damage.
- Skin and overwraps protect spar tubes from incipient nicks, scratches, and environmental damage.
- Prestressing inhibits crack growth and confines damage to immediate area of defect (or ballistic hit).
- Spar tubes, which are essentially pressure vessel structures, can withstand very high internal "blast pressures".
- The prestressed composite spar construction lends itself to reuse for rebuilt blades, since basic spar subassembly is readily stripped from skin with low damage probability.
- Spar tube lends itself to simple non-destructive inspection techniques. High pressure helium can be used to provide a unique high level of detection sensitivity.

3.3.2 Skin

- Superficial nicks and scratches can be ignored due to low notch sensitivity of composites.
- Damage through skin, but not into core, may be repaired with a patch without extensive rework of the damaged skin.
- Distance between edges of adjacent patches can be less than on the B540 metal skinned blade.
- Skin delamination from spar due to ballistic damage of core localized due to overwrap on spar. Joint at aft end of spar eliminated.

- Preparation of fiberglass surfaces for bonding is less critical than of aluminum surfaces.
- Nonmetallic skins and underlying structure will not act as heat sinks when heat is applied during cure cycle.
- Structural strength and fatigue life of skin patches will be at least as great as that of basic blade.¹² Special recurring inspections of repair areas will not be required.

3.3.3 Core

- Core damage up to .0254 meters in diameter does not require installation of core plug. Damage is simply bridged with a skin patch.
- Nomex core material is easily machined using carbide router bit in standard electric router. Cylindrical cavities are thereby created to accept prefabricated plug/patches.
- Low notch sensitivity of the plastic fiber skin allows core routing operation to be performed by relatively unskilled person. Localized excursions up to .00152 meters of router are tolerable.
- Through-holes up to .178 meters in diameter may be repaired by installing 2 plug/patches (one in each side of blade).
- Structural strength and fatigue life of plug/patch repairs will be at least as great as that of basic blade. Special recurring inspections of repair areas will not be required.

3.3.4 Spline

- The skins covering the spline protect spline and become sacrificial material when blending of nicks, scratches, etc., is required.
- Kevlar 49 is corrosion resistant, eliminating corrosion concerns.
- Loss by damage of up to approximately 50% of the spline can be repaired by installation of a "vee" shaped Kevlar doubler.
- Structural strength and fatigue life of "vee" doubler will be at least as great as that of basic blade.¹² Special recurring inspections of repair areas will not be required.

3.3.5 Leading Edge Boot

- Resiliency of boot material will protect underlying structure from small projectiles.
- Small nicks or dents in boot material can be repaired easily with the field application of a patch.

3.3.6 Root Fitting

- The root fitting, a forged 7075-T73 aluminum fitting, has high toughness and is very resistant to stress-corrosion cracking. (13) The fitting is protected from nicks and scratches by the skins and doublers.

3.3.7 Tip Structural Tie

- This aluminum fitting joins the outboard ends of the spar assemblies and provides an anchor for the tip cap. The fitting is protected from damage by the overwraps and skins. Figure 3-5 shows the tip structure. Note the NDI pressure valve to facilitate crack detection by helium leak check technique.

4.0 Technical Discussion

4.1 Structural Analysis

4.1.1 Blade Assembly Structural Analysis

4.1.1.1 General

A preliminary stress analysis was performed on the prestressed spar rotor blade to assess the structural capabilities and feasibilities of the design. The detailed analysis is presented in Appendix 1, Section 7. Two loading conditions were considered in these analysis, the ultimate condition and the fatigue condition. Since the section properties of the prestressed spar rotor blade approximate those of the current AH-1G main rotor blade, loads previously developed for the AH-1G main rotor blades were used to evaluate the prestressed spar rotor blade. Ultimate loads were taken as 1.5 times limit loads. Fatigue loads were calculated from data given in⁽⁷⁾. Critical sections of the prestressed rotor spar analyzed were:

- a) Station 2.03 (80) at the outboard tips of the doublers
- b) Zone between station 1.27 (50) in the vicinity of the tube attachment to the 7075-T73 aluminum fitting.
- c) Station 1.04 (41) at the main bolt attachment area

4.1.1.2 Summary of Blade Assembly Structural Analysis Results

4.1.1.2.1 Blade Section Properties

The design of the basic portion of the prestressed spar rotor blade was tailored to match the section properties of the AH-1G main rotor as closely as possible to insure a dynamically similar blade. Figures 4-1 to 4-7 compare the section properties of the AK-76 prestressed spar rotor blade to those for the AH-1G main rotor blade. Agreement between basic blade section properties is acceptable for this predesign study.

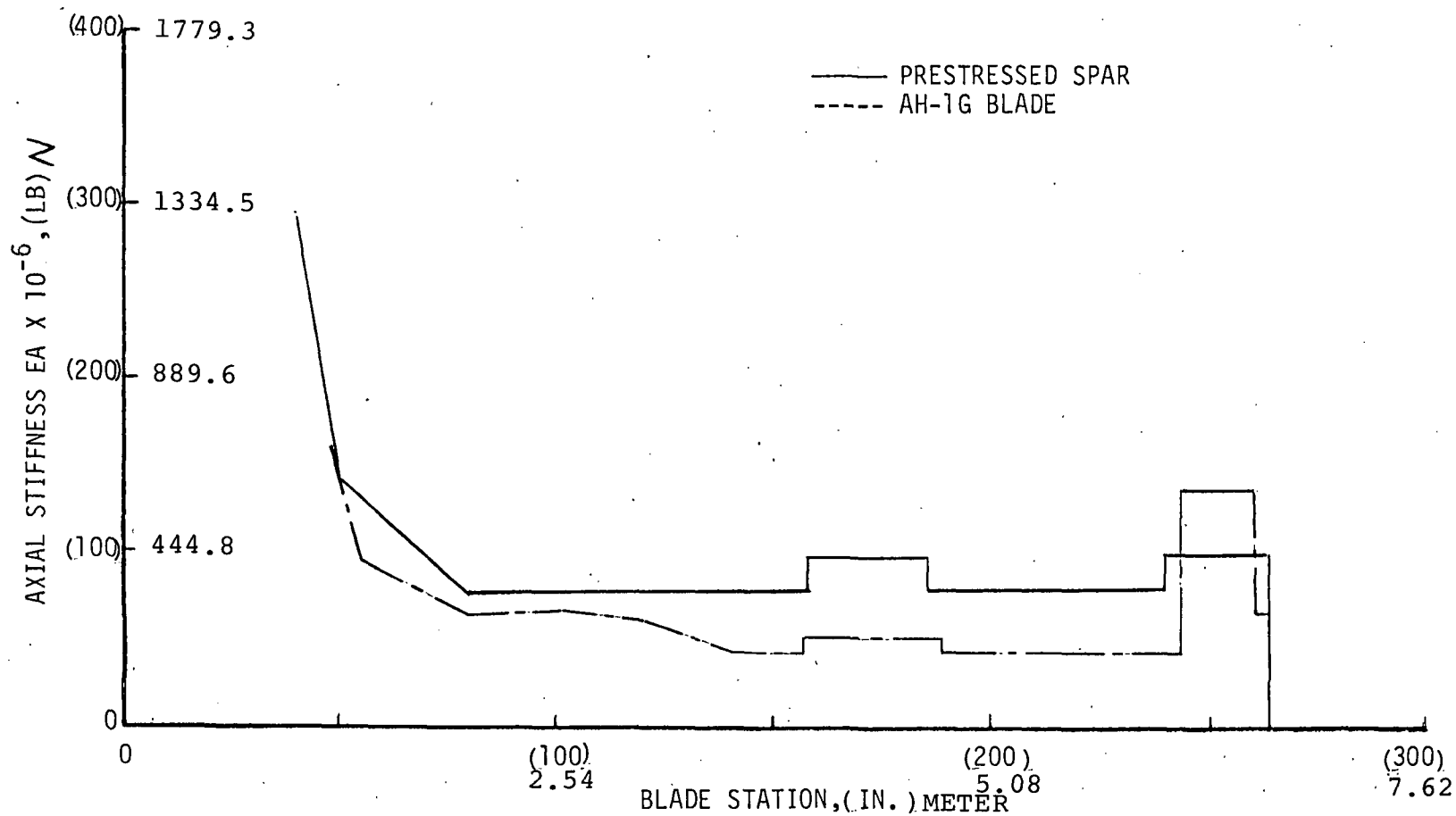


Figure 4-1. Axial Stiffness vs Blade Station

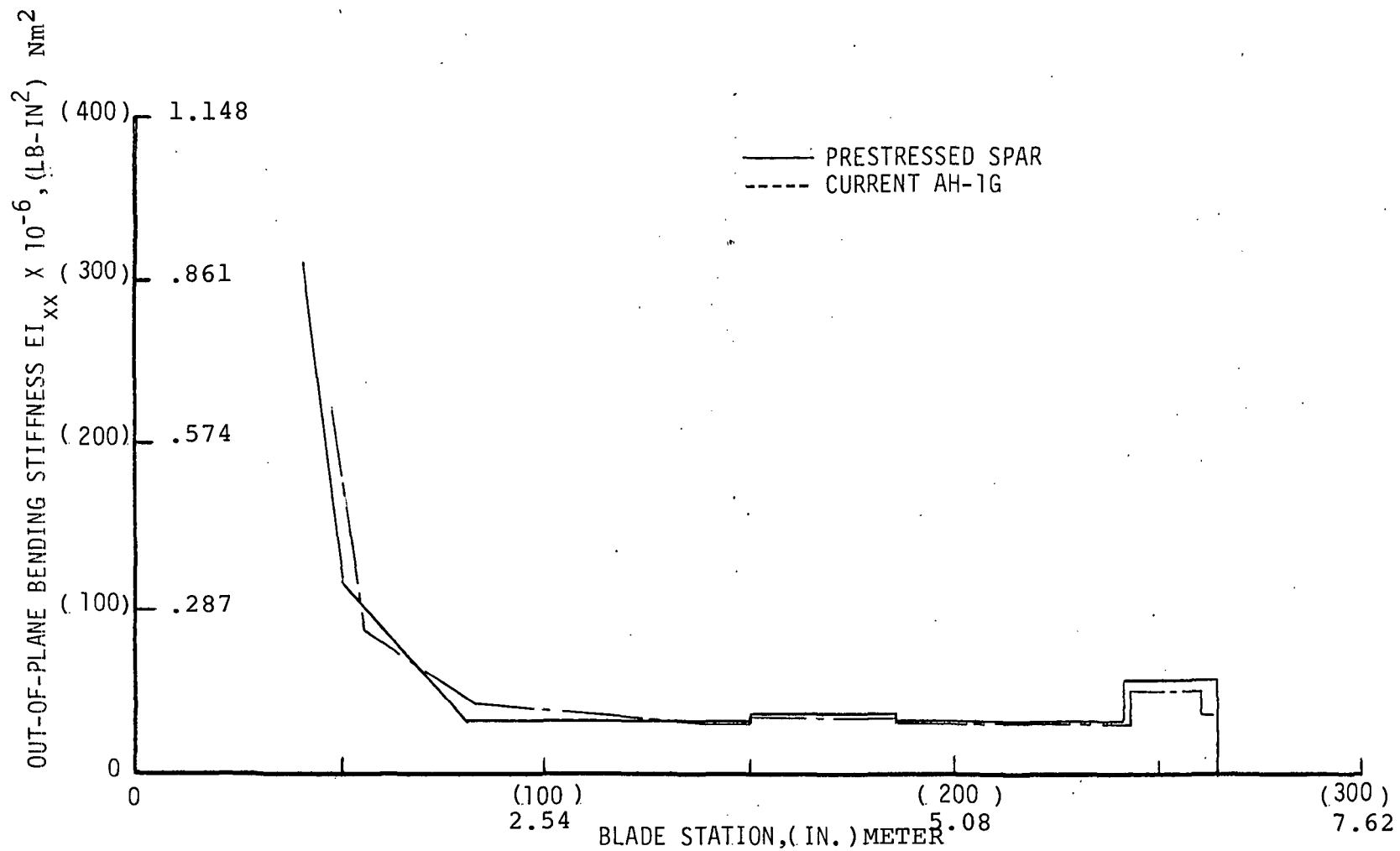


Figure 4 -2. Out-of-Plane Bending Stiffness vs Blade Station

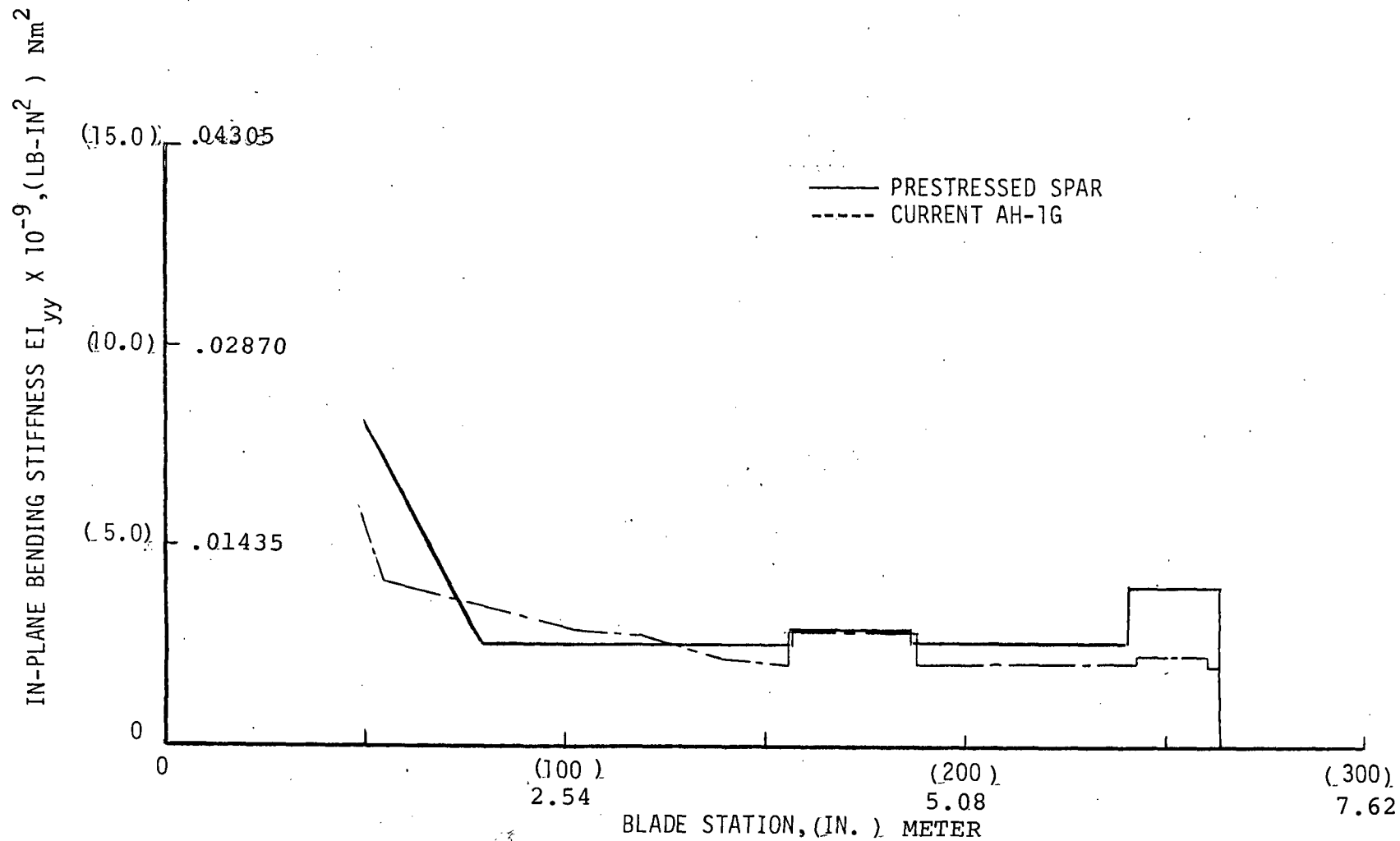


Figure 4-3. In-Plane Bending Stiffness vs Blade Station

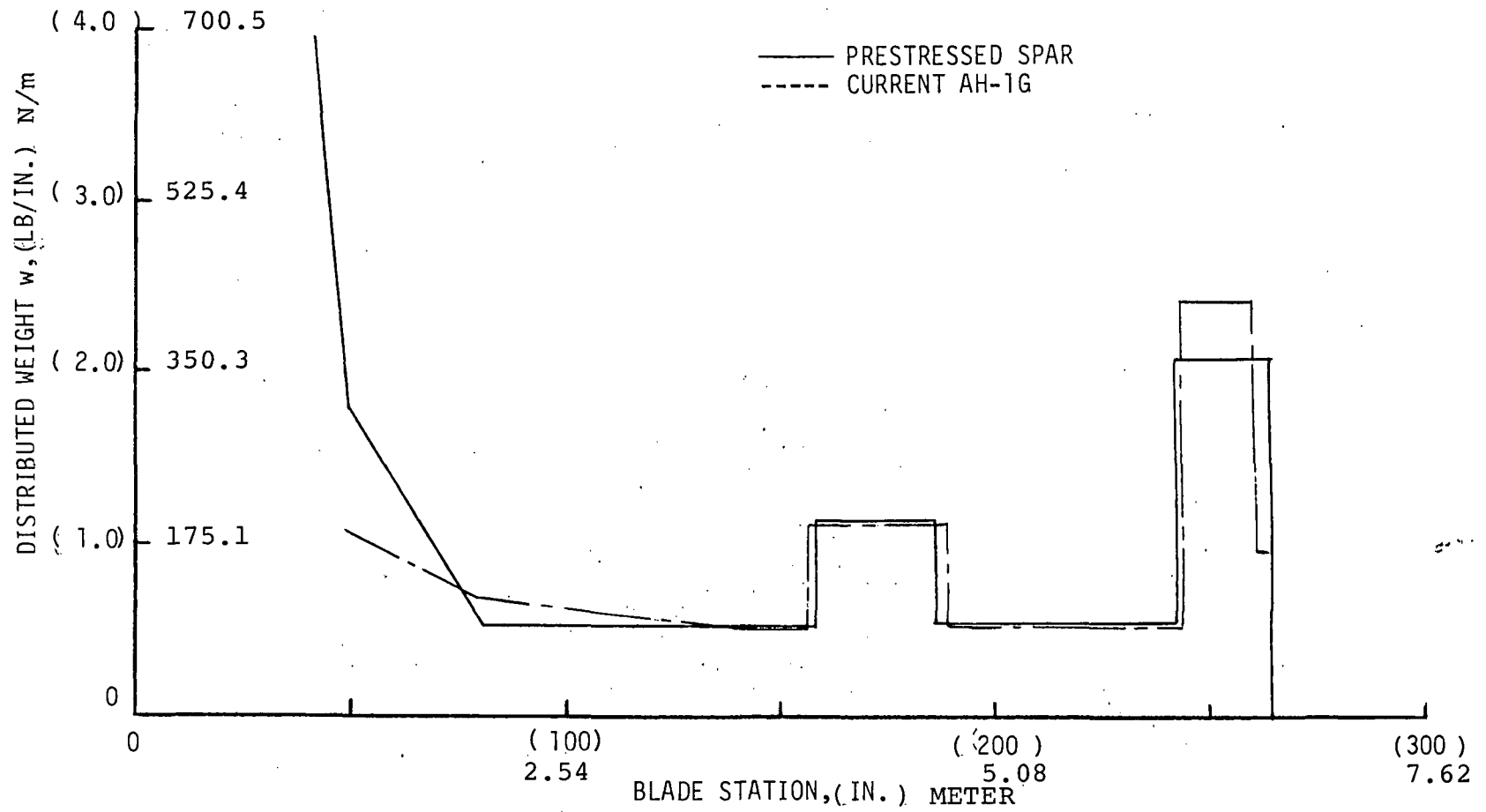


Figure 4 -4. Distributed Weight vs Blade Station

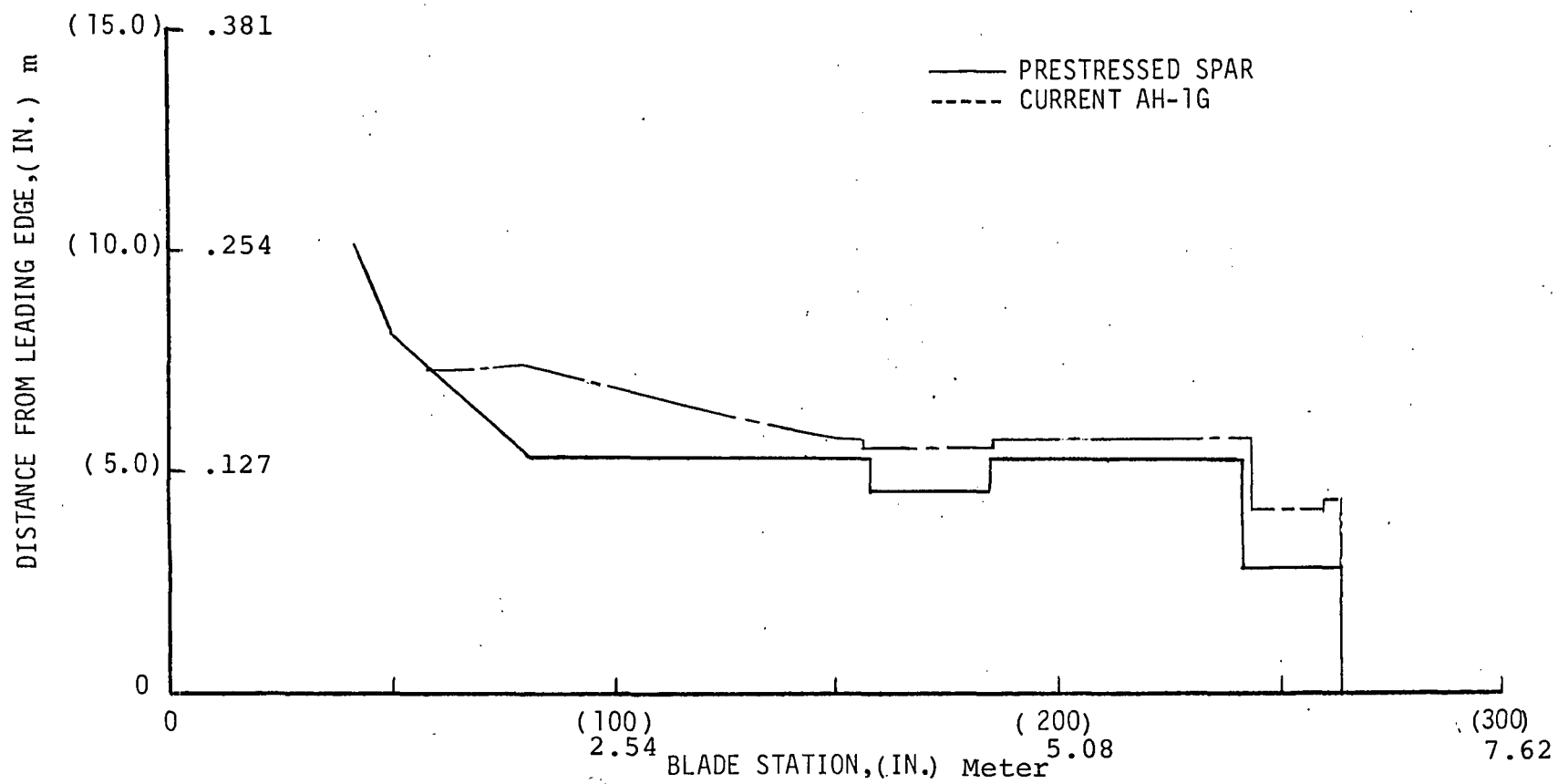


Figure 4-5. Neutral Axis Chordwise Location vs Blade Station

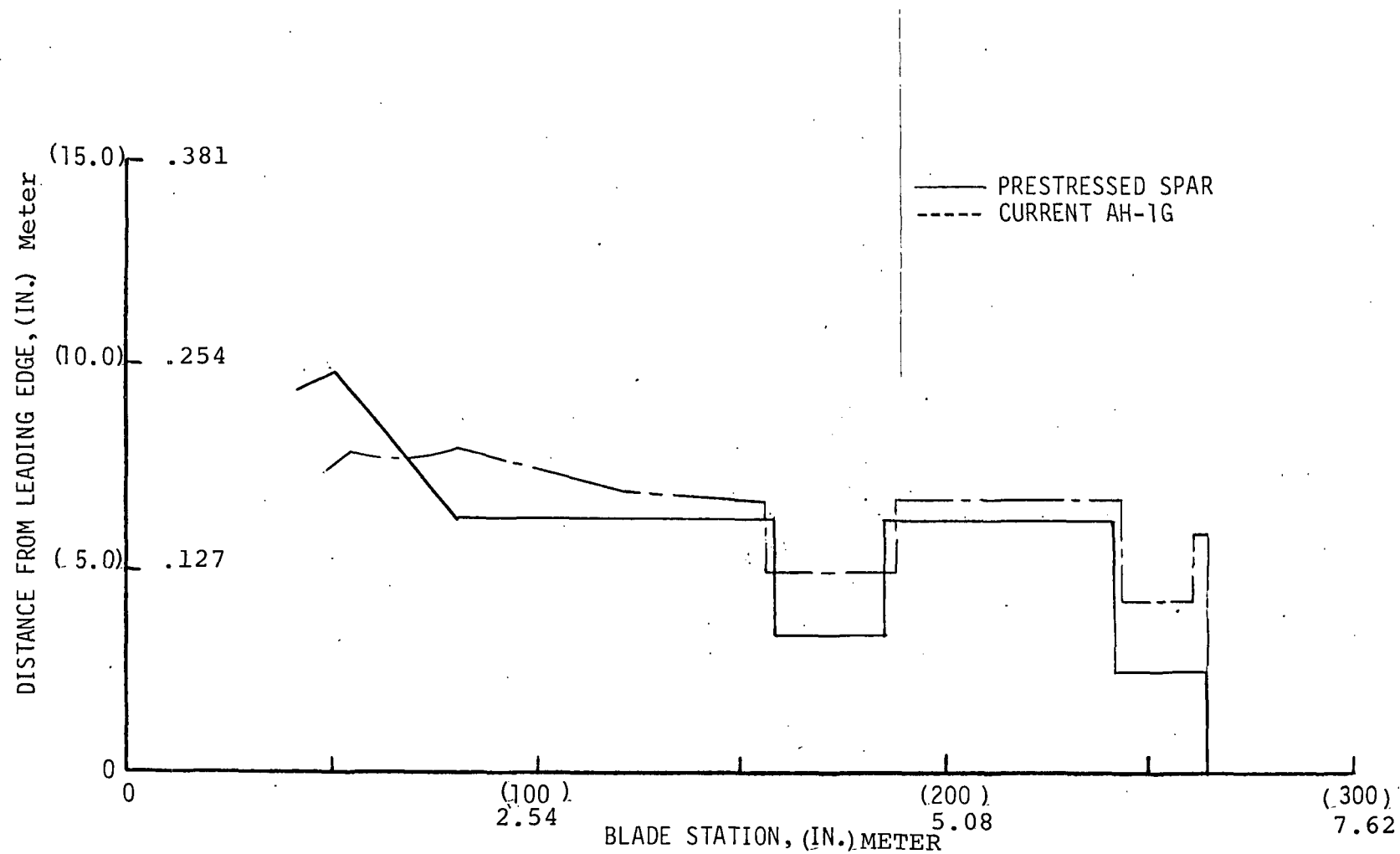


Figure 4-6. Centroidal Axis Chordwise Location vs Blade Station

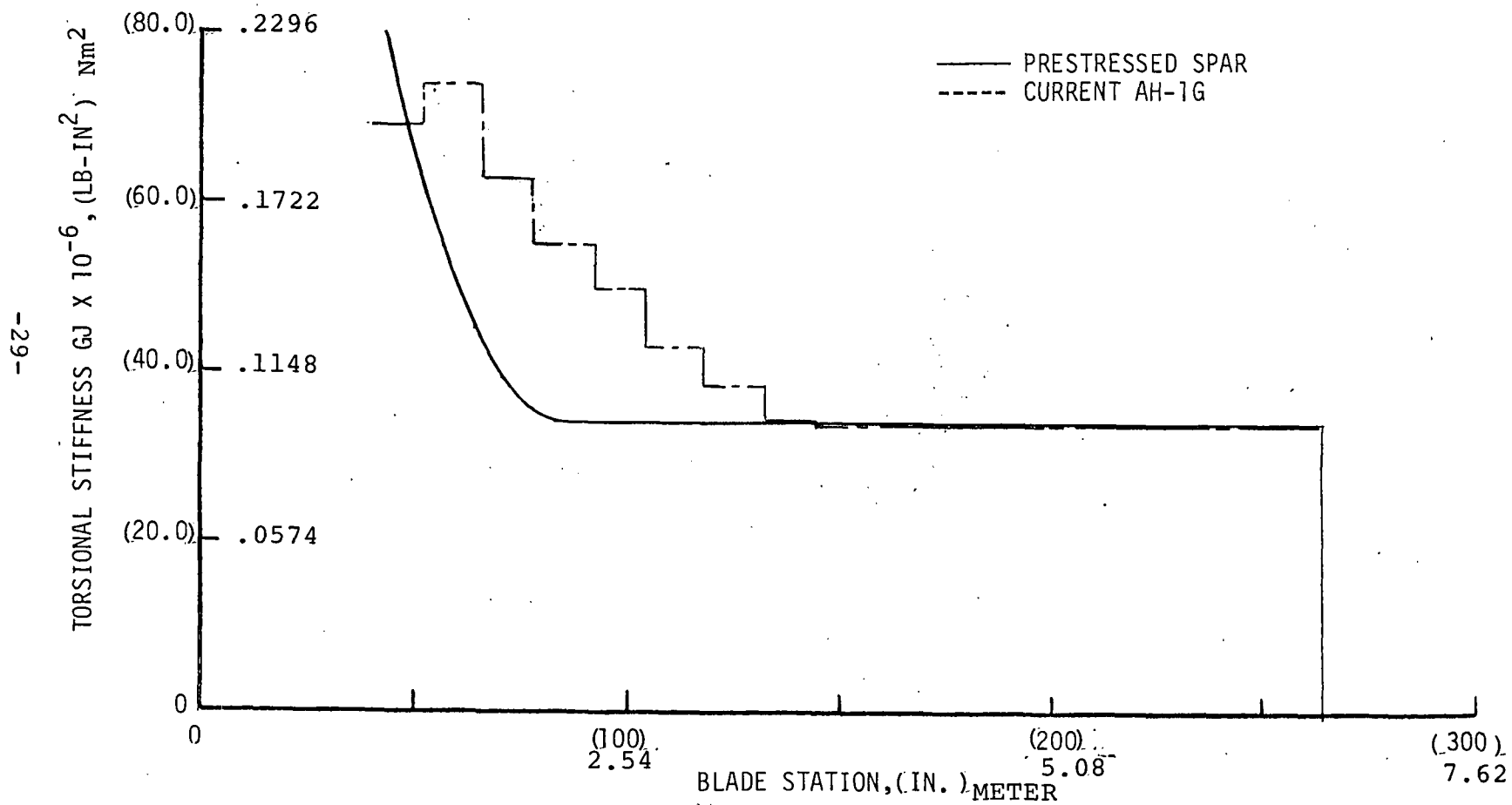


Figure 4-7. Torsional Stiffness vs Blade Station

4.1.1.2.2 Stress and Margins of Safety

Margins of safety at the inboard tube ends (Sections A, B, C, of Figure 4-8) are given in Table 4-1 for the ultimate and fatigue loading conditions. The results are based on conservative assumptions which include neglect of head and fiber wrap load carrying capacity, see Section 7.1.3. Large positive margins of safety exist in all inboard tube and "rod end" lug sections.

Tables 4-2 and 4-3 summarize the stress and margins of safety for prestressed spar rotor structural elements at station 2.032 for the ultimate and fatigue loading conditions, respectively. Prestresses are included, as applicable. All structural components have large positive margins of safety.

Table 4-1

Inboard Tube Ends

Margins of Safety for Stations 1.156 (45.5) to 1.27 (50)

Section	M.S.- (ultimate)	M.S. (fatigue)
A (Sta.50) 1.27	3.17	3.21
B	3.18	4.33
C (Sta. 45.5) 1.156	> 10	> 10

.1.2 Prestressed Composite Spar Tube Structural Analysis

Prestressed composite spar tube structural design formulae, prestress calculations and buckling checks are detailed in Appendices 2, 3, Section 7. Tube and fiber overwrap stresses, based on an overall blade cross-section analysis, have been presented in preceding section 4.1.1.2.2.

TABLE 4-2 STA. 2.032 ULTIMATE LOAD CONDITIONS

ITEM	CONDITION	$E \times 10^{-6}$ (N/m ²)	C_x (m)	C_y (m)	F_u (N/m ²)	f_u (N/m ²)	MS_u
Steel Tube No. 1	1	186158	0.064	0.019	13.1×10^8	-3.146×10^8	3.16
	2	"	"	"		-2.294×10^8	4.71
	3	"	"	"		1.499×10^8	7.74
	4	"	"	"		0.661×10^8	18.82
Steel Tube No. 2	1	"	0.012	0.024		-2.913×10^8	3.50
	2	"	"	"		-2.756×10^8	3.75
	3	"	"	"		0.902×10^8	13.52
	4	"	"	"		0.817×10^8	15.03
Steel Tube No. 3	1	"	-0.046	0.024		-2.272×10^8	4.77
	2	"	"	"		-2.882×10^8	3.55
	3	"	"	"		0.567×10^8	22.10
	4	"	"	"	13.1×10^8	0.748×10^8	16.51
+ $\frac{\pi}{12}$ rad. Wrap Tube No. 1	1	153064	0.064	0.021	14.41×10^8	4.352×10^8	2.31
	2	"	"	"		3.651×10^8	2.95
	3	"	"	"		4.924×10^8	1.93
	4	"	"	"		4.235×10^8	2.40
+ $\frac{\pi}{12}$ rad. Wrap Tube No. 2	1	"	0.012	0.026		4.160×10^8	2.46
	2	"	"	"		4.031×10^8	2.57
	3	"	"	"		4.434×10^8	2.25
	4	"	"	"		4.307×10^8	2.35
+ $\frac{\pi}{12}$ rad. Wrap Tube No. 3	1	"	-0.046	0.026		3.633×10^8	2.97
	2	"	"	"		4.134×10^8	2.49
	3	"	"	"		4.453×10^8	2.24
	4	"	"	"	14.41×10^8	4.307×10^8	2.35
+ $\frac{\pi}{4}$ rad. Wrap Tube No. 1	1	43988	0.064	0.023	7.72×10^8	1.339×10^8	4.77
	2	"	"	"	"	1.137×10^8	5.79
	3	"	"	"	"	1.304×10^8	4.92
	4	"	"	"	"	1.273×10^8	5.06
+ $\frac{\pi}{4}$ rad. Wrap Tube No. 2	1	"	0.012	0.029	"	1.284×10^8	5.01
	2	"	"	"	"	1.247×10^8	5.19
	3	"	"	"	"	1.330×10^8	4.80
	4	"	"	"	"	1.293×10^8	4.97
+ $\frac{\pi}{4}$ rad. Wrap Tube No. 3	1	"	-0.046	0.029	"	1.132×10^8	5.82
	2	"	"	"	"	1.276×10^8	5.05
	3	"	"	"	"	1.214×10^8	5.36
	4	"	"	"	"	1.293×10^8	4.97
Skin Outer Ply (Zero Prestress)	1	23511	-0.028	0.032	3.103×10^8	0.524×10^8	4.92
	2	"	"	"	"	0.570×10^8	4.44
	3	"	"	"	"	0.518×10^8	4.99
	4	"	"	"	"	0.564×10^8	4.50
T.E. Spline (Zero Prestress)	1	75842	-0.553	0.003	-2.758×10^8	-1.485×10^8	0.86
	2	"	"	"	13.79×10^8	1.526×10^8	8.04
	3	"	"	"	-2.758×10^8	-1.339×10^8	1.06
	4	"	"	"	13.79×10^8	1.623×10^8	7.50

TABLE 4-3 RESULTS OF FATIGUE CONDITION STRESS ANALYSIS FOR STATION 2.032

	$E \times 10^{-6}$ (N/m ²)	C_x (m)	C_y (m)	f_f (N/m ²)	F_{tu} (N/m ²)	F_E (N/m ²)	F_a (N/m ²)	$MS_f = \frac{F_a}{F_v} - 1$
Steel Tube No. 1	186158	0.064	0.019	$-0.927 \times 10^8 \pm 0.744 \times 10^8$	13.1×10^8	2.068×10^8	2.215×10^8	1.98
Steel Tube No. 2	186158	0.011	0.024	$-0.895 \times 10^8 \pm 0.808 \times 10^8$	13.1×10^8	2.068×10^8	2.210×10^8	1.73
Steel Tube No. 3	186158	-0.046	0.024	$-0.987 \times 10^8 \pm 0.888 \times 10^8$	13.1×10^8	2.068×10^8	2.224×10^8	1.50
$\pm \frac{\pi}{12}$ rad Tube Wrap No.1	153064	0.064	0.020	$2.937 \times 10^8 \pm 0.673 \times 10^8$	14.41×10^8	2.572×10^8	2.048×10^8	2.04
$\pm \frac{\pi}{12}$ rad Tube Wrap No.2	153064	0.012	0.026	$2.964 \times 10^8 \pm 0.717 \times 10^8$	14.41×10^8	2.572×10^8	2.043×10^8	1.85
$\pm \frac{\pi}{12}$ rad Tube Wrap No.2	153064	-0.046	0.026	$2.889 \times 10^8 \pm 0.782 \times 10^8$	14.41×10^8	2.572×10^8	2.056×10^8	1.63
$\pm \frac{\pi}{4}$ rad. Tube Wrap No. 1	43988	0.064	0.023	$0.903 \times 10^8 \pm 0.215 \times 10^8$	7.72×10^8	1.379×10^8	1.218×10^8	4.67
$\pm \frac{\pi}{4}$ rad. Tube Wrap No. 2	43988	0.012	0.029	$0.911 \times 10^8 \pm 0.228 \times 10^8$	7.72×10^8	1.379×10^8	1.216×10^8	4.33
$\pm \frac{\pi}{4}$ rad. Tube Wrap No. 3	43988	-0.046	0.029	$0.890 \times 10^8 \pm 0.246 \times 10^8$	7.72×10^8	1.379×10^8	1.220×10^8	3.96
** Skin Outer Ply	23511	-0.028	0.032	$0.354 \times 10^8 \pm 0.140 \times 10^8$	3.103×10^8	0.896×10^8	0.794×10^8	4.67
** Trailing Edge Spline	75842	-0.553	0.0026	$0.536 \times 10^8 \pm 0.563 \times 10^8$	1.379×10^8	1.034×10^8	0.994×10^8	0.76

* Prestressed damage "endurance limit" and no crack propagation upper limit per crack propagation test data of Reference 6.

** These members have prestress, $f_i = 0$.

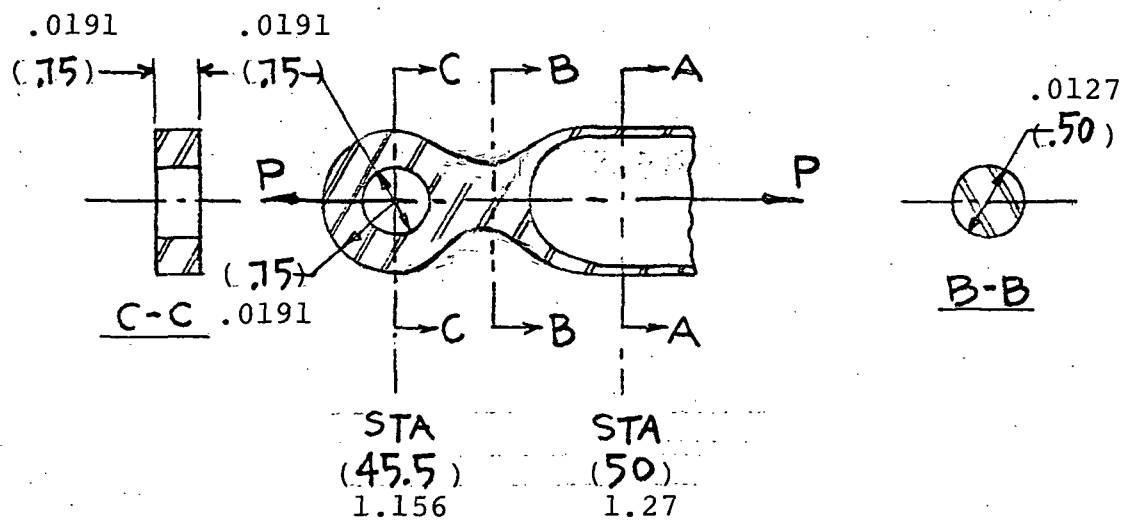


Figure 4-8 - Sketch of Root End Metal Liner Head Cross-Section

Results of the discrete prestressed composite spar tube analysis are summarized below. These relations, as applicable, have been used in the calculations detailed in this report. Notation is defined in Section 7 and Figure 4-9.

a) Prestressed Composite Spar Tube Stiffness Properties

Fiber to Metal Bending Stiffness Ratio, $\frac{k_{fb}}{k_{mb}} = \sum_{j=1}^n \frac{E_{fj} \cos^4 \alpha_j}{E_m} \left(\frac{t_{fj}}{t_m} \right) \left(\frac{D_{fj}}{D_m} \right)^3$ --- (4-1)

Fiber to Metal Torsional Stiffness Ratio, $\frac{k_{ft}}{k_{mt}} = \sum_{j=1}^n \left(2.6 \frac{E_{fj}}{E_m} \right) \sin^2 \alpha_j \cos^2 \alpha_j \left(\frac{t_{fj}}{t_m} \right) \left(\frac{D_{fj}}{D_m} \right)^3$ --- (4-2)

Fiber to Metal Axial Extensional Stiffness Ratio, $\frac{k_{fa}}{k_{ma}} = \sum_{j=1}^n \left(\frac{E_{fj}}{E_m} \right) \cos^4 \alpha_j \left(\frac{t_{fj}}{t_m} \right) \left(\frac{D_{fj}}{D_m} \right)$ --- (4-3)

Composite Bending Stiffness, $k_{cb} = k_{mb} + k_{fb} = \left(1 + \frac{k_{fb}}{k_{mb}} \right) k_{mb}$ --- (4-4)

Composite Torsional Stiffness, $k_{ct} = k_{mt} + k_{ft} = \left(1 + \frac{k_{ft}}{k_{mt}} \right) k_{mt}$ --- (4-5)

Composite Axial Extensional Stiffness, $k_{ca} = k_{ma} + k_{fa} = \left(1 + \frac{k_{fa}}{k_{ma}} \right) k_{ma}$ --- (4-6)

b) Prestressed Composite Stresses

Fiber to Metal Bending (or direct axial) Stress Ratio, $\frac{\sigma_{fx}}{\sigma_{mb}} = \frac{E_f \cos^4 \alpha}{E_m} = \frac{\sigma_f \cos^2 \alpha}{\sigma_{mb}} = \frac{\sigma_{fx}}{\sigma_m}$ --- (4-7)

Metal Bending Stress, $\sigma_{mb} = \frac{M_m C_m}{I_m} = \frac{M}{1 + \frac{k_{fb}}{k_{mb}}} \times \frac{C_m}{I_m}$ --- (4-8)

Metal Direct Axial Stress, $\sigma_{mx} = \frac{F_m}{A_m} = \frac{F}{1 + \frac{k_{fa}}{k_{ma}}} \times \frac{1}{A_m}$ --- (4-9)

c) Prestresses

Spar tube prestresses, designed to provide a net compression in the metal and net tensions in the fibers under operating fatigue load conditions, were computed as:

226

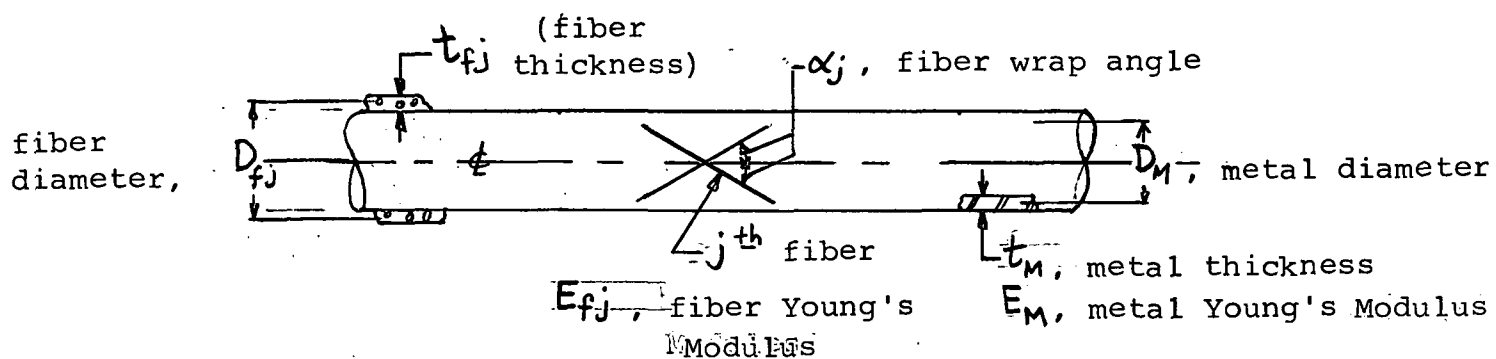


Figure 4-9 - Sketch, Prestressed Composite Spar Tube Notation Description

Metal Longitudinal Compressive Prestress, $\sigma_{Mxi} = -358.5 \times 10^6 \frac{N}{m^2}$

Metal Hoop Compressive Prestress, $\sigma_{M\theta i} = -137.9 \times 10^6 \frac{N}{m^2}$

$\pm \frac{\pi}{12}$ rad ($\pm 15^\circ$) Fiber Tensile Prestress, $\sigma_{f1i} = 77.2 \times 10^6 \frac{N}{m^2}$


$\pm \frac{\pi}{4}$ rad ($\pm 45^\circ$) Fiber Tensile Prestress, $\sigma_{f2i} = 50.3 \times 10^6 \frac{N}{m^2}$

These prestress levels are the same order as those previously demonstrated^{5,6} ($\sigma_{Mi} = -344.7 \times 10^6 \frac{N}{m^2}$ and $\sigma_{fi} = 275.8 \times 10^6 \frac{N}{m^2}$).

Therefore, no significant problems are anticipated.

d) Buckling Checks

Buckling checks of the metal liner were made using prestressed composite structure test data to evolve critical buckling load (stress) improvement factors compared to unprestressed homogeneous material structures. Positive margins of safety against buckling were computed as detailed in Appendix 3, Section 7.



4.2 Performance Evaluation

The AK-76 blade has the same external dimensions - airfoil section, chord, and planform - as the Model 540 blade. Mass and stiffness distributions of both blades match closely. Installed weight of the AK-76 blade is also same as that of the Model 540 blade.

Since the aerodynamic characteristics of the blade and the helicopter weights are unchanged, hover, forward flight, and maneuverability performance of an AH-1G with the new blade will be as good as with the Model 540 blades. Autorotation characteristics will also be uncompromised because the mass distributions - and therefore rotational inertias - of both blades closely match.

Aeroelastic stability and stall flutter boundaries may not be affected. Although such analysis were beyond the scope of present studies, the AK-76 blade responses, amplitudes, and damping rates should closely match those of the Model 540 blade since mass and stiffness characteristics are similar.

The new (AK-76) blade will probably be dynamically compatible with the AH-1G vehicle. Because of similarity in mass and stiffness distributions, natural frequencies and mode shapes of the AK-76 blade should approach those of the Model 540 blade. Dynamic analyses, not funded in this study, are needed to confirm dynamic compatibility.

4.3 Fabrication Considerations

4.3.1 Blade Assembly Fabrication

Figure 4-10A depicts the blade fabrication operation and sequences. Available, developed fabrication techniques are utilized as sketched on Figure 4-10B.

Level 1 operations prepare the prestressed spar tubes for the overwrap windings. The three prestressed spar tubes are mated to the root end attachment and outboard tie fittings and placed in a holding fixture for the winding. The fixture orients the inboard and outboard ends at their proper twist attitudes.

Precut plies for the shear transfer layer are then laid up over the tubes and the precast foam fillers put into position. The fillers will be 4- to 6-foot segments for ease in handling. This uncured "B" stage subassembly is then overwrapped with the KEVLAR 49 filament oriented at $\pm \frac{\pi}{4}$ rad. ($\pm 45^\circ$), binding the tubes and fillers into a unitized "B" stage component.

Level 2 operations complete the spar structure build up. The wrapped tube preassembly is positioned nose-up. The preformed unidirectional KEVLAR 49 nose block segments and the mid span and tip balance weights are tack bonded into place. The assembly is then wrapped with $\pm \frac{\pi}{4}$ rad.-oriented KEVLAR 49 filament. At this stage, the spar structure, except for the tubes, is still in the uncured "B" stage.

Level 3 operations produce the blade basic bonded structure. This phase begins with layup of the uncured upper skin in the primary half-mold bond fixture. The "B" stage spar, afterbody core segments, and the trailing edge spline are positioned in place with foam adhesive in all of the core splice joints and film adhesive where required. The lower skin is then laid on and secured. A flexible caul plate and an air bag are placed over the layup. The bond fixture is then placed into an autoclave, the air bag pressurized to squeeze the bond surfaces, and the structure heated for 60 to 90 minutes at the adhesive cure temperature. The half-mold caul plate tooling assures a smooth accurate contour and sound bonds, and is less expensive than matched closed dies.

Level 4 operations complete the blade bonding operations. The root end doublers and hub attachment area cheek plates are laid up on the cured blade structure, secured and bagged.

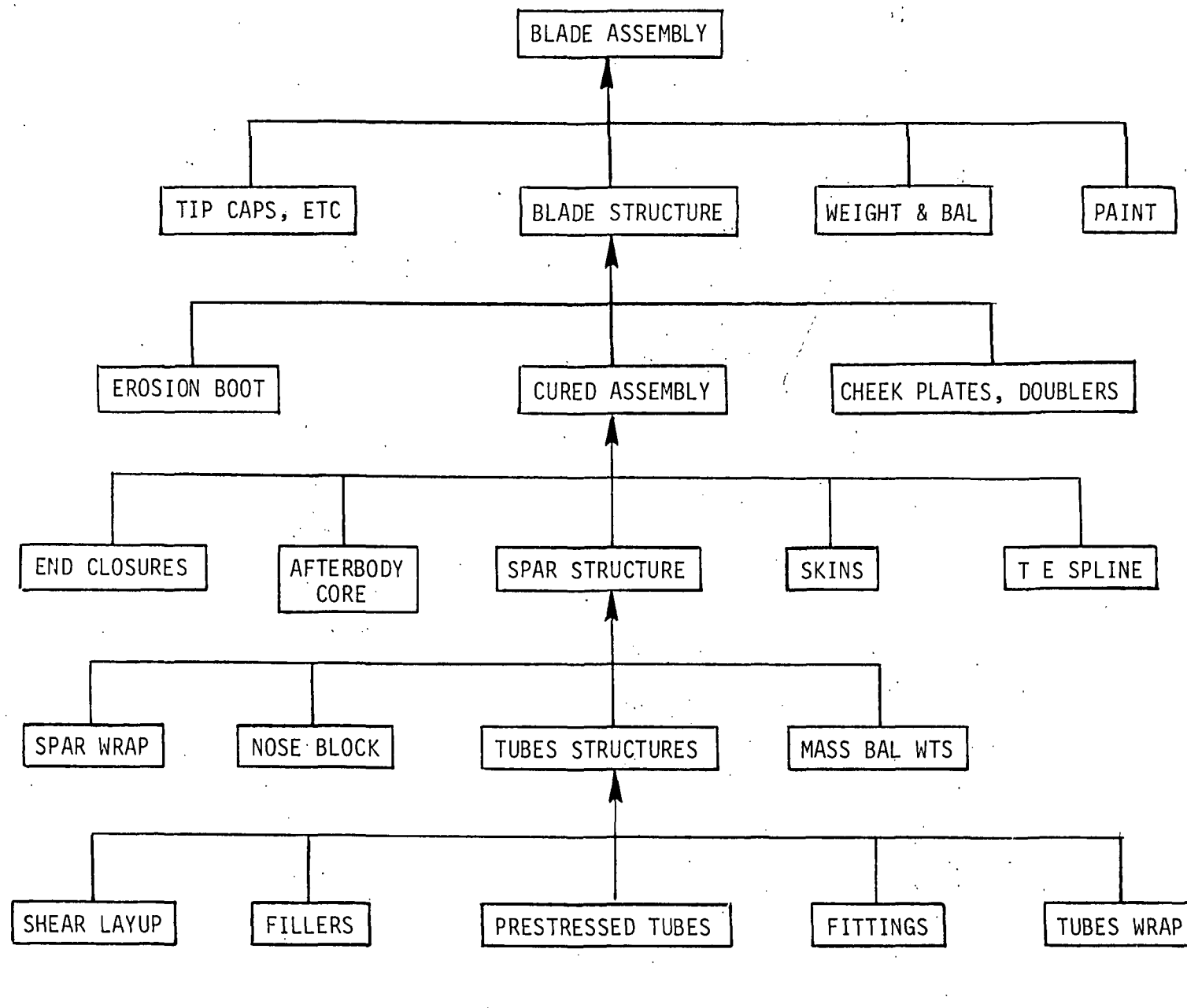
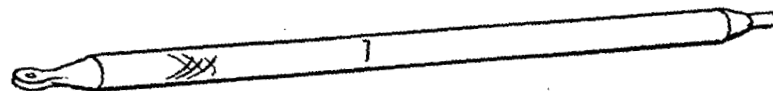
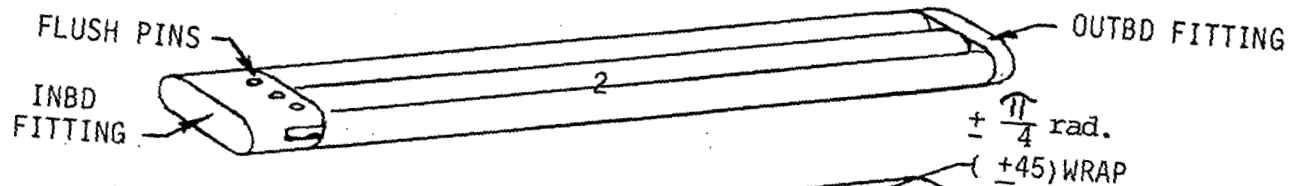


Figure 4-10A Blade Fabrication

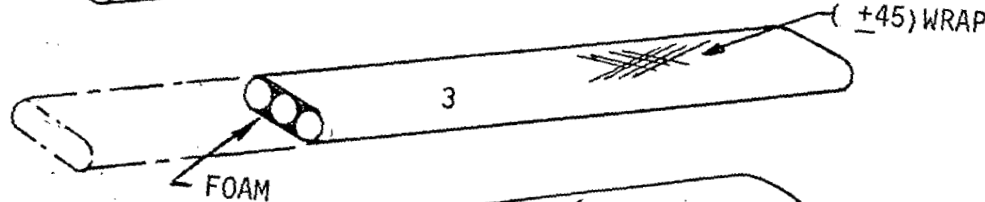
1 TUBE ASSY



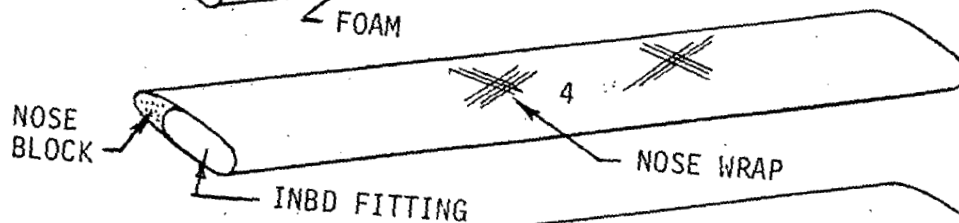
2 TUBES PREPARED FOR SPAR WRAPS



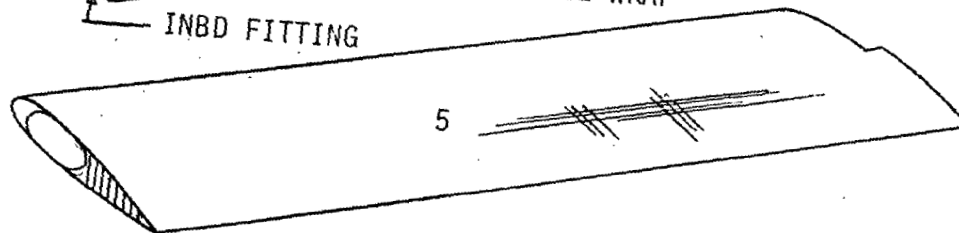
3 SPAR TORSION WRAP, FOAM & TUBE WRAP



4 NOSE BLOCK, BALLAST CUTS, AND NOSE WRAP



5 SKINS AND END RIBS



6 DOUBLERS & CHEEK PLATES ADDED AND MACHINED

MAIN BOLT & DRAG BOLT HOLES REAMED TO SIZE

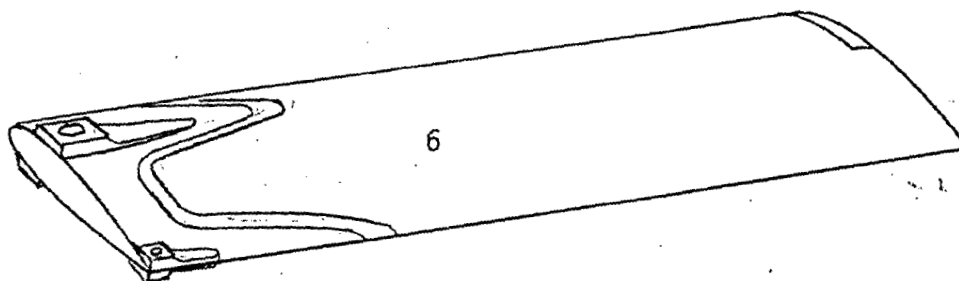


Figure 4-10B Blade Structure Build-Up

The assembly is then cured at approximately 363°K. At this point, the trailing edge is trimmed to the net chord dimension and excess adhesive is cleaned off. The final bonding operation is attachment of the leading edge elastomer erosion boot with lower temperature-cure adhesive.

Level 5 operations complete the blade assembly. The structure is painted, three-scale weighed, and trim balanced with weights to meet the overall weight and center of gravity location specifications. Installations of the end closures and tip cap completes the blade fabrication operations.

4.3.2 Prestressed Composite Spar Tube Fabrication

4.3.2.1 Fabrication Operations and Sequencing

Prestressed composite spar tube fabrication operations and sequencing are shown schematically on Figure 4-11 and described herein.

a) Metal Liner Preform

Automated set-up machined root end and trailing end heads and circular cylindrical tube section (precut to length) are integrated by automatic girth welding techniques to form the 304L liner preform.

b) Inner Fiber Wrap

The metal liner preform is over-wrapped with the $\pm \frac{\pi}{12}$ rad. helix angle HTS graphite fibers plus resin. Fiber wrapping tension is as close to zero as possible. The resin is cured in an oven. The "permanent" metal liner serves as the fiber wrapping mandrel. This construction avoids the problem of stripping the filament wound component from its mandrel, inherent in an all fiber structure. The metal liner can also be "rigidized", if required, by application of internal pressure during the fabrication process.

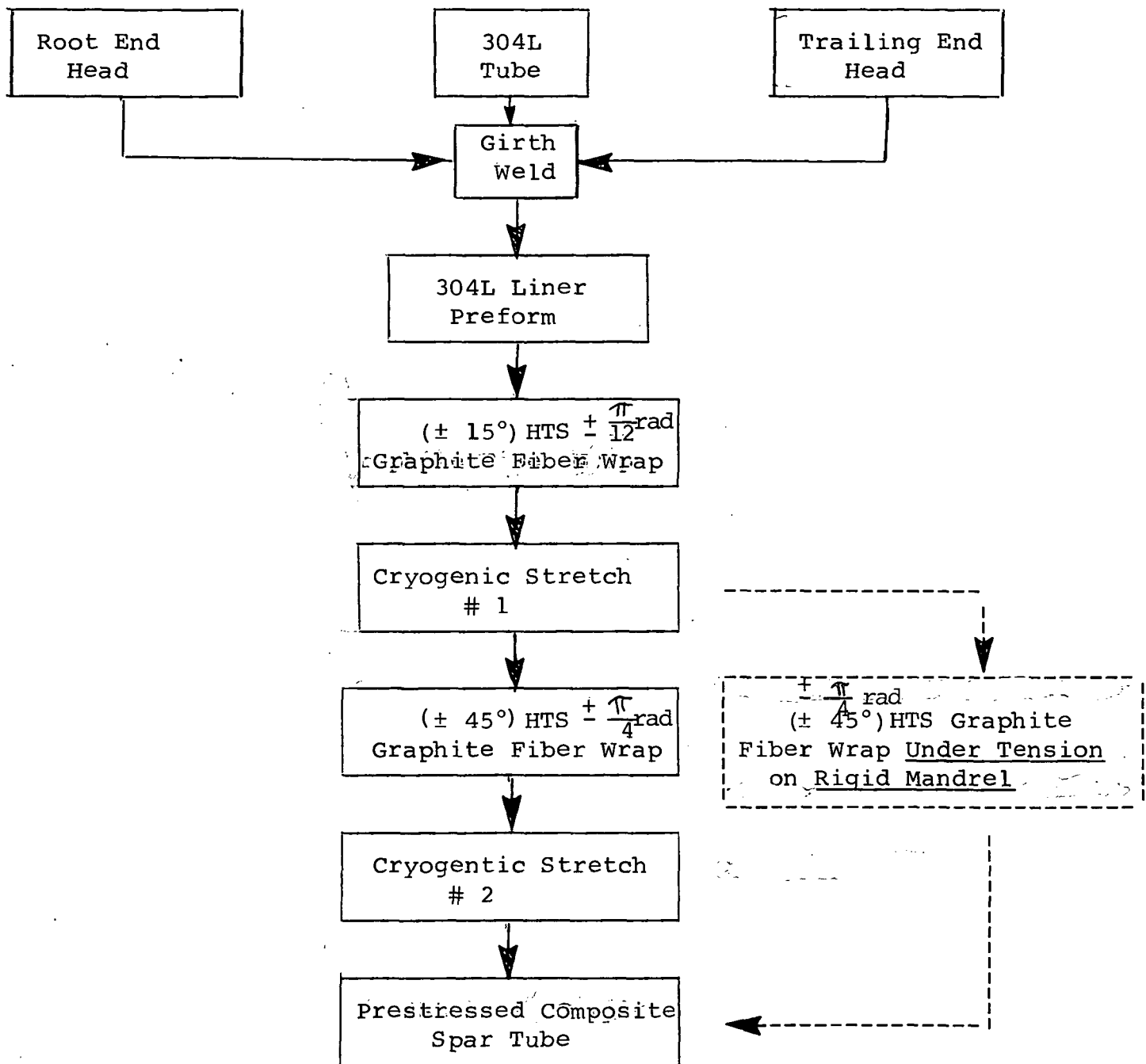


Figure 4-11 - Prestressed Composite Spar Tube Fabrication

c) First Cryogenic Stretchforming Operation

The $\pm \frac{\pi}{12}$ rad. fiber overwrapped 304L tubular liner is cryogenically stretched in a split closed die using liquid nitrogen (LN_2) as the coolant and pressurant. The die is similar in construction to the tooling developed and verified under previous contract efforts (5,6). A two (2) stage cryogenic stretch operation is required because of the strain to rupture limitation of the HTS graphite fibers (about 1% strain). A large hoop cryogenic strain, needed to strengthen the metal liner, can be applied without overstraining the shallow $\pm \frac{\pi}{12}$ rad. angle fibers. On the other hand, if the $\pm \frac{\pi}{4}$ rad. fibers were stretched at the same time, they would rupture.

d) Outer Fiber Wrap

The $\pm \frac{\pi}{12}$ rad. fiber prior overwrapped and cryogenically stretchformed 304L liner is next overwrapped with the $\pm \frac{\pi}{4}$ rad. HTS graphite outer fiber layer. The resin is cured in an oven.

e) Second Cryogenic Stretchforming Operation

The $\pm \frac{\pi}{12}$ rad. and $\pm \frac{\pi}{4}$ rad. fiber overwrapped metal liner is cryogenically stretched in a split closed die to form the prestressed composite spar tube.

4.3.2.2 Alternate Fabrication Option

The second cryogenic stretchforming operation may be eliminated (Figure 4-11) if the outer $\pm \frac{\pi}{4}$ rad. HTS graphite fibers are wound under tension on a "rigidized" mandrel with subsequent mandrel "release". A detailed technical and cost analysis, beyond the scope of the present program, would determine the most suitable fabrication option to be used in hardware applications.

4.3.2.3 Other Options

Circular cylindrical tube sections were chosen for this design study because of simplicity and availability. Sheet metal "roll and weld" techniques, with their inherent flexibility, facilitate design options. This fabrication method can be used to make more structurally efficient oval-shaped

tube sections as demonstrated on prior programs (5,6) as well as variable diameter (tapered) spar tubes to accommodate the advanced blade design configurations as discussed in Section 4.4.2. Variable thickness shapes can be fabricated by using chemical milled or ground tapered thickness starting sheet stock as demonstrated by large thin diaphragm shell forming technology⁽⁹⁾ Welding would be done along the neutral axis to minimize weld stresses. Compressive prestressing, inhibiting crack growth and increasing fatigue life, would add further reliability to the metal spar component.

4.3.3 Processes

The AK-76 blade design lends itself to maximum use of automated processes for fabrication, minimizing expensive "hand" labor, improving quality, and maintaining better dimensional and weight control.

The prestressed spar is fully dependent on and designed around the readily automated filament winding process as discussed above. Metal liner preform fabrication involves use of standard starting tube sizes and automated set-up machined head ends. Head to tube body joining is accomplished by automatic welding techniques. The cryogenic stretch operations of the fiber overwrapped spar tubes in closed split dies are designed to minimize hand labor by using appropriate handling fixtures and "quick opening" die joints.

The fabrication plan also calls for filament winding of skins. The winding will be done on a drum whose circumference is slightly greater than the perimeter lengths of the upper and lower skins. The #120 glass cloth layer can then be wrapped over the wound skin strata to complete the skin structure. The uncured skin is then slit along the length of the drum and removed as sheets for layup into the blade structure.

The trailing edge spline can also be filament wound with a machine such as shown in Figure 4-12. Multistrands of the KEVLAR⁴⁹ filament are directed through a guide eye and resin cup back and forth in a spanwise direction over end pins. Layers of windings are built up toward the forward edge to produce the wedge cross section and a unidirectional spline.

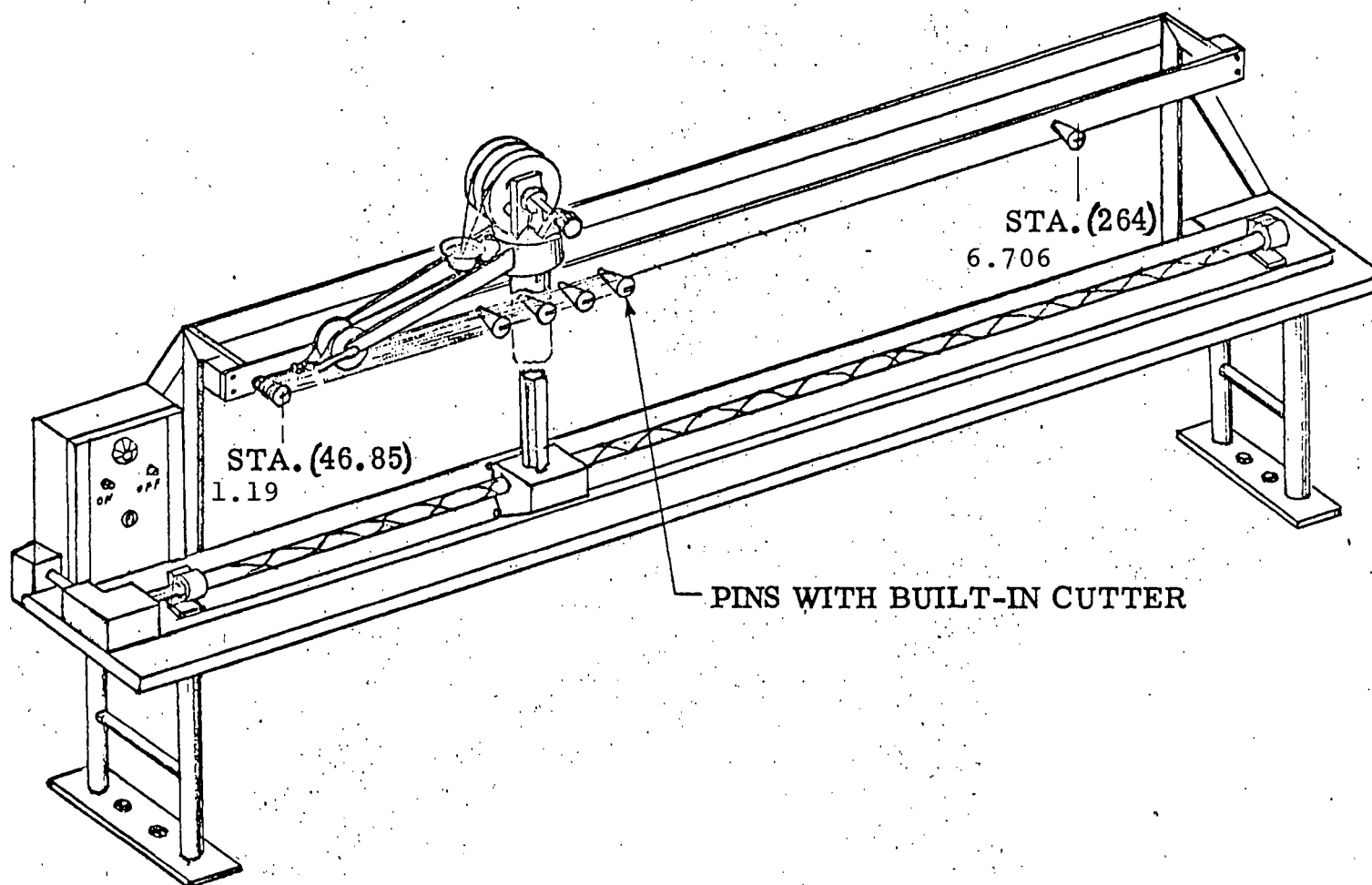


Figure 4-12 - Spline Filament Winding Machine.

4.4 Alternate Applications

4.4.1 Other Rotor Systems

The AH-1G rotor is a two-bladed teetering system. Except for pitch, the blades are attached rigidly to the hub. The blades have to be designed for relatively high flatwise and edgewise bending moments. The prestressed spar blade structure readily accommodates these loads and provides significantly increased safe operational life compared to all metal blades.

The "prestressed spar" blade structure also appears suitable for use with other rotor systems such as the articulated, hingeless, and rigid configurations. The "prestressed spar" structure bending and torsional stiffness can be readily varied together and independently by selective matching of filament material, number of wrap layers, and winding angles to provide the strength and dynamic characteristics required for each rotor concept.

The blade structure can be tailored to be soft or hard inplane with various combinations of torsional stiffnesses to accommodate developed rotor systems or advanced concepts such as the aeroelastically controllable or compliant systems or rotors needing very rigid, high strength blades.

4.4.2 Advanced Design Blades

The "prestressed spar" was successfully integrated into the AK-76 design, a blade with a constant airfoil section, thickness, and chord length. Except for the ends, the spars are constant in diameter and wrap thicknesses.

Some of the advanced rotor concepts discussed in Section 4.4.1 use or can use blades with constant airfoil, thickness and chord geometry. The "prestressed spar" can be applied to these blade structures equally as well as in the AK-76 design.

Others of the advanced blades have different airfoil sections along the span, taper in thickness, incorporate non-linear and large twist, or have swept tips. Used in these structures, the prestressed spar diameter and wrap thickness may have to be varied to attain optimum structural compatibility. Fabrication would be more complex. Filament winding would require drop off of filaments along the span and more winding commands. Variable configuration sheet metal liners can be fabricated using existing "roll and weld" techniques and wall thickness can be varied by chemical milling or grinding as discussed in Section 4.3.2.3.

Accommodation of non-linear twist and higher twist angles may require that tubes for a multi-cell spar be bent, buried deeper into the structure, or spaced by separator elements. Swept and tapered tips would require that the outer span of the spar be bent or tapered. It may be more practical to terminate the spar at the tip juncture and design the tip as an attachable structure. The prestressed spar metallic tube structure simplifies the tip attachment.

The prestressed spar with its advantages can be integrated into most advanced design blades, particularly if the airfoil, thickness, and chord are constant and twist is normal. Application in varying geometry structures is technically feasible. Design and trade-off studies to evaluate the technical and economic benefits are recommended for the varying geometry case.

4.4.3 Non-Rotor Application

Because of the high stiffness-to-weight, infinite fatigue life, excellent tolerance to damage, and survivable-time post-damage life, the prestressed spar structural concept may be an excellent candidate for use in critical helicopter components such as tail rotor drive shafts, control system rods, and landing gear struts or members. All are critical to human safety and machine survivability. Battle or maintenance damage to any can be disastrous since the members are generally highly stressed and/or notch sensitive in fatigue.

Filament wraps on the drive shafts and control rods would reduce their notch damage sensitivity, reduce replacements due to surface scratches and damage, and improve the probability of survival to landing after battle damage.

5.0 BLADE COST ESTIMATE

5.1 Introduction

The major cost elements in introducing and using a new product into service are the acquisition and life cycle costs.

The acquisition costs cover non-recurring and recurring cost elements. Non-recurring items include costs such as design and engineering, test and development, and manufacturing development and tooling. Recurring costs consist of elements such as materials, direct labor, inspection and quality control, and acceptance testing.

Life cycle costs are the user's costs for servicing, maintaining, and overhauling the product during its use. These are dependent on the item's reliability, damage resistance, and serviceability characteristics. Improvement of these characteristics increase "system availability" for use.

As discussed in Section 4.3, the AK-76 blade design permits extensive use of automated processes for high volume filament winding/bonding with relatively simple tooling for production of blades. In addition, prestressed composite spar fabrication is straightforward and readily automated. Design and development based on demonstrated technology should be straightforward without high risk. The new blade price should, therefore, be competitive with those of contemporary blades now appearing on the scene.

With respect to life cycle costs, not only is the AK-76 blade considered more reliable and damage resistant than the Model 540 blade, but its all-composite structure is amenable to field repair of wide ranges of damage types and severity, particularly in the afterbody skin and core. Repair techniques which would be used have already been developed and successfully demonstrated by Kaman in the Army-funded Field Repairable Blade Program.⁽¹²⁾ The demonstrated repair procedures, kit-packaged materials, and supporting tools assure reliable field-repair bonds.

The authorized scope of study permitted only a qualitative estimation by comparison of acquisition and life cycle costs. The basis of these estimates is set forth below.

Kaman has designed, developed, and demonstrated or qualified a number of helicopter advanced blade structures in the past few years - the UH-2"101" rotor blade, the Army-funded Field Repairable Blade (FREB), and a Controllable Twist Rotor (CTR) blade.

Kaman is completing the design of the "Circulation Control Rotor" (CCR) blade for the Navy and is designing, developing, and qualifying an Improved Main Rotor Blade (IMRB) for the AH-1Q helicopter under an Army contract.

These blades utilize and demonstrate many of the AK-76 structural features. The operational "101" and experimental CTR blades both have the honeycomb core - composite skin afterbody structure. Field repair feasibility and reliability of the Nomex core - composite skin afterbody were demonstrated with the Field Repairable blade. Excepting the spar structure and external shape, the AH-1Q IMRB structure is quite similar in design to the AK-76 structure.

Kaman utilized its cost analysis and experience from programs such as the above to estimate the probable development, unit production, and life cycle costs for the AK-76 design.

5.2 Acquisition Costs

Basically the AK-76 uses proven engineering and manufacturing technology. Development risks should be minimal. The main risk area is the prestressed spar. Design, manufacturing and test data for the prestressed composite construction exists, but its technical performance and manufacturing feasibility in the blade application have yet to be demonstrated. However, the risk for the AK-76 defined design appears to be a "normal level" of development risk, and the following cost estimates should be reasonably valid.

5.2.1 Engineering and Development Costs

This category of costs covers the design and engineering; preparation of design and fabrication drawings and data; planning and performance of development tests - such as static, fatigue, and whirl; planning, performance, and support of airworthiness qualification ground and flight tests; development of manufacturing techniques; design and fabrication of test fixtures and manufacturing tooling; manufacture of test hardware; and data documentation normally required by the services. These are essentially the non-recurring cost activities.

Based on Kaman's prior experience, the full program to design, develop, and qualify the blade for production would entail about 90,000 engineering and 40,000 manufacturing man-hours plus approximately \$1,300,000 for material and purchased parts. Using typical industry rates, costs for this will then be:

Engineering:	\$2,700,000
Manufacturing:	700,000
Materials:	1,300,000
Other Direct Charges:	<u>80,000</u>
	\$4,780,000

The above costs include engineering, manufacturing, material, general and administrative overhead burdens. The contractors profit or fee is additional. Flight demonstration only and manufacturing feasibility evaluation programs would cost less. "Flight demonstration only" may likely fall in the \$2.5 to \$3.0 million range. Elements of the above total program can be structured to be performed for as little as \$80 to \$100 thousand.

5.2.2 Unit Production Cost

The unit production cost target for the AH-1Q IMRB blade is \$8,000 or less for a production lot of 200 blades. The estimate after fabrication of several prototype units indicates that the target can be met.

The AK-76 blade is structurally similar to the IMRB blade, excepting the spar. Assembly operations of the after-body and overall blade structure and bonding procedures should be comparable. However, the AK-76 blade with constant chord and thickness is simpler in geometry than the IMRB blade with changing airfoil, section thickness, and tapered tip. It is, therefore, estimated that the unit cost for 200 AK-76 blades will be less than the IMRB blade, probably in the \$7000 to \$7200 range. Apportionment of cost is estimated as:

Spar Materials and Labor	\$2050
Blade Materials	\$2850
Blade Labor	\$2200

The costs, based on early 76 dollars, include overhead and profit.

Relaxation of some of the geometric and mass/stiffness restraints of the present study can result in spar cost reduction by permitting use of lower cost fibers. For example,

substitution of PRD-49 fibers for HTS graphite spar tube fiber overwrap will lead to a reduction of about \$400 in spar unit production cost.

5.3 Life Cycle Cost

Total life cycle costs of a blade are primarily functions of the blade's reliability, maintainability, and repairability. Not only is the AK-76 blade more corrosion and damage tolerant than the all metal 540 blade, it is more highly repairable. (12) Although this study did not include a detail life cycle cost comparison with the Model 540 blade, a synthesis with results of earlier studies to compare the IMRB (all fiber) blade with the Model 540 blade can be utilized to indicate anticipated further improvements by use of the AK-76 blade.

The life cycle cost comparison of Table 5-1 below indicates a \$67,939 Model 540 cost per aircraft as compared to a \$40,654 IMRB cost per aircraft. (7) This corresponds to a 40% life cycle projected cost reduction for the IMRB blade. A reduction of the \$40,654 IMRB cost per aircraft is projected for the AK-76 due to lower new blade cost, improved ballistic survival and improved durability based on non-criticality of long term resin degradation. Therefore, one would anticipate a life cycle cost reduction of more than 40% for the AK-76 blade compared to the 540 blade.

TABLE 5-1 LIFE CYCLE COST¹ COMPARISON

BLADE	540	IMRB	AK-76
New Blade Price	\$ 4,506	\$ 7,800	\$7,200
Mean Time Between Failures (Blade Hours)	1,000	1,558	Further Improvement Overall ↓
Field Repairability	10.5%	64.9%	
Replacements Per Aircraft Life Cycle	11.4	2.9	
Total Initial Procurement Cost	\$12,032	\$20,197	
Total Replacement Cost	\$54,360	\$19,407	
Total Maintenance Cost	\$ 1,547	\$ 1,050	↓
Total Life Cycle Blade Cost Per Aircraft	<u>\$67,939</u>	<u>\$40,654</u>	
Maintenance Man-Hours/Flight Hour	0.029	0.010	
Blade-Related Aircraft Downtime (Hours)	82	29	
¹ Costs are in late 1975 dollars			

6.0 CONCLUSIONS AND RECOMMENDATIONS

6.1 Conclusions

6.1.1 The AK-76 blade design meets the study's prime objective of defining an advanced helicopter rotor blade structure which incorporates the ARDE, INC. prestressed spar and which is functionally equivalent to the current AH-1G helicopter Model 540 rotor blade.

Because the AK-76 composite structure blade

is dimensionally the same as the Model 540 blade,

closely matches the Model 540 blade in mass and stiffness distributions and installed weight,

retrofits without modification to the helicopter, current hover and flight performance, maneuverability, and low speed agility should be maintained.

6.1.2 The prestressed composite (metal/fiber overwrap) spar structure offers a unique combination of advantages and design flexibility, many combinations of which are only available by use of prestressed composite construction. It is projected that benefits would apply for articulated, hingeless and rigid rotors.

a) Life Cycle Cost Savings Projected

• More than 40% compared to Model 540 Rotor Blade

- Project higher durability than all fibers since long term degradation of matrix resin is not critical to the prestressed composite load carrying capability.

b) The use of fiber over the metal enables projection of significantly improved ballistic tolerance over all metal or all fiber construction.

- The metal is retained in compression. Crack growth is retarded. Gun fire resistance has been demonstrated.
- The spar tube acts as a pressure vessel which is capable of sustaining high internal pressure.

- . The metal acts as a redundant load path. Load can be effectively transferred from fiber to metal.

c) Prestressed metal liner in compression during operation is insensitive to flaws and stress raisers and increases life. This is not available in all metal. Tensile prestressed fibers retain full effectiveness under compression loads. This is not available in all fiber.

d) Isotenoid fiber wrap develops full uniaxial fiber strength and minimizes inefficient load transfer by shear through resin. This is not available in all fiber.

e) The fiber members of the composite construction themselves corrosion resistant, protect the inner stainless steel member from moisture, dust, dirt, and the external weather and atmospheric environment. Stainless steel also has a high corrosion resistance. The composite construction therefore maintains improved corrosion resistance compared to all metal blades.

f) Prestressed metal liner allows simple, reliable and structurally efficient blade/rotor attachment. Effective multi-redundant load path root attachments are possible. This is not readily available in all fiber nor all metal.

g) Damage vulnerable after body structure is readily repaired under field repair operating conditions and environment. Repair of all metal construction is more difficult because of the difficulty of obtaining required mating joint surface cleanliness preparation and fit-up under field conditions. All metal is crack/flaw sensitive.

h) Low cost non-destructive inspection by gas leak detection is enhanced. Spar tubes may be pressurized internally with helium to high pressures thus increasing the sensitivity of the leak detection instrumentation. Internal pressure capacity of all metal construction is lower than composite configuration and all fiber construction is porous and would leak, rendering flaw detection by this technique invalid.

6.1.3 As a result of the study, it is projected that the prestressed metal/fiberwrap composite spar offers the

potential for additional unique advantages if some of the geometric, mass and stiffness constraints imposed by this study were removed in order to allow the following:

- 1) Take advantage of the structural "tuning" offered by the prestressed composite.

- a) Use of oval shape spars for improved bending stiffness and packaging.

- b) Modify stiffness distribution by use of varied metal thickness and fiberwrap patterns to provide lighter total blade weight with more mass concentrated at tip region. This would provide the required rotational energy for autorotation needs at a payload advantage. Resulting new blade natural frequencies would be chosen to be compatible with total helicopter system requirements.

- c) Use of less expensive fibers to significantly reduce cost.

- 2) Take advantage of the metal liner to provide easy attachment of various geometric blade tips for aeroacoustic designs.

6.2 Recommendations

Based on the successful results of this study and the projected unique advantages discussed above, the following program(s) to evaluate and demonstrate the prestressed composite spar characteristics are recommended:

1. Dynamic analysis of the AK-76 blade to verify dynamic similarity to the Model 540 blade.

2. Design study of a varying geometry blade to evaluate the technical and economical merits of the "prestressed spar" application in one advanced design blade.

3. Conduct ballistic firing tests on specimen spar structures using larger caliber projectiles such as the 23 mm shells to demonstrate the projected improved survival capability and obtain data for comparison with other blade structures. Specimens can be short length. Firings can be done at the Aberdeen Proving Grounds range where ballistic tests on other helicopter blades have been performed. Such tests should graphically demonstrate a major advantage of the prestressed composite spar.

7.1 Appendix - Blade Assembly Structural Analysis

7.1.1 General

A preliminary stress analysis of the AK-76 composite prestressed spar rotor blade assembly is presented herein. Results have been summarized in Section 4.1.1. Ultimate and fatigue load conditions were investigated in the analysis. Loads previously developed for the AH-1G main rotor blades were used to evaluate the composite prestressed spar rotor blade since the AK-76 blade section properties approximate those of the AH-1G blade. Limit centrifugal forces, in-plane bending moments, and out-of-plane bending moments obtained from Reference 8 are shown in Figures 7-1 through 7-4. Ultimate loads are 1.5 times limit loads. Fatigue condition loads were calculated from data presented in Reference 7. Steady and vibratory in-plane and out-of-plane bending moments used in the fatigue analysis are shown in Figures 7-5 and 7-6.

The basic equations used to convert externally applied loads into internal stresses acting within the composite prestressed spar rotor blade and used to determine the margins of safety are:

a) Ultimate Condition

$$\text{Ult. axial stress, } f_u = 1.5 \left[\frac{CF(EA)}{A(\sum EA)} \pm \frac{M_x C_y (EI_{xx})}{I_{xx} (\sum EI_{xx})} \pm \frac{M_y C_x (EI_{yy})}{I_{yy} (\sum EI_{yy})} \right] + f_i \quad \dots (7-1)$$

$$\text{Ult. margin of safety, } MS_u = \frac{F_u}{f_u} - 1 \quad \dots (7-2)$$

Equation 7-1 expresses the fact that the axial stress in any element of the cross-section due to externally applied CF and bending loads is proportional to the ratio of its stiffness to the stiffness of the entire cross-section. The initial stress, f_i , is superposed, as applicable. The 1.5 factor converts limit to ultimate condition. Equation 7-2 is the "standard" well-known relation for margin of safety.

b) Fatigue Condition

Axial fatigue stress is given by,

$$f_f = (f_s \pm f_v) = (CF) \frac{E}{\sum EA} \pm (M_{xs} \pm M_{xv}) \frac{C_y E}{\sum EI_{xx}} \pm (M_{ys} \pm M_{yv}) \frac{C_x E}{\sum EI_{yy}} + f_i \quad \dots (7-3)$$

33F 33F

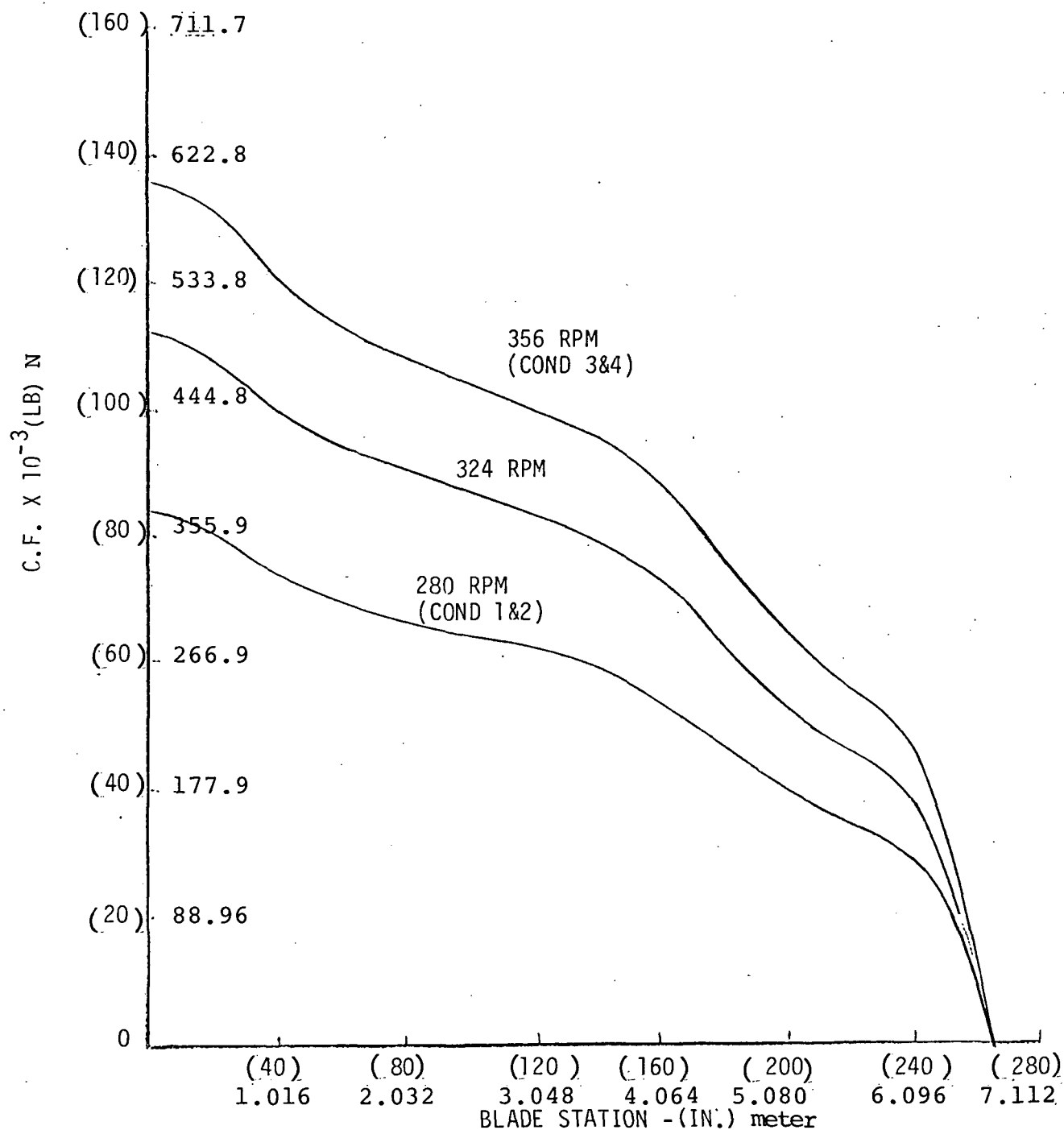


Figure 7-1 Design Loads - AH-1G Model 540 Rotor Centrifugal Force Distribution

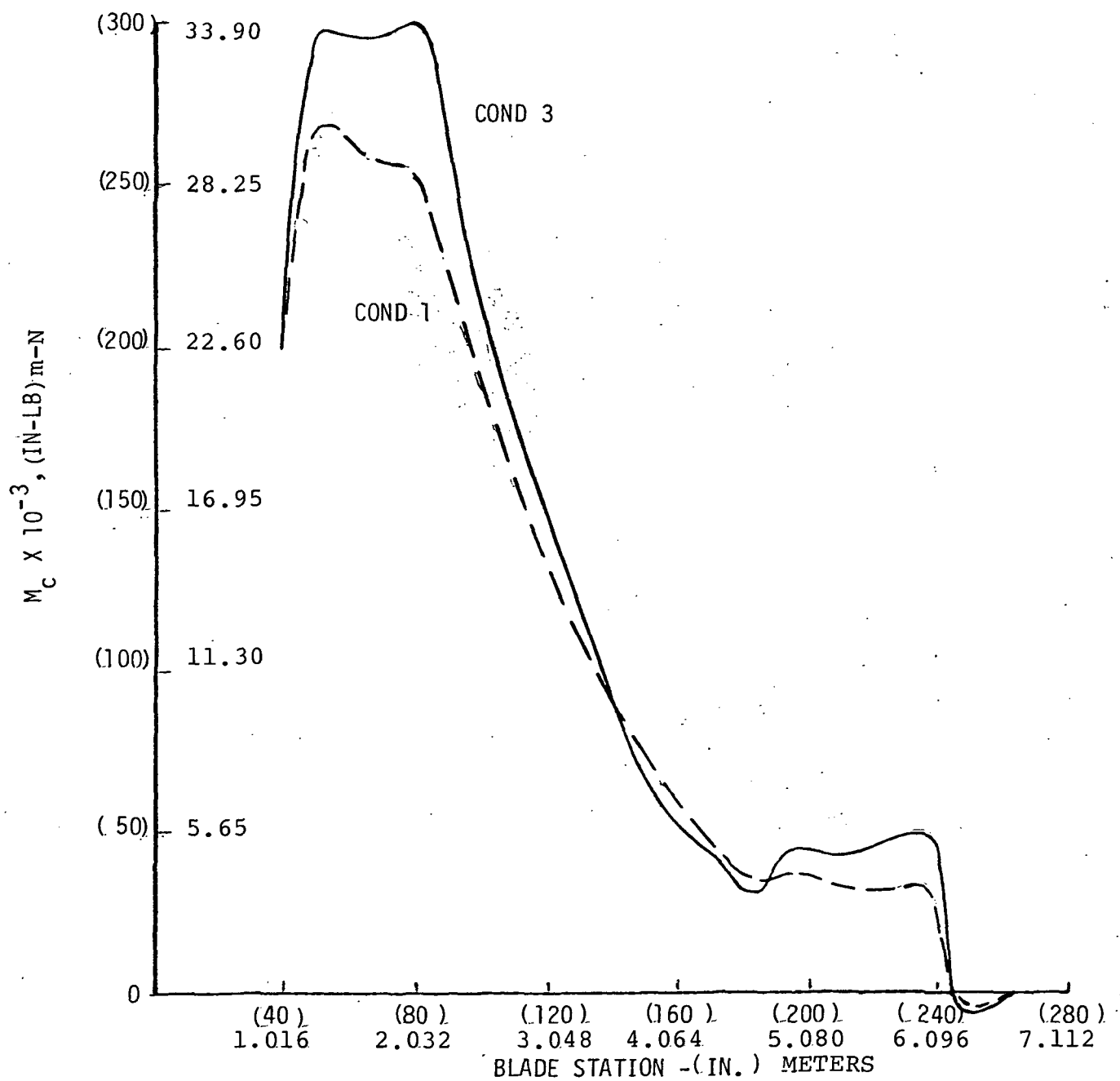


Figure 7-2 Design Loads - AH-1G Model 540 Rotor Limit Chordwise Moment About Blade Neutral Axis

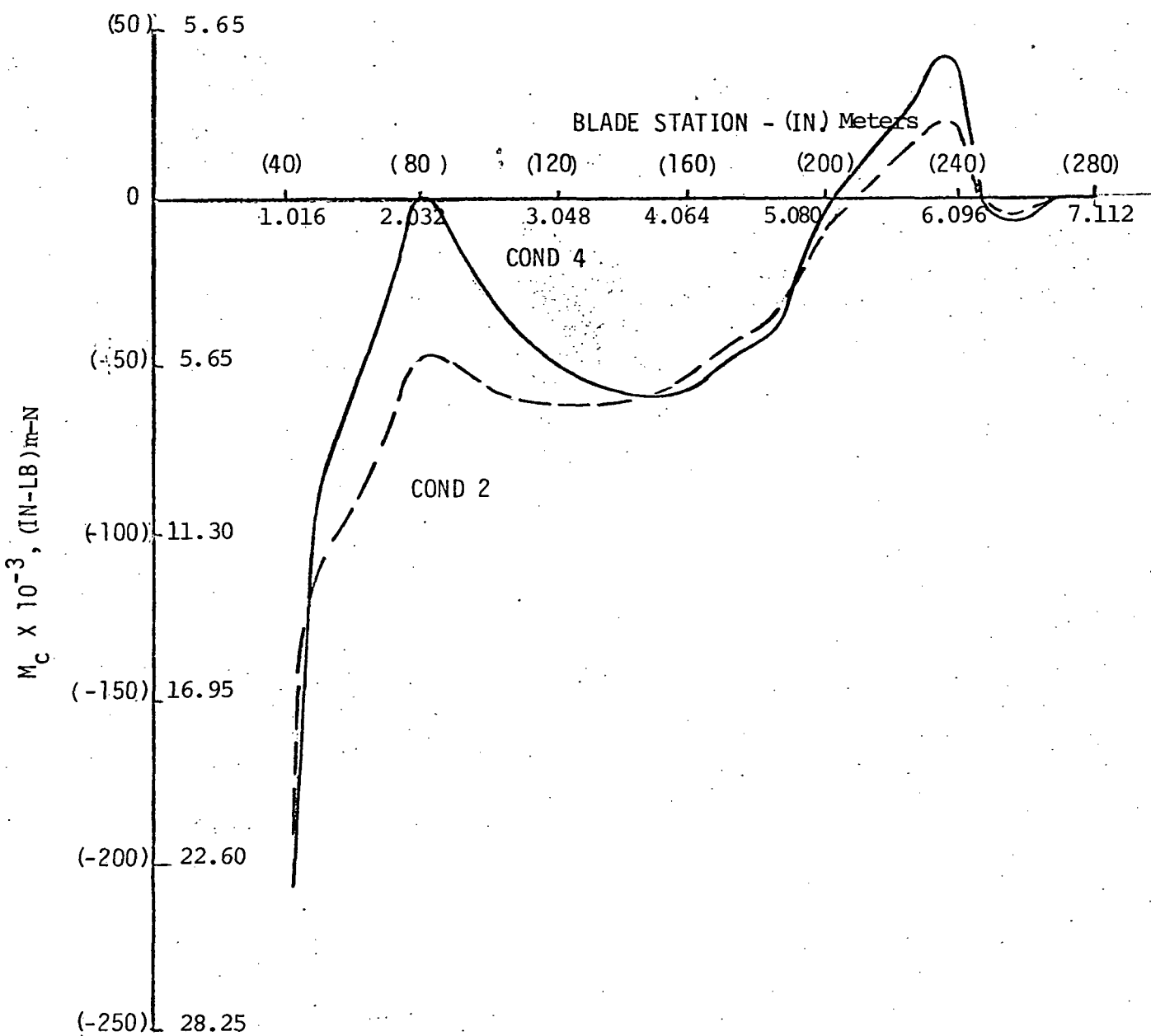


Figure 7-3 - Design Loads - AH-1G Model 540 Rotor Limit Chordwise Moment About Blade Neutral Axis

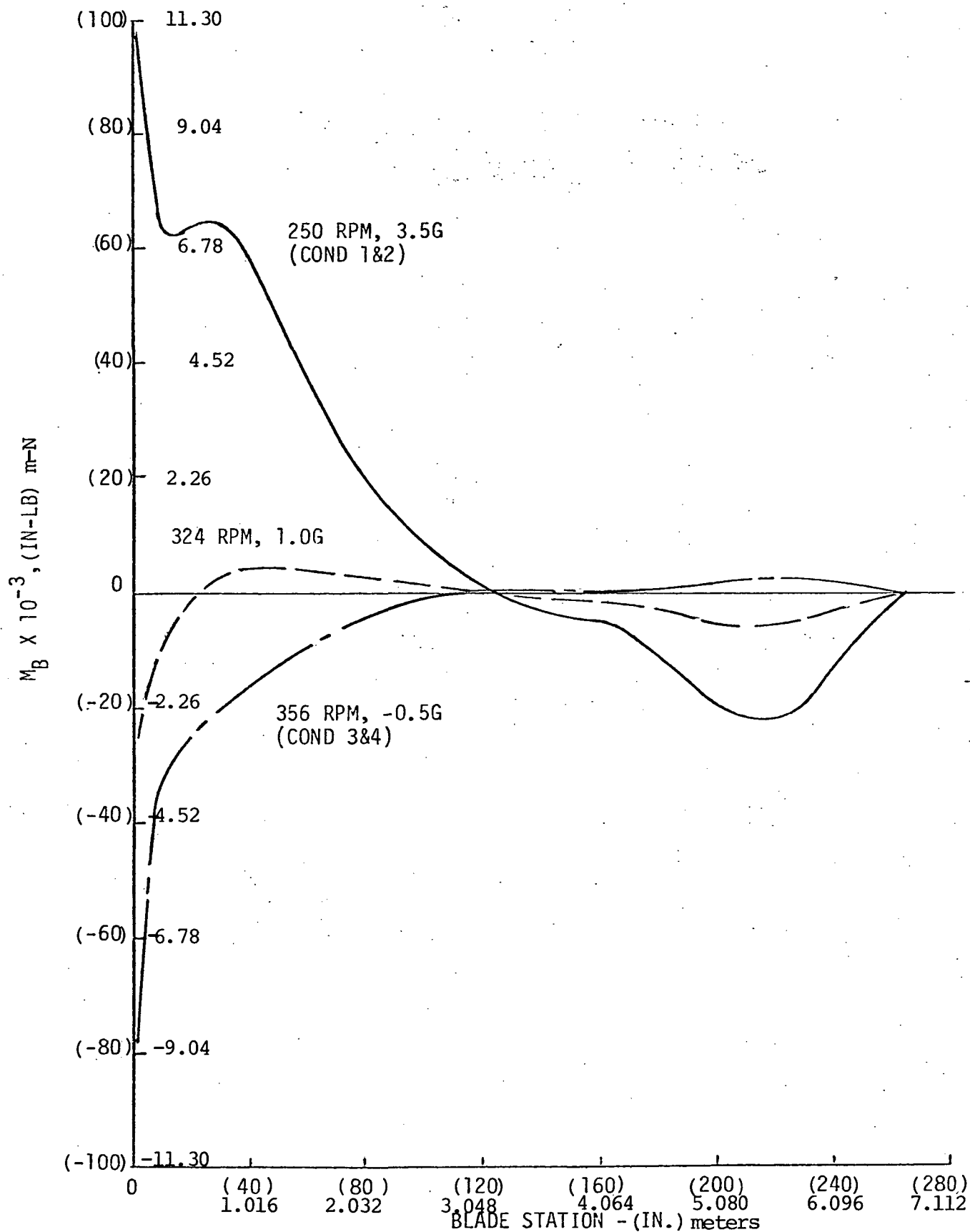


Figure 7-4 - Design Loads - AH-1G Model 540 Rotor Limit Beamwise Moment Distribution

B540 ROTOR
 (140 KNOTS) 72.0 m/sec
 (5000 FT) 1524 m
 324 RPM
 (10000 LB GW) 4536 kg

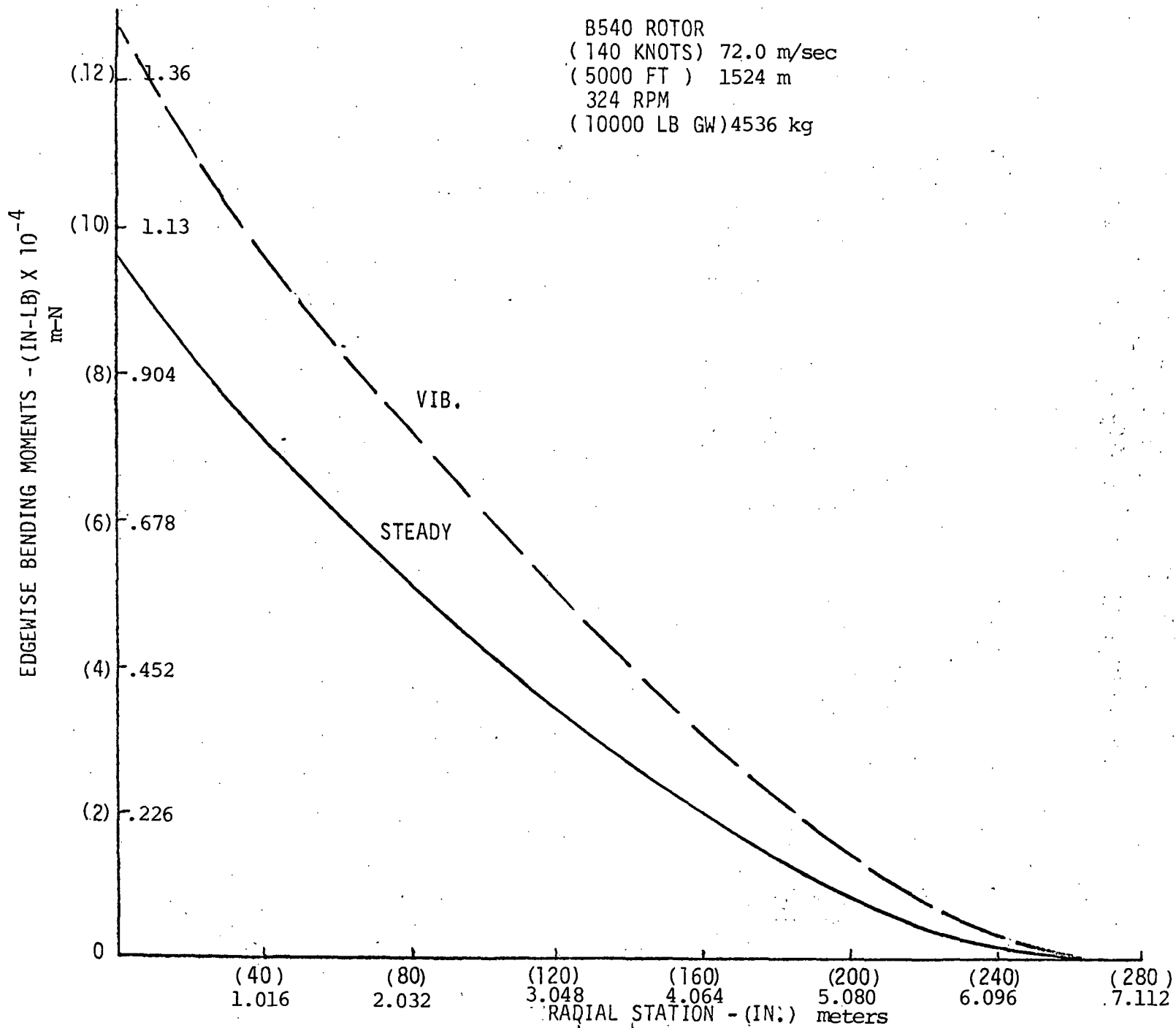


Figure 7-5 - Fatigue Condition - Steady & Vib. Inplane Bending Moment

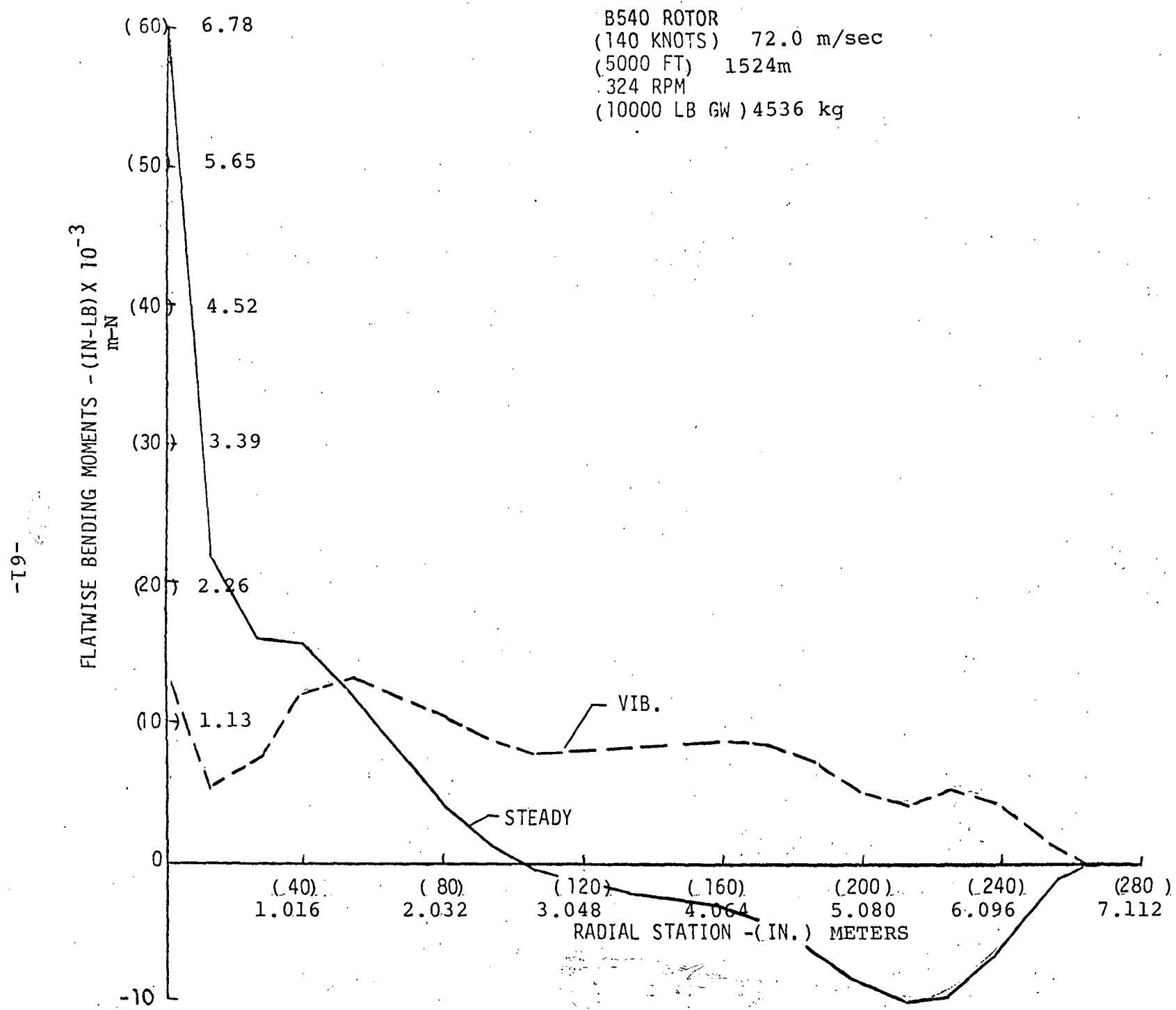


Figure 7-6 - Fatigue Condition - Steady & Vib. Out-Of-Plane Bending Moment

Using a modified Goodman Diagram, the allowable vibratory stress is computed from

$$F_a = F_e \left(1 - \frac{f_s}{F_{tu}} \right) \quad (7-4)$$

The margin of safety in fatigue is then determined from

$$MS_f = \frac{F_a}{f_v} - 1 \quad (7-5)$$

Section properties for the prestressed spar rotor blade used in the stress analysis are compared in Figures 4-1 to 4-7 of Section 4.1.1.2.1 to those for the AH-1G main rotor blade from Reference 8. The design of the basic portion of the prestressed spar rotor blade was tailored to match the section properties of the AH-1G main rotor as closely as possible to insure that natural in-plane and out-of-plane bending frequencies and natural torsional frequencies would be similar to those of the AH-1G blade, thus precluding coupled-mode instability problems.

Physical properties of the materials used in the design of the composite prestressed spar rotor blade are listed in Table 7-1. Since the scope of published data for some of these materials is limited or non-existent, lacking values were estimated. Testing is recommended to verify that these values are conservative enough for final design.

The critical sections of the prestressed spar rotor analyzed are listed below:

- a) Station 2.032 (80) at the outboard tips of the doublers.
- b) Stations 1.041 (41) through 1.27 (50) (main bolt attach area to the vicinity of tube attachment the inboard fitting).

TABLE 7-1. MATERIAL PROPERTY SUMMARY

Item	Material	F_{tu} (N/m^2)	E_x $\times 10^{-6}$ (N/m^2)	G $\times 10^{-6}$ (N/m^2)	F_e (R-1) (N/m^2)	ρ Kg/m^3
Metal Tubes	304L Cryogenically Stretched	13.1×10^8	186158	75842	2.068×10^8 *	7888.77
Tube Wrap	$\pm \frac{\pi}{12}$ rad. High Strength Carbon Graphite Δ	14.41×10^8	187537+	11169	2.572×10^8	1599.90
Tube Wrap	$\pm \frac{\pi}{4}$ rad. High Strength Carbon Graphite Δ	7.722×10^8	43988+	43988	1.379×10^8	1599.90
Spar Wraps & Nose Wrap	$\pm \frac{\pi}{4}$ rad. PRD49, Filament Wound	8.184×10^8	23580	23580	0.517×10^8	1384.00
Nose Block and Trailing Edge Spline	0 rad. PRD 49, Undirectional	13.79×10^8	75842	2068	1.034×10^8	1384.00
Skin Outer Ply	0 rad. - 120 E - Glass	3.10×10^8	23511	3930	0.896×10^8	1937.59
Skin Inner Ply	$\pm \frac{\pi}{4}$ rad. PRD 49	1.93×10^8	6895	6895	0.241×10^8	1384.00
Skin Inner Ply	0 rad. PRD 49	13.79×10^8	75842	2068	1.034×10^8	1384.00
Fiberglass Doublers	$\pm \frac{\pi}{4}$ rad. - 120 E - Glass	1.572×10^8	11921	10611	0.517×10^8	1937.59
Aluminum Doublers	2024-T3 Aluminum Sheet	4.137×10^8	72395	27579	0.414×10^8	2767.99
Grip Plates	2014-T6 Aluminum Forging	4.482×10^8	72395	27579	0.414×10^8	2795.67
Inboard Attachment Fitting	7075 - T73 Aluminum Forging	4.550×10^8	68948	26200	0.414×10^8	2795.67
Mid Span Ballast Wt.	Naval Brass Forging	3.93×10^8	103421	39714	0.414×10^8	8414.69
Outboard Inertia Wt.	Tungsten	15.168×10^8	406791	156442	1.241×10^8	19375.93

* Prestressed damaged "endurance limit" and no crack propagation upper limit per crack propagation test data of reference

ΔF_{tu} (in fiber direction) = $20.684 \times 10^8 N/m^2$ (fiber less resin)

+ E (in fiber direction) = $22.063 \times 10^{10} N/m^2$ (fiber less resin)

7.1.2 Station 2.032(80) Analysis

Section Properties

The basic section properties for Station 2.032 (80) from Table 7-2 used in the stress analysis are:

$$EA = (77.91 \times 10^6 \text{ lb}) \cdot 346.6 \text{ N} \times 10^6$$

$$EI_{xx} = (33.68 \times 10^6 \text{ lb}) \cdot 0.0967 \times 10^6 \text{ N-m}^2$$

$$EI_{yy} = (2510.2 \times 10^6 \text{ lb-in}^2) \cdot 7.204 \times 10^6 \text{ N-m}^2$$

$$\bar{X}_{NA} = (5.212 \text{ in}) \cdot 0.1324 \text{ m from leading edge}$$

The basic dimensions and materials of the three prestressed tubes at Station 2.032 (80) are shown in Figure 7-7.

Ultimate Condition

The limit loads used in the ultimate condition stress analysis of Station 2.032 (80) are:

<u>Condition</u>	<u>CF</u> <u>N(lb)</u>	<u>M_x</u> <u>N-m (lb-in)</u>	<u>M_y</u> <u>N-m (lb-in)</u>
1	293,583(66,000)	2260(20,000)	28,811 (255,000)
2	293,583(66,000)	2260(20,000)	-5649 (-50,000)
3	489,304(110,000)	565(5,000)	33895 (300,000)
4	489,304(110,000)	565(5,000)	0

The ultimate loads are 1.5 times the above limit loads.

Station 2.032(80) ultimate condition stress for the four above loading conditions is summarized in Table 4-2 of Section 4.

TABLE 7-2 BLADE SECTION PROPERTIES, STA 2.032(80)

	A	E (10 ⁶)	EA (10 ⁶)	\bar{X} NA	EA X	EA ² X	EIO YY	EIO XX	ρ	W	W _X	\bar{X} CG
Skins	0.000319	30854	9.831	0.13288	1.301	0.172	0.06773	0.00560	1467	0.4680	0.0619	0.13228
	0.000469	30854	14.468	0.47976	6.941	3.332	0.20475	0.00358	1467	0.6880	0.3301	0.47976
Nose Wrap	0.000215	23580	5.075	0.08578	0.435	0.037	0.01622	0.00331	1384	0.2976	0.0255	0.08578
	0.000056	"	1.317	0.19723	0.260	0.051	0.00011	0.00061	"	0.0775	0.0153	0.19723
Spar Wrap	0.000045	"	1.059	0.05314	0.056	0.003	0.00006	0.00031	"	0.0623	0.0033	0.05314
	0.000129	"	3.043	0.12408	0.378	0.047	0.00304	0.00262	"	0.1785	0.0221	0.12408
	0.000055	"	1.292	0.19690	0.254	0.050	0.00011	0.00056	"	0.0761	0.0150	0.19690
Torsion												
Wrap	0.000088	"	2.066	0.06858	0.142	0.010	0.00057	0.00057	"	0.1218	0.0084	0.06858
	0.000107	"	2.534	0.12065	0.306	0.037	0.00107	0.00107	"	0.1481	0.0179	0.12065
	0.000107	"	2.534	0.17805	0.451	0.080	0.00107	0.00107	"	0.1481	0.0264	0.17805
Front Spar	0.000389	43989	17.113	0.06858	1.174	0.080	0.00414	0.00414	1605	0.6243	0.0428	0.06858
π rad.												
Wrap Next	0.000241	153064	36.834	0.06858	2.526	0.173	0.00707	0.00707	1605	0.3868	0.0265	0.06858
To Tube	0.000047	186158	8.743	0.06858	0.600	0.041	0.00148	0.00148	7889	0.3708	0.0254	0.06858
Mid Spar'	0.000483	43989	21.256	0.12065	2.564	0.309	0.00794	0.00795	1605	0.7752	0.0935	0.12065
	0.000306	153064	46.808	0.12065	5.647	0.681	0.01456	0.01456	1605	0.4991	0.0602	0.12065
	0.000061	186158	11.278	0.12065	1.361	0.164	0.00317	0.00317	7889	0.4812	0.0581	0.12065
Aft Spar'	0.000483	43989	21.256	0.17805	3.785	0.674	0.00794	0.00794	1605	0.7752	0.1380	0.17805
	0.000306	153064	46.808	0.17805	8.334	1.484	0.01456	0.01456	1605	0.4911	0.0874	0.17805
	0.000061	186158	11.278	0.17805	2.008	0.358	0.00317	0.00317	7889	0.4812	0.0857	0.17805
Nose Block	0.000898	75842	68.111	0.03269	2.226	0.073	0.33278	0.01331	1384	1.2428	0.0406	0.03269
2" Spline	0.000183	75842	13.847	0.65250	9.035	5.896	0.00212	0.00003	1384	0.2533	0.1653	0.65250
Nonex Core	0.015192								24.03	0.3651	0.1291	0.35372
Foam	0.002779								33.22	0.0923	0.0141	0.15324
Erosion												
Boot	0.000369								1467	0.5413	0.0352	0.06507
			346.561	0.13238	45.877	12.584	0.69366	0.09666		9.6457	1.5278	0.15839

$$EI_{YY} = \sum EA_x^2 + \sum EIO_{YY} - \sum EA (\bar{X}^2) = 12.584 + .69366 - 346.551 (.13238^2) = 7.204 \times 10^6$$

CHORDWISE STATIONS FROM L.E.

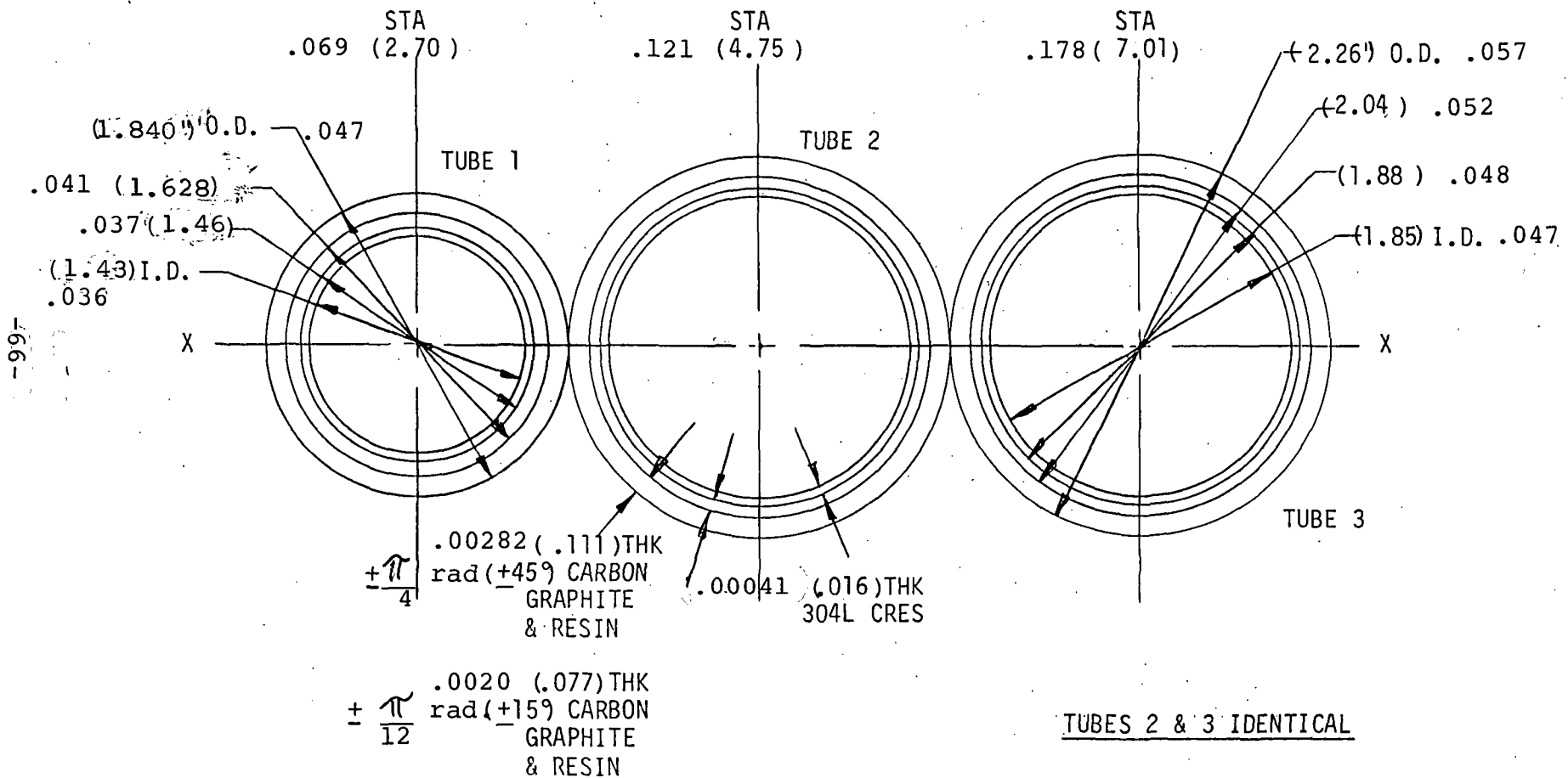


Figure 7-7 Tubes Basic Dimensions & Materials

Fatigue Condition

Fatigue loads for Station 2.032 (80) are:

$$CF = (90,000 \text{ lb.}) \quad 400,340\text{N}$$

$$M_x = (10,000 \pm 15,000 \text{ in-lb}) \quad 1130 \pm 1695\text{N-m}$$

$$M_y = (55,000 \pm 80,000 \text{ in-lb}) \quad 6214 \pm 9039 \text{ N-m}$$

Table 4-3 of Section 4 summarizes the results of the fatigue condition stress analysis for Station 2.032. All components show positive margins indicating infinite fatigue life.

7.1.3 Analysis of Stations 1.041 (41) through 1.27 (50)

Structural adequacy of this portion of the pre-stressed spar rotor blade is conservatively evaluated by using Station 1.27 section properties and Station 1.041 loads.

Station 1.27 section properties from Table 7-3 used in analysis are:

$$\begin{aligned} EA &= (141.1 \times 10^6 \text{ lb}) \quad 627.6 \times 10^6 \text{ N} \\ EI_{xx} &= (116.4 \times 10^6 \text{ lb-in}^2) \quad .334 \times 10^6 \text{ N-m}^2 \\ EI_{yy} &= (8129.5 \text{ lb-in}^2) \quad 23.33 \text{ N-m}^2 \end{aligned}$$

$$\bar{X}_{NA} = (8.159 \text{ in}) \quad .2072\text{m from leading edge}$$

Limit loads at Station 1.041 are:

Condition	CF N (lb)	Mx N-m (lb-in)	My N-m (lb-in)
1	334,506 (75,200)	6666 (59,000)	26,890 (238,000)
2	334,506 (75,200)	6666 (59,000)	-17,965 (-159,000)
3	540,459 (121,500)	1864 (16,500)	26,890 (238,000)
4	540,459 (121,500)	1864 (16,500)	-17,965 (-159,000)

TABLE 7-3 BLADE SECTION PROPERTIES, STA 1.27 (50)

	A	E (10 ⁶)	EA (10 ⁶)	\bar{X} NA	EA \bar{X} (10 ⁶)	EA \bar{X}^2 (10 ⁶)	EIo YY	EI XX	p	W	W X	\bar{X} C.G.
Clean Blade For 3"	-	-	346.551	0.13238	45.877	12.584	0.69366	0.09666	-	9.6457	1.5278	0.15839
Spline	0.000228	75842	17.272	0.62151	10.735	6.672	0.00092	0.00012	1383.995	0.3156	0.1961	0.62151
Alum Dblr.A												
1A	0.000272	72395	19.663	0.14130	2.778	0.393	0.11383	0.01308	2795.670	0.7604	0.1074	0.14130
2A	0.000060	72395	4.344	0.30322	1.317	0.399	0.00126	0.00321	"	0.1677	0.0508	0.30322
3A	0.000129	72395	9.341	0.62230	5.813	3.617	0.01256	0.00041	"	0.3606	0.2244	0.62230
Alum Dblr.B												
1B	0.000268	72395	19.430	0.14257	2.770	0.395	0.11059	0.01318	"	0.7492	0.1068	0.14257
2B	0.000050	72395	3.596	0.29814	1.072	0.320	0.00071	0.00289	"	0.1398	0.0417	0.29814
3B	0.000110	72395	7.940	0.63182	5.017	3.170	0.00770	0.00043	"	0.3075	0.1943	0.63182
Alum Dblr.C												
1C	0.000265	72395	19.336	0.14384	2.781	0.400	0.10741	0.01589	"	0.7464	0.1074	0.14384
2C	0.000033	72395	2.382	0.28989	0.690	0.200	0.00021	0.00230	"	0.0923	0.0268	0.28989
3C	0.000097	72395	7.006	0.63818	4.471	2.853	0.00518	0.00048	"	0.2712	0.1731	0.63818
Alum Dblr.D												
1D	0.000265	72395	19.196	0.14511	2.786	0.404	0.10428	0.01748	"	0.7408	0.1075	0.14511
2D	0.000023	72395	1.635	0.28481	0.466	0.133	0.00007	0.00177	"	0.0643	0.0183	0.28481
3D	0.000084	72395	6.072	0.64452	3.913	2.522	0.00345	0.00054	"	0.2348	0.1513	0.64452
Alum Dblr.E												
1E	0.000261	72395	18.916	0.14638	2.769	0.405	0.10122	0.01898	"	0.7297	0.1068	0.14638
2E	0.000058	72395	0.420	0.27656	0.116	0.032	0	0.00015	"	0.1621	0.0448	0.27656
Aluminum Check Plate	0.001057	72395	76.505	0.12700	9.716	1.234	0.25713	0.09610	"	2.9550	0.3753	0.12700
$\pm \frac{7}{4}$ rad. FG												
Dblr												
1	0.002845	11921	33.917	0.13299	4.511	0.600	0.26325	0.02371	1937.593	5.5124	0.7331	0.13299
2	0.004188	11921	49.922	0.47976	23.950	11.490	0.70642	0.02663	1937.593	8.1146	3.8931	0.47976
			627.637	0.20722	130.044	47.792	2.48986	0.33404		32.7765	8.1271	0.24795

$$EI_{YY} = \sum EA \bar{X}^2 + \sum EI_{YY} - \sum EA (\bar{X})^2 = 47.792 + 2.48986 - 627.537 (.20722^2) = 23.335 \times 10^6$$

Fatigue loads at Station 1.041 are:

$$CF = (100,000 \text{ lb}) 444,822N$$

$$M_x = (15,500 \pm 12,500 \text{ in-lb}) 1751^{+}1412m-N$$

$$M_y = (71,000 \pm 97,500 \text{ in-lb}) 8022^{+}11016m-N$$

Spar Attachment to Inboard Fitting

The metal spar tube ends were assumed to carry the above loadings in the redundant root end structure as a conservative approach. The load carrying capacity of the fiber overwrap in this area has been omitted and the beneficial effects of metal prestressing have been disregarded, which is also conservative. Figure 4-8 of Section 4 shows the spar ends design. All are similar except for basic diameters at Section A-A.

Section A-A (STA. 50) 1.27

Coordinates, areas, and moduli of elasticity for the critical sections of the three 304L stainless steel tubes at Station 1.27 are:

Tube No.	m	C _x (in.)	m	C _y (in.)	m ²	A _t (in ²)	$\frac{N}{m^2}$	E x 10 ⁻⁶ (psi)
1	.1387	(5.459)	.0186	(.732)	.0000470	(.0728)	186,158	(27.0)
2	.0866	(3.409)	.0239	(.942)	.0000606	(.0939)	186,158	(27.0)
3	.0292	(1.149)	.0239	(.942)	.0000606	(.0939)	186,158	(27.0)

Ultimate steel tube stresses, margins of safety, and equivalent axial tube loads for Section A-A are summarized in the following Table 7-4. Neglecting prestresses, the equivalent ultimate axial load of each tube is conservatively assumed to be:

$$P_u = A_t f_u \text{ ---- (7-5)}$$

TABLE 7-4

STATION 1.27 (50) TUBE ULTIMATE MARGINS OF SAFETY

Con- di- tion	$N/m^2 f_u$	Tube No. 1			Tube No. 2			MS_{u3}	N
		MS_{u1}	N	N/m^2	MS_{u2}	N	N/m^2		
1	2.97×10^8	3.40	13,950	3.100×10^8	3.22	18,780	2.915×10^8	3.49	17659
2	2.226×10^8	4.88	10,453	2.635×10^8	3.97	15,965	2.759×10^8	3.74	16712
3	3.140×10^8	3.17	14,750	3.056×10^8	3.28	18,514	2.871×10^8	3.56	17392
4	2.396×10^8	4.46	11,254	2.591×10^8	4.05	15,698	2.715×10^8	3.82	16445

Fatigue condition stresses, margins of safety in fatigue, and the equivalent axial fatigue load acting on each tube at Section A-A are:

Tube Number	$N/m^2 f$	MS_f	P_f
1	$2.384 \times 10^8 \pm 0.402 \times 10^8$	3.21	11201 ± 1890
2	$2.412 \times 10^8 \pm 0.397 \times 10^8$	3.26	14612 ± 2402
3	$2.357 \times 10^8 \pm 0.321 \times 10^8$	4.28	14279 ± 1944

The equivalent axial fatigue load is conservatively in the absence of prestress,

$$P_f = A_t f_f \text{ ---- (7-6)}$$

Ultimate and fatigue tube loads calculated above are assumed to act at both Sections B-B and C-C as defined in Figure 4-8 of Section 4.

Section B-B

The cross sectional area of each tube at Section B-B is:

$$A_t = \frac{\pi}{4} (.0127)^2 = .0001267m^2$$

The ultimate stresses, $f_u = P_u/A_t$, and margins of safety, $MS = F_u/f_u - 1$, for each tube at Section B-B are presented in Table 7-5. It is assumed that these portions of the tubes will not be fully work-hardened. The ultimate tensile strength allowed, therefore, is $620.5 \times 10^6 \frac{N}{m^2}$

TABLE 7-5						
SECTION B-B ULTIMATE MARGINS OF SAFETY						
Condi- tion	Tube No. 1		Tube No. 2		Tube No. 3	
	f_u N/m ² (psi)	MS UL	N/m ² (psi)	MS u2	N/m ² (psi)	MS u3
1	1.103×10^8 (16000)	4.63	1.485×10^8 (21541)	3.18	1.396×10^8 (20255)	3.44
2	0.827×10^8 (11990)	6.51	1.262×10^8 (18311)	3.92	1.322×10^8 (19168)	3.70
3	1.166×10^8 (16918)	4.32	1.464×10^8 (21235)	3.24	1.375×10^8 (19949)	3.51
4	0.890×10^8 (12908)	5.97	1.241×10^8 (18005)	4.00	1.300×10^8 (18862)	3.77

Fatigue stresses and their respective margins of safety for each tube at Section B-B are given below. A conservative endurance limit of $124.1 \times 10^6 \text{ N/m}^2$ has been used for this annealed region.

Tube Number	f_f N/m ²	f_f (psi)	MS _f
1	$88.439 \times 10^6 \pm 14.927 \times 10^6$	(12827 [±] 2165)	6.13
2	$115.38 \times 10^6 \pm 18.967 \times 10^6$	(16735 [±] 2751)	4.33
3	$112.68 \times 10^6 \pm 15.348 \times 10^6$	(16343 [±] 2226)	5.61

Section C-C

The results of a simplified ultimate lug analysis are presented in the following table. Maximum ultimate loads derived from the four limit loading conditions in Table 7-4 are used with the following areas and equations:

$$\text{Tensile Area, } A_t = (.0381 - 0.01905) (.01905) = .0003629\text{m}^2$$

$$\text{Shear Area, } A_s = 2(.01905) (.01905) = 0.0007258\text{m}^2$$

$$\text{Bearing Area, } A_{br} = (.01905) (.01905) = 0.0003629\text{m}^2$$

$$F_{tu} = P_u / A_t, MS_{tu} = (F_{tu} / f_{tu}) - 1, f_{su} = P_u / A_s, MS_{su} = (F_{su} / f_{su}) - 1,$$

$$f_{bru} = P_u / A_{br}, \text{ and } MS_{bru} = (F_{bru} / f_{bru}) - 1$$

Allowable ultimate stresses are: $F_{tu} = 620.53 \times 10^6 \text{ N/m}^2$, $F_{su} = 372.32 \times 10^6 \text{ N/m}^2$
and $F_{bru} = 1379 \times 10^6 \text{ N/m}^2$

Table 7-6 summarizes margins of safety at Sections C-C:

TABLE 7-6
SECTION C-C ULTIMATE MARGINS OF SAFETY

Tube Number	P_u N	f_{tu} N/m ²	MS_{tu}	f_{su} N/m ²	MS_{su}	f_{br} N/m ²	MS_{br}
1	14,750	40.679×10^6	14.25	20.326×10^6	17.3	40.679×10^6	Ample
2	18,780	51.793×10^6	10.98	25.876×10^6	13.4	51.793×10^6	Ample
3	17,659	48.705×10^6	11.74	24.332×10^6	14.3	48.705×10^6	Ample

Fatigue stresses in the lug at Section C-C are also low, giving high margins of safety. Therefore, this condition was not evaluated further.

7.1.4 Inboard Attachment Fitting

Material 7075-T73

aluminum forging. Stresses in the aluminum inboard fitting for both the ultimate and fatigue conditions are considerably lower than are those in the tube clevis. No formal stress analysis is presented for this component.

7.2 Appendix 2 - Prestressed Composite Spar Tube Structural Analysis

7.2.1 Stiffness and Stresses

7.2.1.1 Prestressed Composite Spar Tube Bending Stiffness

Figure 7-8 shows a sketch of a fiber strain, ϵ_f , produced by metal hoop and longitudinal strains, ϵ_θ and ϵ_x , respectively.

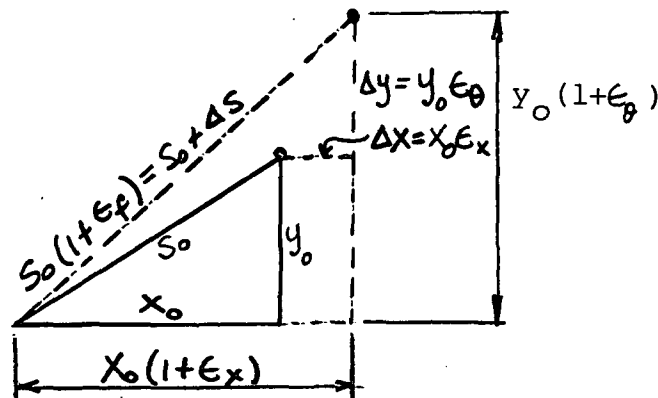


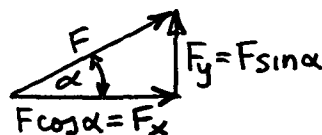
Figure 7-8 Fiber Strain Due to Bending

Noting that
$$\left[x_0 (1 + \epsilon_x) \right]^2 + \left[y_0 (1 + \epsilon_\theta) \right]^2 = \left[s_0 (1 + \epsilon_f) \right]^2$$

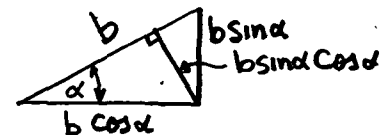
and $x_0/s_0 = \cos \alpha$, $y_0/s_0 = \sin \alpha$, we have (retaining only the first order terms in strains) the relation between fiber and metal strains,

$$\epsilon_f = \epsilon_x \cos^2 \alpha + \epsilon_\theta \sin^2 \alpha \quad \dots (7-7)$$

Fiber force and cross-sectional width components are sketched on Figure 7-9, a and b.



(a) Fiber Force Components



(b) Fiber Width Components

Figure 7-9 Fiber Forces and Widths

We then have,

$$\sigma_f = \text{Fiber Stress} = \text{Fiber Force/Fiber Area} =$$

$$\sigma_f = \frac{\text{Fiber Force}}{\text{Fiber Width} \times \text{Thickness}} = \frac{F}{(b \sin \alpha \cos \alpha) t_f} \dots (7-8)$$

$$\sigma_{fx} = \text{Longitudinal Fiber Stress Component} = \frac{F \cos \alpha}{(b \sin \alpha) t_f} \dots (7-9)$$

From (7-8) and (7-9),

$$\sigma_{fx} = \sigma_f \cos^2 \alpha \dots (7-10)$$

Similarly,

$$\sigma_{fo} = \text{Hoop Fiber Stress Component} = \frac{F \sin \alpha}{(b \cos \alpha) t_f} = \sigma_f \sin^2 \alpha \quad (7-11)$$

Treating shaft as narrow beam, i.e., taking Poissons Ratio = 0 corresponding to hoop strain $\epsilon_o = 0$, we have from (7-7) and (7-10) utilizing Hookes Law,

$$\sigma_{fx} = \sigma_f \cos^2 \alpha = (E_f \epsilon_f) \cos^2 \alpha = (E_f \cos^4 \alpha) (\epsilon_x) \dots (7-12).$$

Taking the bending strain (proportional to the bending curvature K) as linear with the thickness coordinate Z, we have the metal and fiber bending stresses,

$$\begin{aligned} \sigma_{Mb} &= E_M \epsilon_x = E_M KZ \\ \sigma_{fb} &= \sigma_{fx} = E_f \cos^4 \alpha KZ \end{aligned} \dots (7-13)$$

Since both the metal and fibers resist part of the total moment, we have the differential moments,

$$dM = dM_f + dM_M = \sigma_{fb} Z (dA_f) + \sigma_{Mb} Z (dA_M)$$

Using (7-13) and integrating yields, the total moment resisted by the composite spar tube,

$$M_C = \int dM = K \left[E_f \cos^4 \alpha \int Z^2 dA_f + E_M \int Z^2 dA_M \right]$$

Noting that the integrals represent fiber and metal moments of inertias, we have the composite bending stiffness, k_{bc} , as

$$\frac{M}{K} = k_{bc} = (E_f \cos^4 \alpha) I_f + E_M I_M = k_{bf} + k_{bM} \dots (7-14)$$

The first term represents the fiber bending stiffness and the second term is the metal bending stiffness. For thin-walled cross-sections, the moments of inertia are very closely proportional to the thickness times the cube of the diameter. We then obtain from (7-14) for a cross-section consisting of j fibers of thickness t_{fj} and wrap angle α_j , plus a metal element of thickness t_M , the bending stiffness ratios,

$$\frac{k_{bc}}{k_{bM}} = 1 + \frac{k_{bf}}{k_{bM}} = 1 + \sum_{j=1}^n \left(\frac{E_{fj} \cos^4 \alpha_j}{E_M} \right) \left(\frac{t_{fj}}{t_M} \right) \left(\frac{D_{fj}}{D_M} \right)^3 \dots (7-15)$$

For a thin-walled metal circular cylindrical tube of diameter and thickness D_M and t_M respectively, we have (Ref. 11),

$$k_{bM} = E_M I_M \approx (E_M) \frac{\pi}{8} D_M^3 t_M \dots (7-16)$$

From (7-13) and (7-14), we have after simplification the metal and fiber bending stress relation, .

$$\sigma_{Mb} = \left(\frac{M_C Z}{I_M} \right) \left(\frac{1}{1 + \frac{k_{bf}}{k_{bM}}} \right) = \sigma_{fbj} \left(\frac{E_M}{E_{fj} \cos^4 \alpha_j} \right) \equiv \sigma_{fx} \left(\frac{E_M}{E_{fj} \cos^4 \alpha_j} \right) \dots (7-17)$$

where, maximum $Z \equiv C_M$ = metal extreme fiber distance from the neutral axis.

43E

7.2.1.2 Prestressed Composite Spar Tube Torsional Stiffness

Figure 7-10 is a sketch of a fiber before and after being twisted* through an angle of twist per unit length, θ , due to an applied torque, T .

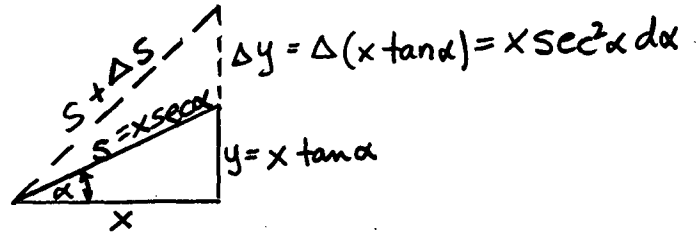


Figure 7-10 - Fiber Strain Due to Torsion

Noting that $[y + \Delta y]^2 + x^2 = [S + \Delta S]^2$, $\sin \alpha = y/S$ and $x^2 + y^2 = S^2$, we find (after neglecting squares of infinitesimals) that the fiber strain is,

$$\epsilon_f = \frac{\Delta L}{S} = \frac{(\Delta y) \sin \alpha}{S} = \frac{x \sec^2 \alpha d\alpha \sin \alpha}{x \sec \alpha} = \tan \alpha (d\alpha) \dots (7-18)$$

From geometry for cylinder of radius R_f we have,

$\Delta y = x \sec^2 \alpha (d\alpha) = R_f (x\theta)$ or, fiber angle change due to twist per unit length θ is,

$$d\alpha = R_f \theta \cos^2 \alpha \dots (7-19)$$

From Hooke's Law, the fiber stress due to twist is then,

$$\sigma_f = E_f \epsilon_f = E_f \tan \alpha (d\alpha) = E_f (R_f \theta) \sin \alpha \cos \alpha \dots (7-20)$$

If ΔS is the fiber differential arc length (width) along the circle of radius R_f , the elemental fiber area, dA_f (normal to the fiber force) is thus,

$$dA_f = (\Delta S \cos \alpha) t_f$$

as can be seen from the sketch of Figure 7-11.

* One fiber of a pair is elongated by angle change $(+d\alpha)$ and other fiber is shortened by angle change $(-d\alpha)$ due to applied torque.

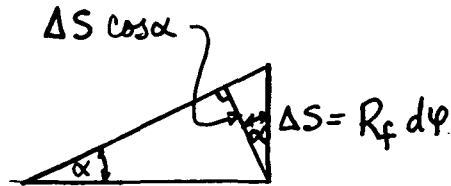


Figure 7-11 - Fiber Width

Now from (7-20) and above, one has the differential fiber force,

$$dF_f = \sigma_f dA_f = E_f R_f \theta \sin \alpha \cos^2 \alpha t_f \Delta S = \theta E_f t_f R_f^2 \sin \alpha \cos^2 \alpha d\varphi$$

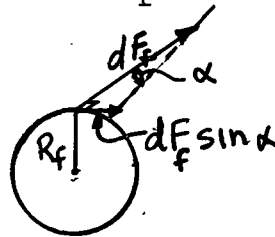


Figure 7-12 - Differential Fiber Force

The differential fiber resisting torque, dT_f , due to dF_f is then (see Figure 7-12)

$$dT_f = R_f dF_f \sin \alpha = \theta E_f t_f R_f^3 \sin^2 \alpha \cos^2 \alpha d\varphi$$

Integrating between $\varphi = 0$ and 2π gives the total fiber resisting torque and fiber torsional stiffness, k_{Tf} , as

$$\frac{T_f}{\theta} = k_{Tf} = E_f 2\pi R_f^3 t_f \sin^2 \alpha \cos^2 \alpha = E_f D_f^3 \frac{\pi}{4} t_f \sin^2 \alpha \cos^2 \alpha \dots (7-21)$$

Neglecting the effect of axial stresses, the metal torsional stiffness (Ref.11) is,

$$k_{TM} = \frac{T_M}{\theta} = G_M J_M = \frac{E_M}{2(1+\nu)} \times \frac{\pi D_M^3}{4} t_M = \frac{E_M}{2.46} \times \frac{\pi D_M^3}{4} t_M \dots (7-22)$$

Since the metal and fibers both resist the applied torque,

$$T = T_c = T_M + T_f \quad \text{or}$$

$$\frac{T_c}{\theta} = k_{Tc} = \frac{T_M}{\theta} + \frac{T_f}{\theta} = k_{TM} + k_{Tf}$$

For j fibers and one (1) metal element the torsional stiffness ratios are then,

$$\frac{k_{Tc}}{k_{TM}} = 1 + \frac{k_{Tf}}{k_{TM}} = 1 + \sum_{j=1}^n (2.6) \left(\frac{E_{fj}}{E_M} \right) \sin^2 \alpha_j \cos^2 \alpha_j \left(\frac{t_{fj}}{t_M} \right) \left(\frac{D_{fj}}{D_M} \right)^3 \dots \quad (7-23)$$

7.2.1.3 Prestressed Composite Spar Tube Axial Stiffness

Axial equilibrium with applied CF force F , pounds per unit of tube circumference, requires,

$$\sigma_{fx} t_f + \sigma_{Mx} t_M = F \quad \dots (7-24)$$

Noting that $\sigma_{Mx} = E_M \epsilon_x$ and using equation (7-12), we find from (7-24) that

$$\frac{\sigma_{Mx} t_M}{F} = \frac{E_M t_M}{E_f \cos^4 \alpha t_f + E_M t_M} = \frac{k_{Ma}}{k_{fa} + k_{Ma}} = \frac{k_{Ma}}{k_{ca}} \quad \dots (7-25)$$

$$\frac{\sigma_{fx} t_f}{F} = \frac{E_f \cos^4 \alpha t_f}{E_f \cos^4 \alpha t_f + E_M t_M} = \frac{k_{fa}}{k_{fa} + k_{Ma}} = \frac{k_{fa}}{k_{ca}} \quad \dots (7-26)$$

$$k_{ca} = \frac{F}{\epsilon_x} = k_{fa} + k_{Ma} = E_f \cos^4 \alpha t_f + E_M t_M \quad \dots (7-27)$$

7.2.2 Composite Spar Tube Prestresses

The sketch of Figure 7-13 defines the metal longitudinal and hoop initial stresses (prestresses) σ_{Mxi} and σ_{Mei} , respectively, as well as the initial stress in the j^{th} fiber at helix angle α_j . Consider a two (2) fiber system ($j = 1, 2$) where fiber and metal thicknesses and fiber helix angles are; t_{f1} , t_{f2} , t_M , α_1 , and α_2 , respectively. If σ_{f1i} and σ_{f2i} are the fiber initial stresses in fibers 1 and 2, longitudinal and hoop equilibrium at zero external load require,

$$\sigma_{f1} \cos^2 \alpha_1 t_{f1} + \sigma_{f2} \cos^2 \alpha_2 t_{f2} + \sigma_{Mxi} t_M = 0 \quad \dots (7-28)$$

$$\sigma_{f2} \sin^2 \alpha_1 t_{f1} + \sigma_{f2} \sin^2 \alpha_2 t_{f2} + \sigma_{Mei} t_M = 0 \quad \dots (7-29)$$

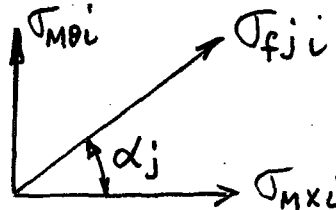


Figure 7-13 - Sketch, Fiber and Metal Initial Stresses

For Ak-76 Design:

$$\alpha_1 = \frac{\pi}{12} \quad \cos^2 \frac{\pi}{12} = .9330, \quad \sin^2 \frac{\pi}{12} = .0670$$

$$\alpha_2 = \frac{\pi}{4} \quad \cos^2 \frac{\pi}{4} = .5000, \quad \sin^2 \frac{\pi}{4} = .5000$$

$$t_{f1} = \frac{.00196}{\text{Volume Ratio}} = \frac{.00196}{1.45} = .00135m \text{ (fiber less resin thickness)}$$

$$t_{f2} = \frac{.00282m}{1.45} = .00194m, \quad t_M = .000406m$$

Substituting numerical values into equations

(7-28) and (7-29) gives,

$$3.091 \sigma_{f1} + 2.406 \sigma_{f2} = -\sigma_{Mxi} \quad \dots (7-30)$$

$$0.222 \sigma_{f1} + 2.406 \sigma_{f2} = -\sigma_{Mei} \quad \dots (7-31)$$

Solving simultaneously yields,

$$\sigma_{fli} = - .3486 \sigma_{Mxi} - \sigma_{Mei} \quad \dots (7-32)$$

$$\sigma_{f2i} = .03216 \sigma_{Mxi} - .4478 \sigma_{Mei} \quad \dots (7-33)$$

Using equation 7-1 together with station 2.032 (80)

section properties and limit loads, one computes with prestress $\sigma_{fi} = 0$, a maximum tube axial tensile stress of $348.9 \frac{MN}{m^2}$ (tube No. 2). Here, the 1.5 factor of equation 7-1 has been changed to 1.0, corresponding to the operating condition. Choose then metal tube axial compressive prestress, $\sigma_{Mxi} = -358.5 \frac{MN}{m^2}$ provides a net compressive stress in all the metal tubes under operating conditions, thereby suppressing crack growth and increasing ballistic resistance and operating life.

Select also metal hoop compressive prestress,

$\sigma_{Mei} = -137.9 \frac{MN}{m^2}$. Substituting the above values of σ_{Mxi} and σ_{Mei} in (7-32) and (7-33) one obtains the fiber tensile prestresses,

$$\sigma_{fli} = 76.9 \frac{MN}{m^2} \quad (\pm \pi/12 \text{ fibers})$$

$$\sigma_{f2i} = 50.2 \frac{MN}{m^2} \quad (\pm \pi/4 \text{ fibers})$$

The axial components of the fiber prestresses are,

$$\sigma_{flxi} = \sigma_{fli} \cos^2 \alpha_1 = 76.9 \times .933 = 71.8 \frac{MN}{m^2}$$

$$\sigma_{f2xi} = \sigma_{f2i} \cos^2 \alpha_2 = 50.2 \times .5 = 25.1 \frac{MN}{m^2}$$

Net fiber tensions are thus maintained even if the CF operating stresses shown in Table 4-2 are substantially reduced. All fibers are thus always fully effective in providing stiffness and load resisting capability with minimum need for shear transfer in the resin.

The prestresses are imparted by means of a two (2) stage cryogenic stretchforming fabrication sequence as discussed in Section 4.3. Relatively large cryogenic hoop plastic strain is imparted to the metal in the first stretch operation in order to substantially strengthen the metal. The small $\pm \frac{\pi}{12}$ fiber wrap helix angle permits this large hoop straining without exceeding the 1% strain to rupture limitation of the HTS graphite fibers. The second cryogenic stretch operation subsequent to overwrapping the outer $\pm \frac{\pi}{4}$ HTS graphite fibers is accomplished at a relatively small metal plastic strain magnitude.

7.3 Appendix 3 - Prestressed Composite Liner Buckling Data

7.3.1 Simplified Buckling Considerations

Buckling loads for a fiber overwrapped prestressed member (liner) are much higher than would be predicted by classical theory for buckling of the "unwrapped" liner. The interaction of the fibers and the liner results in local "inward cusp-like" buckling mode shapes quite different from the outward and inward "classical" buckling mode shapes. These "cusp" shapes require much higher buckling loads than classical theory would predict. Test data on prestressed composite pressure vessels (spheres and cylinders) and for actual prestressed spars on previous NASA-ARMY programs (Reference 5,6) verify this. Significantly higher (many orders of magnitude higher) buckling loads have been observed. As a "first cut estimate" of buckling load improvement, we will utilize composite prestressed structure data in an oversimplified way. Additional test data will help define the maximum improvements that can be achieved with prestressed composite construction.

A prestressed composite spar liner was subjected to bending and compression (Ref. 6) as follows:

$$\left\{ E \frac{t}{r} \text{ was } 1565 \times 10^6 \frac{\text{N}}{\text{m}^2} \right\}$$

a) Liner Did Not Buckle:

$$\text{Direct compression, } R_c = \frac{\sigma_{\text{direct}}}{\sigma_{\text{cr}}} = 1.43 =$$

$$\frac{268.9 \times 10^6}{10^6 \times 1565C} \quad \begin{array}{l} \text{Buckling} \\ \text{Coefficient} \end{array}$$

$$\text{Bending, } R_b = \frac{\sigma_{\text{bending}}}{\sigma_{\text{cr}}} = 1.25 = \frac{234.4 \times 10^6}{1565C \times 10^6}$$

From Ref. 11,

$$\text{M.S.} = \frac{1}{R_b + R_c} - 1 = 0 \quad \begin{array}{l} \text{(Theoretical} \\ \text{Buckling Limit)} \end{array}$$

or,

$$C = \frac{268.9 + 234.4}{1565} \approx \frac{1}{3} \quad (\text{value of } C \text{ used was } .12)$$

So one would predict a minimum buckling load increase of .33 or about 3 .
.12

- b) The liner was severely overloaded (factor of 3 in bending) and Plastic Buckle occurred with local "cusp-like" buckle shape observed. This data, together with cylinder data, can be used to estimate the order of magnitude of the maximum buckling load increase.

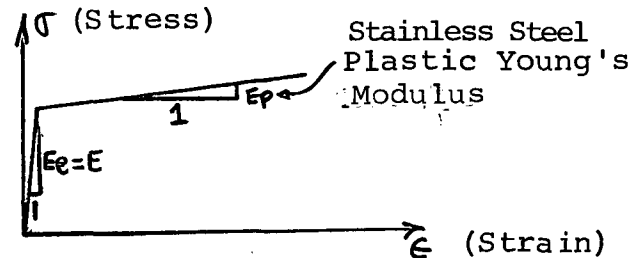


Figure 7-14 Idealized Stress-Strain Curve

Buckling relation of the form, $\sigma_{cr} = C E_p \frac{t}{r}$ for both direct compression and bending (Ref. 11).

$$R_c = \frac{268.9 \times 10^6}{C \frac{E_p}{E} \times 1565 \times 10^6}; \quad R_b = \frac{(3 \times 234.4 = 703.2)}{C \frac{E_p}{E} \times 1565}$$

$$M.S. = 0 = \frac{1}{R_b + R_c} - 1 = \frac{1}{(-703.2 + 268.9) / 1565 C \frac{E_p}{E}}$$

or,

$$C = \frac{(703.2 + 268.9)}{1565 \frac{E_p}{E}}; \quad C = .62 \frac{E}{E_p} \text{ as maximum effective buckling coefficient}$$

$$\left\{ \begin{array}{l} \text{used } C \approx .12 \\ \frac{.62}{.12} \approx 5 \end{array} \right\}$$

47B

then approximately,

$$3 < \frac{(\sigma_{cr})}{(\sigma_{cr})} \begin{array}{l} \text{prestressed composite} \\ \text{classical theory} \end{array} < 5 \frac{E}{E_p}$$

Now (Figure 7-14)

$$\frac{E}{E_p} \approx 20 \rightarrow 50 \text{ then,}$$

$$3 < \frac{(\sigma_{cr})}{(\sigma_{cr})} \begin{array}{l} \text{prestressed composite} \\ \text{classical theory} \end{array} < \begin{array}{l} 100 \text{ to} \\ 250 \text{ } \\ \text{(Plastic} \\ \text{Buckle)} \end{array}$$

based on shallow angle ($\pi/12$ - $\pi/9$)
prestressed composite spar data.

- c) NASA LRC Data on Fiber Overwrapped Cylinders
(Ref. 10) ($\alpha = \pi/2$ - Hoop Wrap) see Fig. 7-15
Herein.

$$\frac{\sigma_{cr} \text{ (prestressed fiber = } 150,000 \left(\frac{t}{D}\right)^3 = 136.5 \times 10^3 \left(\frac{t}{D}\right)^3}{\sigma_{cr} \text{ Classical Cylinder } \left(\frac{1}{.91}\right) \left(\frac{t}{D}\right)^2}$$

$$\text{our } t_{M/D} \approx \frac{.0004064}{.0475} = 8.6 \times 10^{-3}$$

$$\text{Then, } \frac{\sigma_{cr} \text{ prestressed overwrapped}}{\sigma_{cr} \text{ classical}} =$$

$$136.5 \times 10^3 \times 8.6 \times 10^{-3}$$

$$\frac{\sigma_{cr} \text{ overwrapped prestressed}}{\sigma_{cr} \text{ classical}} \approx 1174 \text{ say } 1170$$

predicated on 90°
hoop wrap data

485

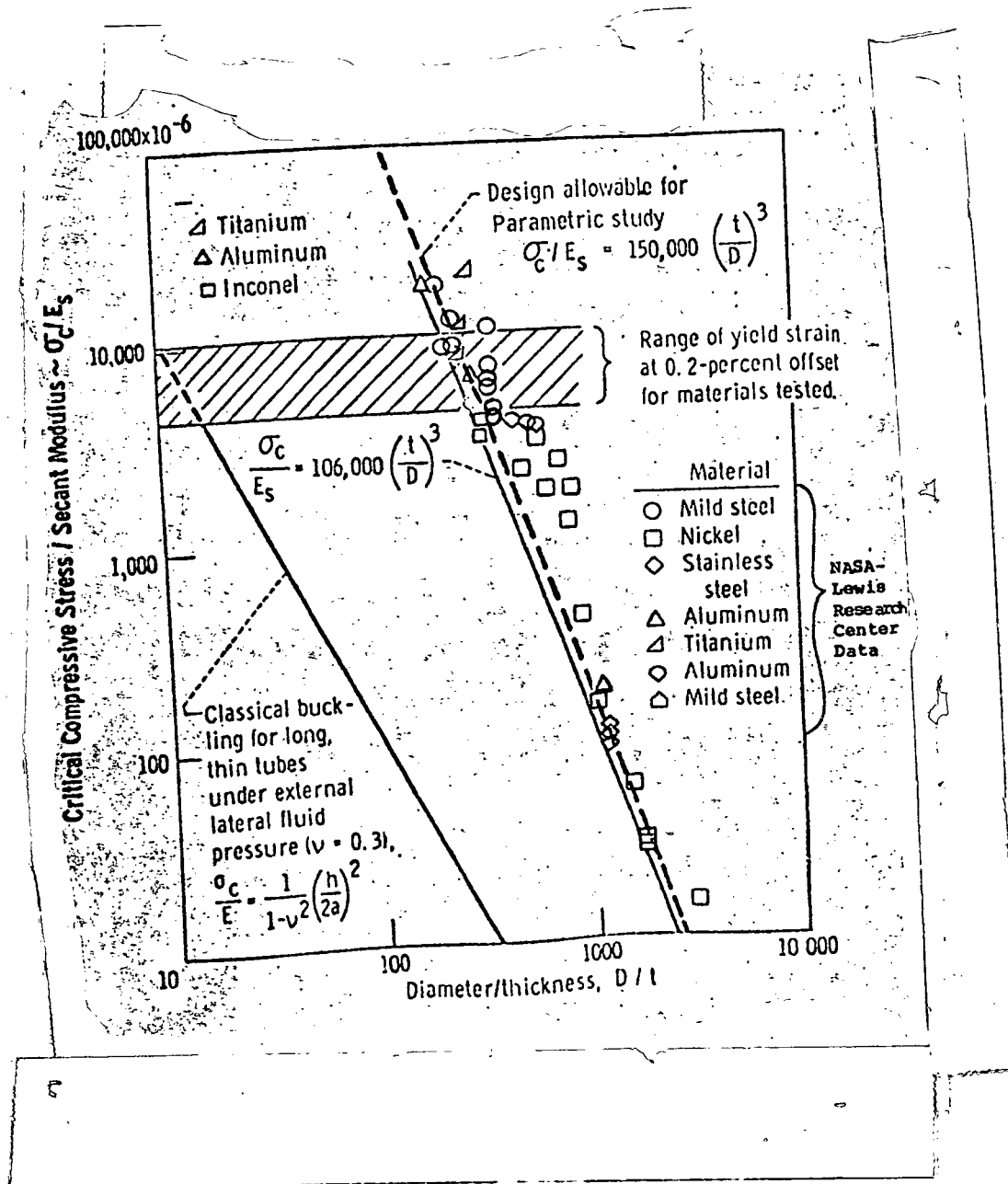


Figure 7-15 - Constrictive-Wrap Buckling Strengths for Cylindrical Tubes

- d) Based on Item (a) \rightarrow (c) analysis and test data, we would project buckling load increases of the order of
- 3 $\left\langle \begin{array}{l} (\sigma_{cr}) \text{ prestressed composite} \\ \sigma_{cr} \text{ classical theory} \end{array} \right\langle \begin{array}{l} 100 \text{ to } 250 \text{ plastic} \\ \text{buckle} \\ 1170 \text{ elastic} \\ \text{buckle} \end{array}$
- e) For preliminary design estimates therefore, say conservatively take buckling load improvement ≈ 10 to 15 (for bending and/or axial compression of long cylindrical shapes). Use Figure 7-15 for buckling due to hoop fiber bearing pressure. Assume the same order of improvement factors hold for very long prestressed cylinders, which in the absence of the pretensioned fiber overwrap, would "attempt" to buckle in the classical Euler type instability mode. Test data are needed to determine the precise magnitude of the buckling load improvement factors for this length range. Such test data could be obtained from the fabricated spar hardware utilized on the follow on program recommended in Section 5 herein.

7.3.2 Buckling Checks of AK-76 Design Point

The critical design condition is in "as fabricated" tube state (zero external load condition) since there is no CF tension help and tube fiber ties as well as tube bundle fiber overwraps and support fittings are not yet in place.

- a) Check as Long Cylinder (classisical diamond buckle pattern unprestressed and unwrapped)

$$\sigma_{cr}' \approx .12 \frac{Et}{r} \quad (\text{axial compression})$$

For Tube #1,

$$\sigma_{cr}' \approx .12 \times 186.16 \times 10^9 \times \frac{.0004064}{.01839} = 493.7 \times 10^6 \frac{N}{m^2}$$

$$\sigma_{cr} = \sigma_{cr}' \text{ times improvement factor}$$

$$\sigma_{cr} = (10) \times 493.7 \times 10^6$$

$$MS = \frac{\sigma_{cr}}{\sigma_{direct}} - 1 = \frac{493.7 \times 10^6 \times (10)}{344.7 \times 10^6} = \text{large}$$

b) Check as "Euler Type" Instability

①	②	③	④	⑤	⑥	⑦	⑧	⑨	⑩	⑪ =
t_M	\bar{D}_M	\bar{D}_{fj}	t_{fj}	α_j	$\cos^4 \alpha_j$	$E \times 10^{-6}$	$10^{-6} \times \left(\frac{\bar{D}_{fj}}{\bar{D}_M} \right)$	$\frac{t_{fj}}{t_M}$	$\frac{t_{fj}}{t_M}$	$\frac{k_{fjb}}{k_{Mb}} = \frac{⑦ \times ⑥ \times ⑨ \times ⑩}{⑧}$
.00041	0.03678	0.0391	0.00135	$\pi/12$.87	220632	186158	1.205	3.313	4.116
		0.0439	0.0020	$\pi/4$.25	220632		1.702	4.813	2.427
										6.543

(Ref. Section 7.2)

$$k_{Mb} = E_M I_M = 186.16 \times 10^9 \times \frac{\pi}{8} (.03678)^3 \times .0004064 = 1478 \text{ N-m}^2$$

$$k_c = (EI)_c = 7.543 \times 1478 = 11,149 \text{ N-m}^2$$

Assuming that simply supported Euler column equation applies without fiber wrap influence on buckling mode shape,

$$P_{cr} = \frac{\pi^2}{L^2} \times (EI)_c = \frac{\pi^2}{(5.334)^2} \times 11,149 = 3867 \text{ N}$$

$P_{cr} = 3867$ times improvement factor

Projecting a buckling load improvement factor of $\frac{(2 \times 10)}{3}$ due to influence

of the fiber wrap on the buckling mode shape we have then,

$$P_{cr} = \frac{20}{3} \times 3867 = 25,780 \text{ N}$$

Direct axial prestress is,

$$F_x = \sigma_{Mxi} \times A_M = 358.5 \times 10^6 \times 2\pi \times .01839 \times .0004064 = 16,835N$$

$$MS = \frac{P_{cr}}{F_x} - 1 = \frac{25780}{16,835} - 1 > 0, \text{ O.K.}$$

50F

8.0 REFERENCES

- 1) Meredith, Seiferth and Rummel: A Graphite/Epoxy Compression Panel for the Space Shuttle. Society of Aerospace Material and Process Engineers, Space Shuttle Materials, Vol. 3, National SAMPE Technical Conference, Oct. 5-7, 1971, Huntsville, Alabama, pp. 99-110.
- 2) Lager, J.R.: Composite Space Shuttle Engine Support Structure. Society of Aerospace Materials and Process Engineers, Space Shuttle Materials, Vol. 3, National SAMPE Technical Conference, Oct. 5-7, 1971, Huntsville, Alabama, pp. 149-156.
- 3) Gleich, D.: Cryogenically Formed Prestressed Fiber-Metal Structures for O₂/H₂ High Pressure Gas Tanks. Society of Aerospace Materials and Process Engineers, Space Shuttle Materials, Vol. 3, National SAMPE Technical Conference, Oct. 5-7, 1971, Huntsville, Alabama, pp. 527-547.
- 4) Gleich, D. : Development of a Filament Overwrapped Cryoformed Pressure Vessel. (ARDE, INC.; NASA Contract NAS 3-11194.) NASA CR-72753, 1971.
- 5) Gleich, D.: Final Report, Feasibility Study of Applying an Advanced Composite Structure Technique to the Fabrication of Helicopter Rotor Blades. (ARDE, INC.; NASA Contract NAS1-10028.) NASA CR-112191, 1972.
- 6) Gleich, D.: Final Report, Fabrication and Testing of Prestressed Composite Rotor Blade Spar Specimens. (ARDE, INC.; NASA Contract NAS1-11594.) NASA CR-132611, 1974.
- 7) Maloney, P., et al: Preliminary Design Study of an Improved Blade for AH-1Q Helicopter. Tech. Report R-1314, Kaman Aerospace Corp., 1975.
- 8) Gravely, A.: Structural Analysis of 540-011 Hub and Blade Assembly for Model 209/AH-1G Helicopter. Tech. Data Report 209-099-067, Bell Helicopter Co., 1967.

- 9) Gleich, D.: Six-Foot Diameter Multicycle Metallic Diaphragms for Subcritical Cryogenic Fluid Storage and Expulsion. ARDE, INC.; USAF Contract AF33 (615)-2827. Technical Report AFAPL-TR-70-95, 1971.
- 10) Johns & Kaufmann: Filament Overwrapped Cylindrical Pressure Vessels. NASA TMX-52171, 1966.
- 11) Bruhn: Analysis and Design of Flight Vehicle Structures, Tri-State Offset Company, 1965.
- 12) Kaman Aerospace Corp.: Development Program for Field-Repairable/Expendable Main Rotor Blades. USAA MRDL-TR-76-9, 1976.
- 13) MIL-HDBK-5B, Military Standardization Handbook, Metallic Materials and Elements for Aerospace Vehicle Structures, 1971.

NASA Contractor Report 159086

Distribution List

NAS1-13816

No.
Copies

NASA Langley Research Center Hampton, VA 23665 Attn: Report and Manuscript Control Office, Mail Stop 180A Technology Utilization Office, Mail Stop 139A Dr. Felton D. Bartlett, Jr., Mail Stop 266	1 1 10
NASA Ames Research Center Moffett Field, CA 94035 Attn: Library, Mail Stop 202-3	1
NASA Dryden Flight Research Center P. O. Box 273 Edwards, CA 93523 Attn: Library	1
NASA Goddard Space Flight Center Greenbelt, MD 20771 Attn: Library	1
NASA Lyndon B. Johnson Space Center 2101 Webster Seabrook Road Houston, TX 77058 Attn: JM6/Library	1
NASA Marshall Space Flight Center Marshall Space Flight Center, AL 35812 Attn: Library, AS61L	1
Jet Propulsion Laboratory 4800 Oak Grove Drive Pasadena, CA 91103 Attn: Library, Mail 111-113	1
NASA Lewis Research Center 21000 Brookpark Road Cleveland, OH 44135 Attn: Library, Mail Stop 60-3	1
NASA John F. Kennedy Space Center Kennedy Space Center, FL 32899 Attn: Library, NWSI-D	1
National Aeronautics and Space Administration Washington, DC 20546 Attn: RTM-6	1

No.
Copies

NASA Scientific and Technical Information Facility
6571 Elkridge Landing Road
Linthicum Heights, MD 21090

29 plus
original

1. Report No. NASA CR-159086		2. Government Accession No.		3. Recipient's Catalog No.	
4. Title and Subtitle FINAL REPORT DESIGN STUDY OF PRESTRESSED ROTOR SPAR CONCEPT				5. Report Date JAN 1980	
				6. Performing Organization Code	
7. Author(s) D. GLEICH				8. Performing Organization Report No. 41005	
9. Performing Organization Name and Address ARDE, INC. 19 Industrial Avenue Mahwah, New Jersey 07430				10. Work Unit No.	
				11. Contract or Grant No.	
12. Sponsoring Agency Name and Address NATIONAL AERONAUTICS AND SPACE ADMINISTRATION Langley Research Center Hampton, Virginia 23665				13. Type of Report and Period Covered Contractor Report	
				14. Army Project No. AVRADCOM Structures Laboratory	
15. Supplementary Notes					
16. Abstract A design study of the prestressed composite spar concept as applied to the Bell Helicopter 540 Rotor System of the AH-1G helicopter was performed. The stiffness, mass and geometric configurations of the Bell blade were matched, to give a dynamically similar prestressed composite blade. A multi-tube, prestressed composite spar blade configuration was designed for superior ballistic survivability at low life cycle cost. Principal structural elements include three (3) prestressed composite spar tubes, KEVLAR 49 fiber skins and interconnections, a Nomex honeycomb afterbody and KEVLAR 49 fiber nose and trailing edge members. The tube liners were designed to provide redundant attachment to the rotor hub. An outer skin ply of #120 woven fiberglass cloth increases tear resistance to external damage. The composite spar prestresses, imparted during fabrication, are chosen to maintain compression in the high strength cryogenically stretchformed 304-L stainless steel liner and tension in the over-wrapped HTS graphite fibers under operating loads. This prestressing results in greatly improved crack propagation and fatigue resistance as well as enhanced fiber stiffness properties. Advantages projected for the prestressed composite rotor spar concept include increased operational life and improved ballistic survivability at low life cycle cost.					
17. Key Words (Suggested by Author(s)) Composite spar, prestressed, cryogenic stretch forming, crack retardation, enhanced fatigue life			18. Distribution Statement Unclassified - Unlimited		
19. Security Classif. (of this report) Unclassified		20. Security Classif. (of this page) Unclassified		21. No. of Pages 93	
				22. Price*	